International Scientific-Technical and Production Journal

The Paton WELDING JOURNAL

March 2011 # 3

English translation of the monthly «Avtomaticheskaya Svarka» (Automatic Welding) journal published in Russian since 1948

Founders: *E.O. Paton Electric Welding Institute of the NAS of Ukraine*
International Association «Welding»

Publisher: *International Association «Welding»*

Address:
E.O. Paton Electric Welding Institute,
International Association «Welding»,
11, Bozhenko str., 03680, Kyiv, Ukraine
Tel.: (38044) 287 67 57, 200 82 77
Fax: (38044) 528 04 86, 200 82 77
E-mail: journal@paton.kiev.ua
http://www.nas.gov.ua/pwj

State Registration Certificate
KV 4790 of 09.01.2001

Subscriptions:
$324, 12 issues per year,
postage and packaging included.
Back issues available.

CONTENTS

DIFFUSION BONDING OF γ-TiAl BASE ALLOY IN VACUUM BY USING NANOLAYERED INTERLAYERS

G.K. KHARCHENKO, A.I. USTINOV, Yu.V. FALCHENKO, A.N. MURAVEJNIK, T.V. MELNICHENKO and **L.V. PETRUSHINETS**
E.O. Paton Electric Welding Institute, NASU, Kiev, Ukraine

The effect of nanolayered interlayers Ti/Al, Ni/Ti and Ni/Al on structure of the diffusion bonds made in vacuum on γ-TiAl base alloy was studied. It is shown that when using the nanolayered interlayers of a composition differing from that of the base alloy it is necessary to conduct homogenising annealing to lower the degree of chemical heterogeneity in the bonding zone.

Keywords: *diffusion bonding in vacuum, intermetallic titanium-aluminium alloy based on γ-TiAl, nanolayered interlayer, homogenising annealing, joint, heterogeneity, structure, microhardness*

Titanium aluminides and alloys on their base belong to a new class of light heat-resistant materials, which are intended for operation at a temperature of 700–1100 °C, that is much higher than the service temperature of modern titanium superalloys ($T \le 600$ °C). The interest in titanium aluminides is caused by their high potential for application in aerospace engineering instead of titanium and nickel superalloys.

Studies [1, 2] investigated joinability of titanium aluminides (Ti–45 at.% Cr–2 at.% Nb) when using the Ti–Al system nanolayered interlayers of the Ti–(48–50) at.% Al composition, which were deposited on the mating surfaces by magnetron sputtering. Thickness of the interlayers was 2.0–2.5 μm, thickness of the individual layers being 4 nm. The TiAl nanocrystals with a higher hardness than that of the base metal form in the interlayers during deposition of a film. The authors of the above studies consider the following parameters of the process to be the optimal ones: bonding temperature $T_{bond} = 1000$ °C, pressure $P = 50$ MPa, and bonding time $t_{bond} = 1$ h.

It is shown in study [3] that the optimal parameters for diffusion bonding of γ-TiAl alloys through the nanolayered interlayer Ti/Al produced by vacuum deposition are as follows: $T_{bond} = 1200$ °C, $P = 10$ MPa, and $t_{bond} = 20$ min. With these parameters the bonding zone is free from pores and cracks.

No investigation results on the possibility of using other compositions of nanolayered interlayers are available in the literature.

The purpose of this study was to investigate peculiarities of formation of permanent bonds on the γ-TiAl base alloy by using nanolayered interlayers of the Ti/Al, Ni/Ti and Ni/Al systems in the form of foils 15–30 μm thick, produced by electron beam evaporation and vapour-phase deposition in vacuum [4, 5]. The foils consist of alternating nanolayers of the components, in which solid-phase reactions of synthesis of intermetallics take place during heating.

The following interlayers were chosen for bonding of samples of alloy Ti–48 at.% Al–2 at.% Nb–2 at.% Mn: Ti/Al (Ti–38 at.% Al), Ni/Ti (Ti–44 at.% Ni) and Ni/Al (Al–46 at.% Ni).

Diffusion bonding of the 10 × 10 × 6 mm samples of intermetallic Ti–48 at.% Al–2 at.% Nb–2 at.% Mn (below referred to as γ-TiAl) was performed by using unit U-394. The electron beam heater was employed as a heat source. The mating surfaces were preliminarily prepared by removing the cold worked layer with a diamond wheel, and then by degreasing. Bonding was carried out under the following conditions: heating temperature $T_h = 1200$ °C, heating time $t_h = 20$ min, $P = 20$ MPa, and vacuum in the working chamber at a level of $1.33 \cdot 10^{-3}$ MPa.

Microstructure and chemical composition of the base metal and bonds were analysed by using optical microscope «Neophot-32», as well as scanning microscope «CamScan» equipped with energy-dispersive system «Energy 200» for local analysis. Phase composition was evaluated by the X-ray diffraction analysis method using diffractometer DRON-3 in Cu_{K_α} radiation. Microhardness of the samples was measured with meter PMT-3 under a load of 0.1–0.5 N.

Results of X-ray diffraction phase analysis show that the γ-TiAl alloy in the initial state contains two phases — TiAl (γ-phase) and Ti_3Al (α_2-phase). The volume content of the α_2-phase in the alloy, with respect to the γ-phase, is 7 %. A fragment of the diffraction pattern of the γ-TiAl alloy is shown in Figure 1.

As revealed by metallography, the alloy in the initial state has a fully lamellar structure. The alloy consists of homogeneous, practically equiaxed grains approximately 60–120 μm in size, having the γ- and α_2-phase lamellae of a certain orientation inside them (Figure 2).

It is noted in study [6] that normally the α_2-phase is present in the lamellar structure in the form of thin

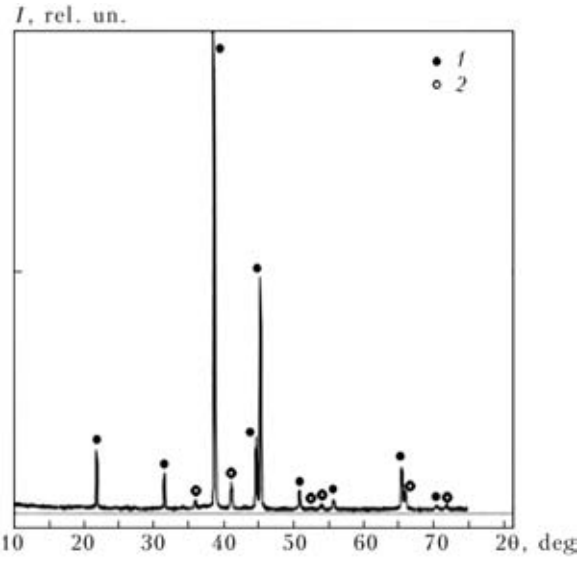

Figure 1. Fragment of diffraction pattern of γ-TiAl alloy in the initial state: *1* — TiAl phase; *2* — Ti_3Al phase; *I* — radiation intensity; 2θ — diffraction angle

plates at the twin boundaries of the γ-phase, which may inhibit its growth. Moreover, dispersed dark inclusions of a different shape form in the alloy at the background of the lamellar structure. These inclusions are uniformly distributed in the bulk of the matrix and have the increased niobium content. The alloy comprises isolated micropores. No coarse pores and cracks were detected. Microhardness of the alloy in the initial state was *HV* 3000–4000 MPa.

Earlier the authors of study [3] conducted metallographic examinations of the bond on the γ-TiAl alloy produced by diffusion bonding in vacuum without an interlayer. As seen in Figure 3, *a*, structure of the transition zone has a clearly defined interface, and no common grains form within the bonding zone. The presence of an interlayer of intermetallic Ti_3Al was revealed at the interface in microstructure of the alloy at high magnifications in the phase contrast mode (Figure 3, *b*).

Bonding through interlayers Ti/Al. Microstructures of the bond made through the nanolayered interlayer Ti/Al are shown in Figure 4, *b*, *c*. Here the points where microhardness and local chemical composition were investigated are designated by numerals.

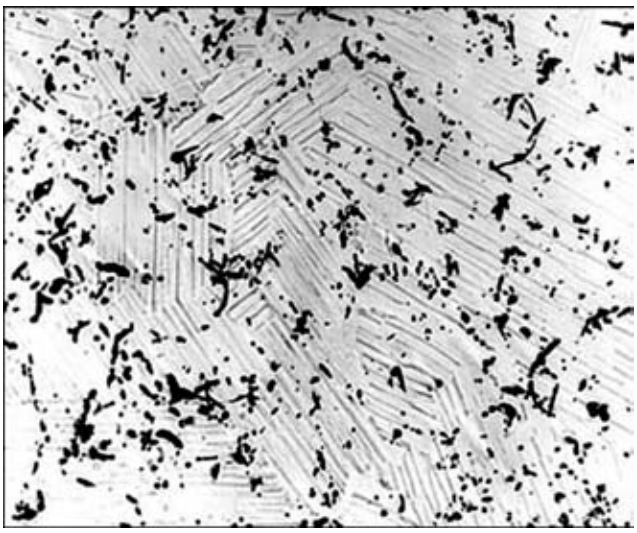

Figure 2. Microstructure (×400) of γ-TiAl alloy in the initial state

The metallography results showed that the bonds were free from defects in the form of pores, oxide inclusions and cracks. A homogeneous transition zone about 20 μm thick formed in the bond (Figure 4, *a*). According to the data of local chemical analysis, this zone had a composition of 49.26 at.% Al–50.07 at.% Ti–0.67 at.% Mn, which is close to the composition of the main intermetallic phase γ-TiAl. When using the Ti/Al interlayer, fine equiaxed grains growing into the base metal formed within the bonding zone (see Figure 4, *b*). However, this did not deteriorate strength properties of the bond. Microhardness of the bonding zone was *HV* 3500–4200 MPa, and that of the base metal was *HV* 3000–4000 MPa.

To understand the role of nanolayered foils in formation of the bonds and investigate the intensity of the diffusion processes occurring in the bonds, we performed bonding by using radioactive isotopes preliminarily deposited on titanium aluminide. It was established [7] that application of the nanolayered interlayers Ti/Al for diffusion bonding in vacuum considerably increased mobility of atoms ^{63}Ni within the bonding zone. In bonding through the nanolayered interlayer the diffusion zone grew approximately 4 times in size, compared to bonding without the interlayer. The calculated value of the effective diffusion coefficient in bonding without the interlayer is about

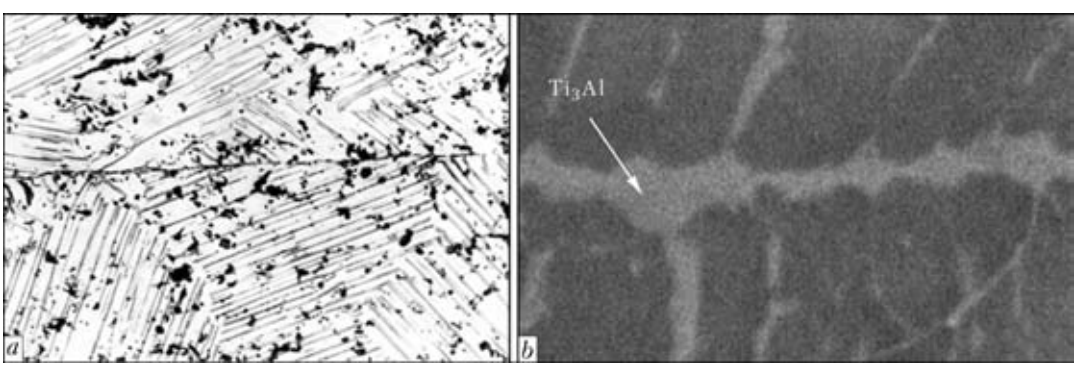

Figure 3. Microstructures of the bonding zone on γ-TiAl alloy in bonding without an interlayer, obtained by optical (*a* — ×500) and scanning electron microscopy (SEM) in phase contrast mode (*b* — ×3000)

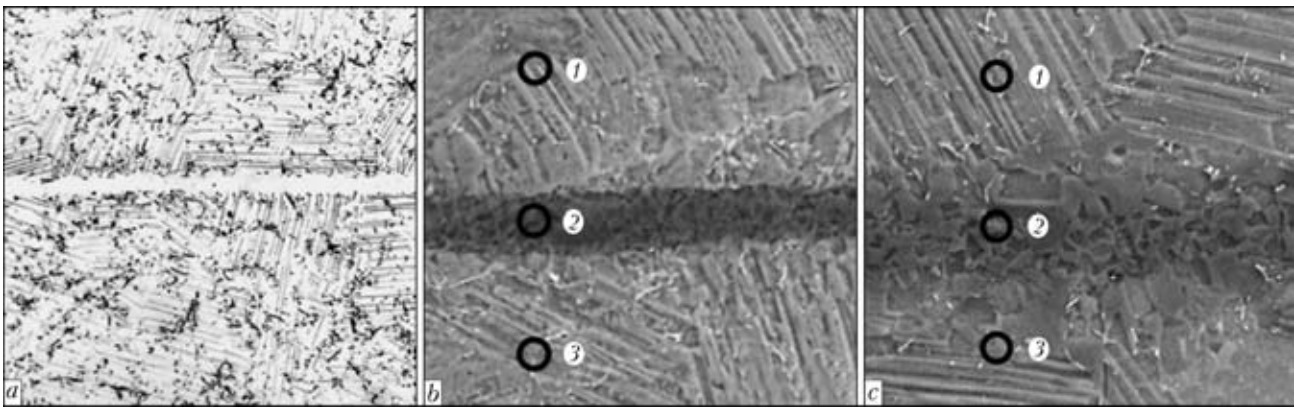

Figure 4. Microstructures of the bonding zone on γ-TiAl alloy in bonding through nanolayered interlayer Ti/Al, obtained by optical microscopy (*a* — ×200), SEM (*b* — ×300) and SEM after bonding and homogenising annealing at 1200 °C for 2 h (*c* — ×300)

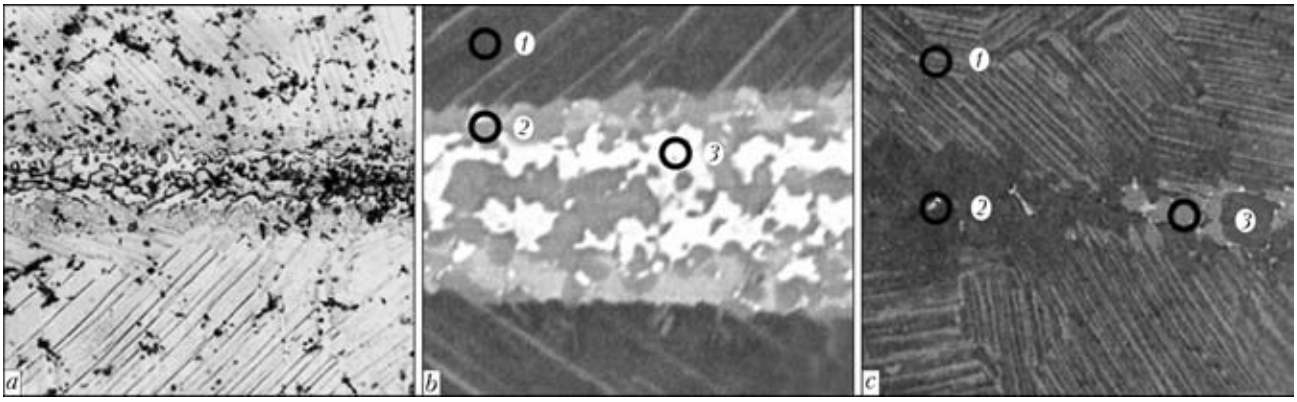

Figure 5. Microstructures of the bonding zone in bonding through nanolayered interlayer Ni/Ti, obtained by optical microscopy (*a* — ×400), SEM (*b* — ×1000) and SEM after bonding and homogenising annealing at 1200 °C for 2 h (*c* — ×200)

$1 \cdot 10^{-7}$, and with the interlayer — about $1 \cdot 10^{-5}$ cm^2/s. Therefore, when using the nanolayered interlayer the mobility of atoms ^{63}Ni increases almost by two orders of magnitude.

Activation of the diffusion processes is evidenced by the presence of manganese in the bonding zone (Table 1). Unlike manganese, niobium does not transfer from the base metal into the interlayer during bonding. As heterogeneity of structure and chemical composition of the bond is probably related to an insufficiently long thermal effect during bonding, the resulting samples were subjected to homogenising annealing in vacuum for 2 h at a temperature of 1200 °C in order to increase homogeneity of the composition and structure. After annealing, levelling of chemical compositions of the interlayer and base metal took place in the bond (see Figure 4, *c* and Table 1).

Bonding through interlayers Ni/Ti. As revealed by metallographic examinations, the nanolayered interlayer Ni/Ti causes a considerable activation of the diffusion processes within the bonding zone. The transition zone of a variable thickness (about 30 μm), which is heterogeneous in structure and composition and consists of two phases (Figure 5, *a*, *b*), forms during bonding in place of the initial interlayer. According to the data of local chemical analysis (Table 2), the dark-gray phase component contains the following elements, at.%: up to 0.7 Ni, 59.2 Ti, 37.4 Al, 1.8 Nb, and 0.9 Mn. The light phase compo-

Table 1. Indicators of the bonding zone on γ-TiAl alloy produced through nanolayered interlayer Ti/Al

Treatment method	Investigated points*	Chemical composition, at.%				*HV*, MPa
		Al	Ti	Mn	Nb	
Bonding	*1*	45.58	50.97	1.44	2.01	5000
	2	49.26	50.07	0.67	—	4000
	3	43.05	54.18	0.99	0.78	4500
Bonding + annealing	*1*	44.57	52.03	1.36	2.04	3800
	2	46.69	51.39	1.02	0.90	3500
	3	43.18	53.85	0.84	2.13	3900

*Here and in Tables 2 and 3, see Figure 4, *b*, *c*.

Table 2. Indicators of the bonding zone on γ-TiAl alloy produced through nanolayered interlayer Ni/Ti

Treatment method	Investigated points	Chemical composition, at.%					*HV*, MPa
		Al	Ti	Mn	Ni	Nb	
Bonding	*1*	44.1	52.4	1.2	0	2.3	3900
	2	37.4	59.2	0.9	0.7	1.8	5500
	3	43.0	36.0	2.3	16.9	1.8	9000
Bonding + annealing	*1*	44.8	51.8	1.4	–	2.0	4200
	2	45.8	50.3	0.9	0.9	2.0	4400
	3	41.3	54.5	1.2	0.9	2.1	5300

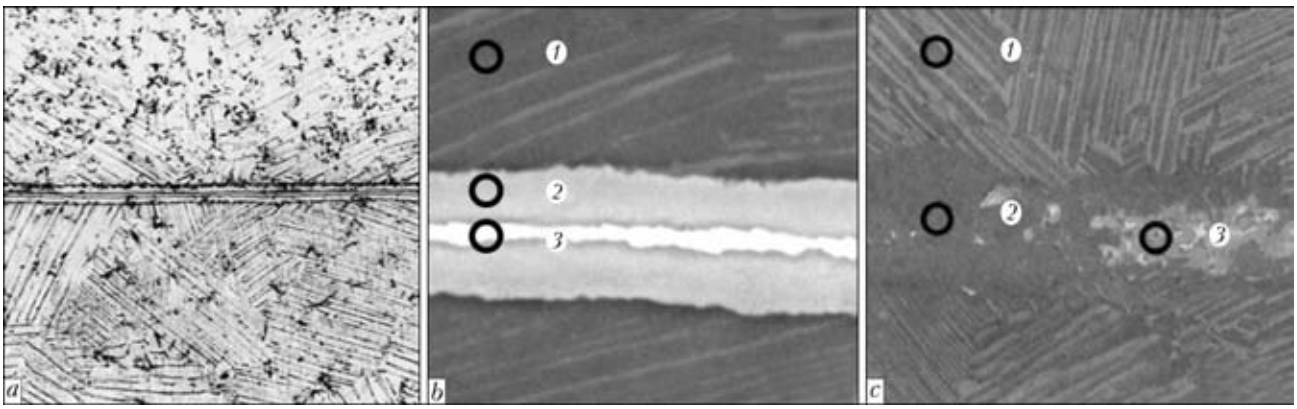

Figure 6. Microstructures of the bonding zone in bonding through nanolayered interlayer Ni/Al, obtained by optical microscopy (*a* — ×200), SEM (*b* — ×1000) and SEM after bonding and homogenising annealing at 1200 °C for 2 h (*c* — ×200)

Table 3. Indicators of the bonding zone on γ-TiAl alloy produced through nanolayered interlayer Ni/Al

Treatment method	Investigated points	Chemical composition, at.%					*HV*, MPa
		Al	Ti	Mn	Ni	Nb	
Bonding	*1*	44.5	51.5	1.2	0.5	2.3	4100
	2	41.6	34.8	1.1	21.0	21.0	11400
	3	44.7	9.7	0.25	45.2	0.15	7900
Bonding + annealing	*1*	43.0	53.3	1.3	0.2	2.2	4200
	2	48.5	48.2	0.9	0.4	2.0	4000
	3	43.2	46.5	2.1	6.6	1.6	10300

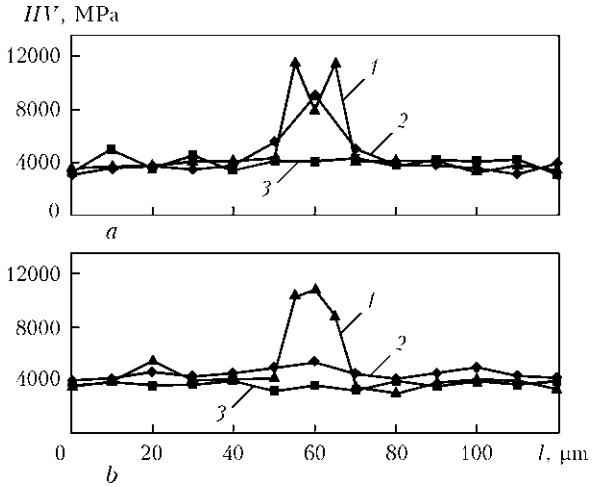

Figure 7. Distribution of microhardness in the bonding zone after bonding through nanolayered interlayers Ni/Al (*1*), Ni/Ti (*2*) and Ti/Al (*3*) (*a*), and after bonding and homogenising annealing at 1200 °C for 2 h (*b*): *l* — distance between indenter impressions

nent contains the following elements, at.%: 16.9 Ni, 36 Ti, 43 Al, 1.8 Nb, and 2.3 Mn. Niobium, like manganese, penetrates into the transition zone through all its thickness during the process of diffusion bonding (see Table 2). Nickel concentrates mostly in the light phase component, which is a complex intermetallic (Ti, Ni)Al. Microhardness of the dark-gray diffusion regions is *HV* 4500–5500 MPa, and that of the central region consisting mostly of the complex intermetallic is *HV* 8000–10000 MPa, which is much higher than microhardness of the base metal (*HV* 3500–3900 MPa). No marked changes of structure in the base metal regions adjoining the transition zone were detected, the lamellar structure persisting (see Figure 5, *b*). After annealing, levelling of the distribution of manganese and niobium, which are contained in the alloy and interlayer, take place in the bond. The nickel content of the bond decreases to 0.9 at.% (see Figure 5, *c* and Table 2).

Bonding through interlayers Ni/Al. Metallographic examinations of the bonds produced through the Ni/Al interlayer showed that the transition zone about 20 μm thick, which is heterogeneous in structure and composition (Figure 6, *a*, *b*), formed within the bonding zone. The Ni/Al base intermetallic layer 3–4 μm thick formed in its central part. The central region of the transition zone (Figure 6, *b*; Table 3) contained the following elements, at.%: 45.2 Ni, 44.7 Al, 9.7 Ti, 0.25 Mn, and 0.15 Nb. It should be noted that niobium did not practically penetrate into the central part of the transition zone. Its peripheral part contained the following elements, at.%: 21 Ni, 41.6 Al, 34.8 Ti, 1.1 Mn, and 1.4 Nb. It is a complex intermetallic (Ti, Ni)Al alloyed with niobium and manganese. Microhardness of the peripheral region of the transition zone was *HV* 9000–11400 MPa.

Also investigated was the character of changes of microhardness in the γ-TiAl bonding zone produced through nanolayered interlayers Ni/Ti, Ni/Al and Ti/Al. The character of changes of microhardness in the bonds produced through the Ni/Ti and Ni/Al interlayers is indicative of the fact that the bonding zone contains regions of a material with a high microhardness, much higher than that of the base metal. When using the Ti/Al interlayers, which are close in composition to the base metal, microhardness in the bonding zone remains almost unchanged.

After annealing, microhardness of the bonds produced through the Ti/Al and Ni/Ti interlayers is close in value to that of the base metal (*HV* 4000–5000 MPa). In the case of using the Ni/Al interlayers, annealing has no effect on microhardness (*HV* 10000–11000 MPa) of the bonds.

CONCLUSIONS

1. Application of nanolayered interlayers Al/Ti for diffusion bonding in vacuum of intermetallic alloy Ti–48 at.% Al–2 at.% Nb–2 at.% Mn allows producing the bonds with a uniform distribution of the alloying elements contained in the base alloy.

2. When using nanolayered interlayers Ni/Al, additional annealing does not remove heterogeneity of chemical composition and structure, and has no effect on microhardness of the bond.

3. Additional annealing of the bonds produced through nanolayered interlayers Ni/Ti provides the bonds with a chemical composition close to that of the base metal.

The authors express sincere gratitude to Prof. A.I. Ishchenko and Dr. V.K Sabokar for their participation in the study.

1. Duarte, L.I., Ramos, A.S., Vieira, M.F. et al. (2006) Solid-state diffusion bonding of γ-TiAl alloys using Ti/Al thin films as interlayers. *Intermetallics*, **14**, 1151–1156.
2. Ramos, A.S., Vieira, M.T., Duarte, L.I. et al. (2006) Nanometric multilayers: a new approach for joining TiAl. *Ibid.*, 1157–1162.
3. Ustinov, A.I., Falchenko, Yu.V., Ishchenko, A.Ya. et al. (2009) Producing permanent joints of γ-TiAl based alloys using nanolayered Ti/Al interlayer by vacuum diffusion welding. *The Paton Welding J.*, **1**, 12–15.
4. Ustinov, A.I., Olikhovskaya, L.A., Polishchuk, S.S. (2006) Metastable nanostructural states in coatings of Ni–Al, made by vapor phase deposition. *Metallofizika i Nov. Tekhnologii*, **6**, 32–37.
5. Ustinov, A.I., Olikhovskaya, L.A., Melnichenko, T.V. et al. (2008) Solid-phase reactions in heating of multilayer foils Al/Ti made by electron-beam deposition method. *Sovremen. Elektrometallurgiya*, **2**, 21–28.
6. Romankov, S.E., Volkova, T.V., Melikhov, V.D. (2002) Phase-structural transformations of alloy Ti–48 % Al–2 % Nb in artificial ageing. *Fizika Metallov i Metallovedenie*, 93(**4**), 50–61.
7. Kharchenko, G.K., Mazanko, V.F., Ustinov, A.I. et al. (2009) Studies of diffusion processes in welded joints of titanium aluminide (TiAl). *Visnyk Ch. DTI. Series Tekhn. Nauky*, **37**, 117–119.

FRACTURE SURFACE MORPHOLOGY AT FATIGUE OF MIG-WELDED JOINTS OF AMg6 ALLOY

T.M. LABUR, V.A. SHONIN, T.G. TARANOVA, V.A. KOSTIN, V.S. MASHIN and **I.N. KLOCHKOV**
E.O. Paton Electric Welding Institute, NASU, Kiev, Ukraine

Results of examination of structure of fracture surface on samples of MIG-welded joints of AMg6 alloy after cyclic tests with loading cycle asymmetry $R_\sigma = 0.4$ and $R_\sigma = -1$ are given. Peculiarities of morphology in different fracture regions have been revealed and mechanism of fatigue crack propagation has been established. It is noted that fracture of the welded joints at a microlevel is of a mixed and multi-site nature. High-frequency peening in a narrow AMg6 alloy weld to base metal transition zone using steel strikers provides formation of a smoother geometry of the weld to base metal transition zone and decrease in average values of the stress concentration factor.

Keywords: *arc welding, aluminium alloy, consumable electrode, welded joints, fatigue testing, fracture surface morphology*

Application of traditional materials and development of new ones requires knowledge of the change of physical and structural characteristics under the conditions of cyclic loading, as they reflect the level of material resistance to macrocrack development in a specified structural state and operation modes. Loading periodicity increases localization of plastic deformation in a material, changes its stressed state and causes restructuring in microvolumes, which is a response to external impact [1–6]. Exhaustion of material capability for further plastic deformation leads to its fracture.

In welded joints structural zones are singled out, in which complex multiphase structures form under the impact of the thermal cycle of welding. Differences between heterogeneous base metal grains and weld crystallites formed in welding cause the appearance of stress concentration gradient in the welded joint. An increase of the width of intergranular space in the heat zone is accompanied by an increase of the number of eutectic phases forming as a result of development of chemical inhomogeneity by the main alloying elements and impurities, because of their segregation along the grain boundaries [2]. This results in a change of the dimensions, shape and configuration of the location of phase precipitates, coagulation of intermetallic phase inclusions, leading to formation of coarser structure regions in the joint zone, that influences the localization of plastic deformations in the HAZ metal, leading to realization of different fracture micromechanisms, accompanying the processes of crack initiation and propagation [3].

The purpose of this work is establishment by the method of fractographic analysis of morphological and structural features of microrelief on fatigue fracture surface of welded joints of high-strength AMg6 aluminium alloy 12 mm thick, made by consumable electrode. Welding of samples was performed in a mixture of argon and helium (50 + 50 %) by a pulsed arc in the following mode: I_w = 220 A, U_a = 23 V, v_w = = 30 m/h using TPS-450 power source (Fronius, Austria). Samples of welded joints across the weld with technological reinforcement and without it were cut out of butt joints.

After welding some joints of the alloy were subjected to mechanical peening in the narrow zone of weld to base metal transition by applying a single-row group of steel strikers of 5 mm diameter, brought into directed motion by a small-sized portable ultrasonic generator (of 0.3 kW power) and manual tool with piezoceramic converter of ultrasonic oscillations into mechanical oscillations [7]. The speed of striker displacement along the weld was equal to 5 mm/s.

Fatigue testing was conducted under the conditions of alternating load along sample axis with 5–6 Hz frequency by a standard procedure in MTS-318.25 machine with maximum axial load of 25 t. Error of measurement of the applied force did not exceed 1 %.

Condition of the metal after welding and performance of high-frequency mechanical peening of the surface of the zone of weld fusion with the base metal was studied by fractographic analysis. Change of the shape and dimensions of individual fragments of the relief of welded joint fracture was examined in the scanning electron microscope JSM-840 with a system of Link-860/500 microanalyzer (at accelerating voltage of 15, 25 and 30 kV).

Visual analysis of fracture surface of samples of AMg6 alloy welded joints after testing at cyclic load with coefficient of asymmetry $R_\sigma = 0$ showed that the fatigue crack initiates on the boundary of weld fusion with the base metal and propagates in the HAZ direction with further transition into the base metal, forming the main crack (Figure 1). Fracture contains three characteristic relief zones: purely fatigue fracture, fatigue fracture with a rough surface as a result of plastic deformation, final fracture zone, which was formed by tough fracture mechanism. Presence of dif-

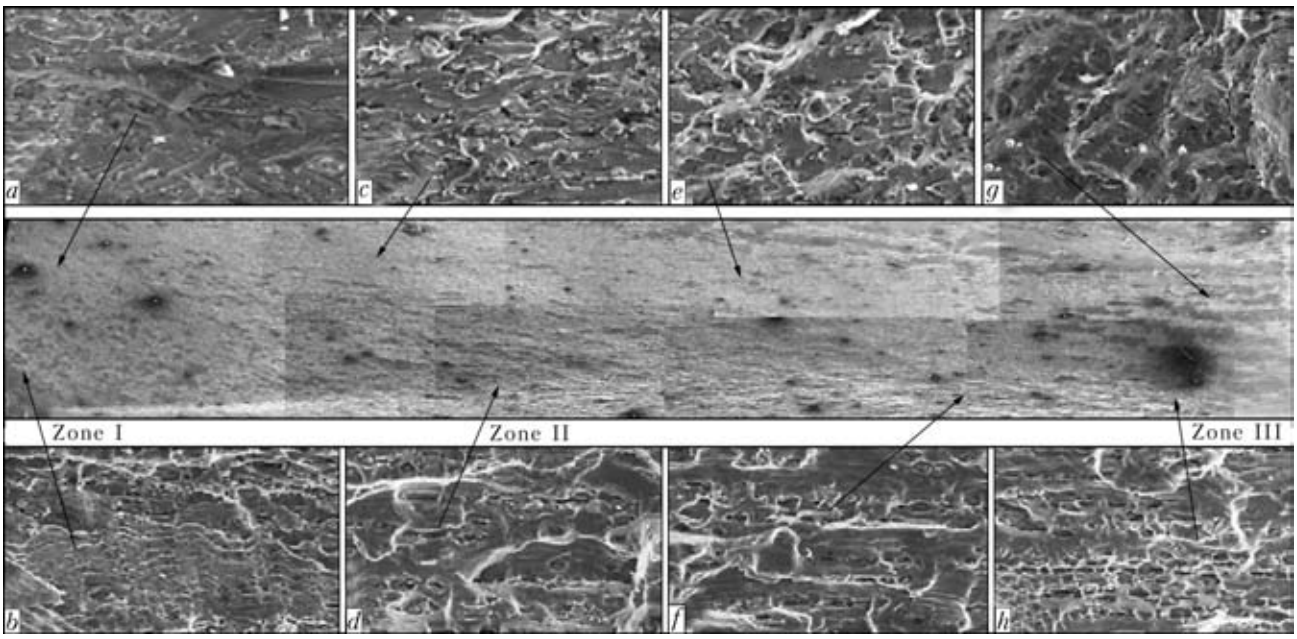

Figure 1. Fracture panorama (×13) and fractographs of its individual fragments (×500) in MIG-welded joints of AMg6 alloy tested at cyclic loading with coefficient of asymmetry $R_\sigma = 0$ (for *a*–*h* see the text)

ferent topography of the relief regions on fractures of the studied samples points to different degrees of plastic deformation, which accompanies the processes of initiation and propagation of the main fatigue crack during testing. The colouring of fracture regions, where the fatigue crack initiates and propagates, is bright, and the final fracture zone is of mat colour. Its relief has several deep cracks, which run in-depth of the sample and are oriented along the axis of application of cyclic load. Their extent on the fracture surface is equal to 10–50 μm, which is attributable to insufficient quality of the alloy working during manufacturing of the semi-finished product.

Topography of the region, where the site of fatigue crack initiation formed, is due to the characteristic features of the structure of weld metal on AMg6 alloy and conditions of cyclic testing (Figure 1, *a*–*h*). Level of local microstresses, which remained on the boundary of weld metal crystallites after phase transformation during the welding cycle, affects the process of microcrack initiation. Change of activation energy in the metal and concentration of plastic shears in individual, most stressed weld crystallites at achievement of the critical value of stress range, is accompanied by their localization, formation of slip bands, shifting of one part of the crystal relative to another along crystallographic surfaces of the same orientation [4, 5]. This not only causes appearance of the fatigue crack source, but also determines the nature of its further propagation.

In the fracture plane the crack is a flat surface in the form of a fan, propagating in the radial direction relative to the oxide film located in the weld near the fusion zone. This is indicative of the fact that the film is the site of fatigue crack initiation. Flat regions of intergranular fracture are present on the fracture surface. Indications of brittle crack initiation with kink steps (Figure 1, *b*) are also observed, which are manifested when the crack tip runs into screw dislocations crossing the cleavage plane [4, 6]. These may be dislocations, present in the alloy, or generated by the fatigue crack tip. Traces of the action of tough micromechanism, which is realized as a result of plastic deformation localization under the conditions of an alternating loading, are insufficient. A considerable number of deformed weld crystallites on the fracture surface of the studied sample in as-welded condition, is indicative of the fact that slip bands are intensively developing during crack propagation.

During the period of stable growth the main crack propagates in an intercrystalline mode along the boundaries of grains, which are fringed with intermetallic phases. Their coagulation during welding heating, as well as increase of the width of the intercrystalline space, volume of eutectic phases formed as a result of segregation of alloying elements and impurities, cause metal softening in the near-boundary regions and intensive initiation of microcracks by the cleavage mechanism. Morphological relief elements that are formed in this case, can be compared by their size with the matrix (solid solution), regions of intermetallic phase location, and facet structure elements. The width of longitudinal microcracks does not change as they propagate, remaining equal to 1.5–2.0 μm. Crack length is increased through coalescence of individual microcracks, and its path acquires a zigzag shape (Figure 1, *c*, *d*).

Located beyond the fatigue crack is the zone of action of mixed fracture mechanism, in which alongside flat sections of the relief, indications of plastic deformation realization at propagation of the main crack by the tearing mechanism are also observed (Fi-

gure 2). Transition to the zone of mixed fracture occurs as a result of increase of the number of deformed grains. Branching of microcracks observed in the fracture indicates that location of coarse phase particles on the crystallite boundary prevents the translational motion of the main crack. This leads to its deceleration, increase of additional local deformation in the metal microvolume and, consequently, to a change of its propagation direction. All these processes are accompanied not only by a change of relief structure near the crack, but also development of fatigue striation, similar to facet structure bands (see Figure 1, *e*, *f*), manifestation of which is related to increase of dislocation density [8]. There are also relief regions, where the crack propagates through the crystallite that is in a transcrystalline mode. Relief protrusion of fatigue striations indicates the direction and nature of propagation of the main crack.

Specific marks, which are called «track traces» can be also seen on the surface of this fracture region (Figure 2, *a*). They are considered to be indications of fatigue fractures, forming at failure of aluminium and its alloys [8]. The marks are characterized by an exceptionally clear-cut pattern, and are found only in the smooth portions of the relief. They form paths between them, coinciding with the direction of the main crack propagation. Quantity of marks in different fracture sections does not coincide, and the distance between them decreases with increase of the row length (Figure 2, *b*). Publications do not provide an accurate substantiation of the causes for «track traces» appearance in the relief of fatigue fractures. They are associated with manifestation of the secondary effect of the influence of inclusions, phase precipitates or solid insoluble structural components, which protrude above the crack surface during its displacement, as well as the result of interaction of local tangential and normal alternating stresses [9–11].

Presence of a considerable quantity of pits of a parabolic shape, forming in case of shear mechanism of fracture, should be regarded as one of the features of relief structure of final fracture zone (see Figure 1, *f*–*h*). They form from micropores as a result of development of plastic deformation and plastic decohesion under the conditions of cyclic loading [9]. Such processes usually run along the boundaries between the inclusions and matrix in those cases, when the forces of adhesion between them are insufficient, and cause an increase of local stress concentration leading to initiation of microcracks. This is indicated by presence of fragments of broken inclusions or phase precipitates on the pit bottom. Microcracks were observed along grain boundaries. Change of pit orientation and increase of the number of microcracks in the relief of final fracture region, compared to the total panorama of fracture of the studied sample, are indicative of the difference in the local conditions of plastic deformation at the stage of completion of the fracture process.

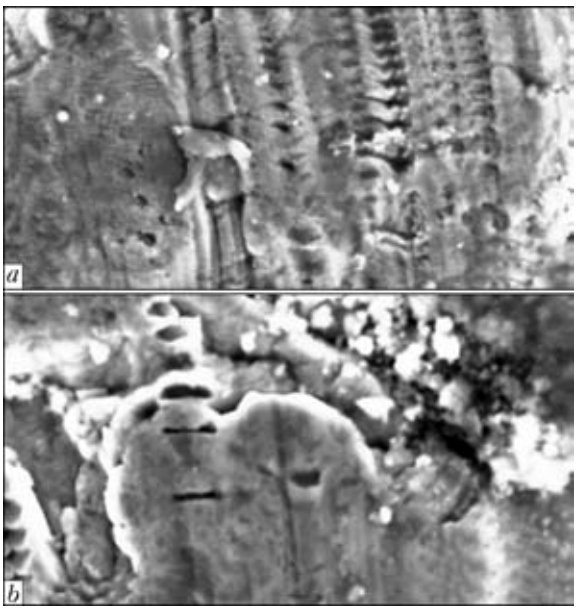

Figure 2. Fracture fractograms (×1000) with characteristic patterns of specific «track traces» marks (for *a*, *b* see the text)

Generalizing the obtained information, the following characteristic features of structure morphology in the fracture of AMg6 alloy welded joint can be noted: fatigue crack initiation site is located on the surface near the zone of weld fusion with the base metal; oxide film is the initiator of fatigue crack; presence of three relief zones in the fracture is indicative of a mixed and multi-site nature of fracture of samples under the conditions of cyclic loading.

Change of the coefficient of asymmetry at cyclic testing from $R_\sigma = 0$ up to more complicated conditions ($R_\sigma = -1$) causes an intensification of plastic deformation localization, and, consequently, change of the nature of fracture relief in the studied samples of welded joints (Figure 3). Fatigue crack initiates beyond the weld in the HAZ metal and propagates in the direction of the base metal, forming the main crack. Its propagation is the result of coalescence of individual microcracks, developing along the slip steps or at crossing of slip planes of two systems. Main crack develops in the intercrystalline mode along grain boundaries, causing brittle intercrystalline fracture with traces of small plastic deformations. Such fractures form under the conditions of lowering of cohesion forces between the structural components located on the boundaries between the grains. Their level in this case should be lower than cohesion in the cleavage plane or slip plane [1–4]. The greatest degree of lowering of adhesion between the grains is noted in samples at cyclic testing with the coefficient of asymmetry $R_\sigma = -1$, which is indicated by three times reduction of the number of cycles to fracture (490,120 cycles). The above phenomenon may be the consequence of brittle nature of intermetallic phases or presence of residual stress as a result of segregation of alloying elements and impurities under the conditions of welding.

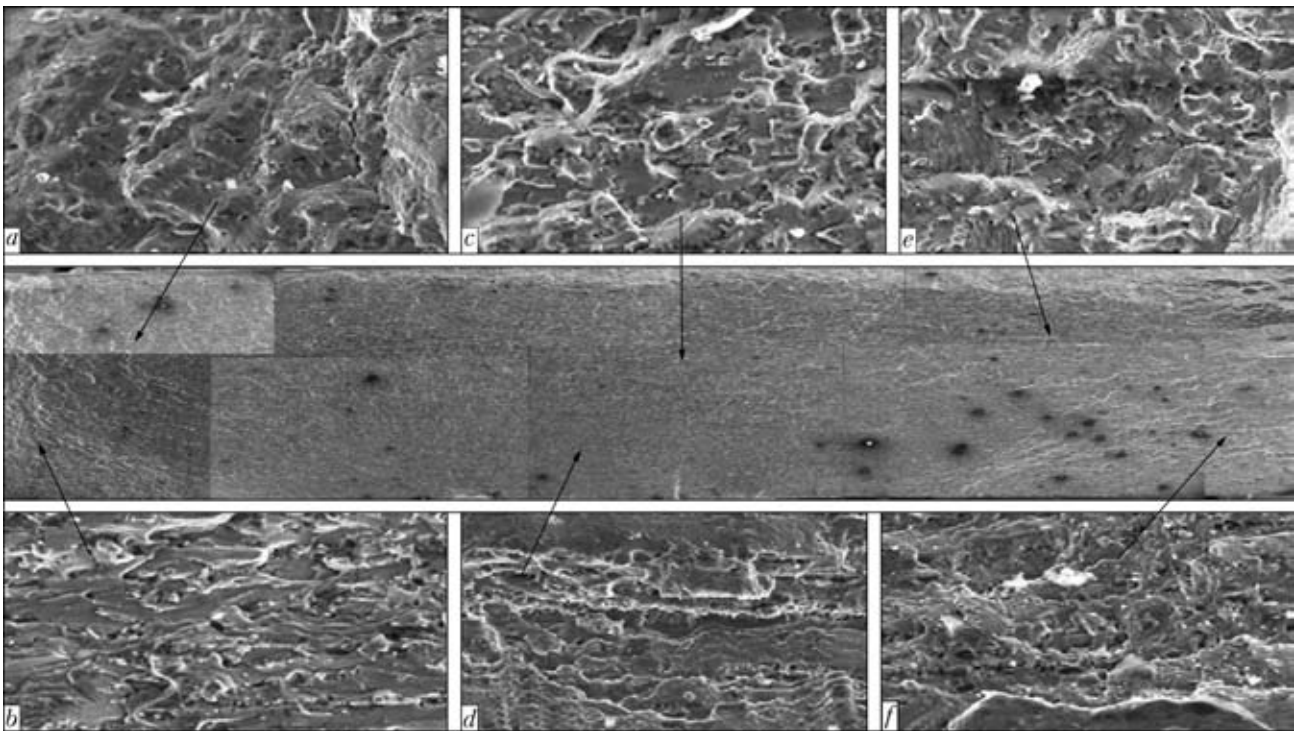

Figure 3. Fracture panorama (×13) and fractographs of its individual fragments (×500) in MIG-welded joints of AMg6 alloy tested at cyclic loading with coefficient of asymmetry R_σ = 0.4 (for *a–f* see the text)

Increase of loading frequency at R_σ = 0.4 is accompanied by increase of the degree of striation disorientation relative to the direction of microcrack movement and appearance of fine secondary striation, slip traces, and steps (Figure 3, *a–c*). A decrease of fatigue striation step and increase of the number of secondary microcracks is noted, the microcracks initiating on the fatigue striation and propagating normal to the fracture surface in-depth of the material. The non-simultaneous nature of realisation of the movement of individual microcracks at testing causes coalescence of the steps and leads to a change of the mechanism of fatigue crack propagation from the brittle to the mixed type (Figure 3, *d–f*). Here the number of ductile bridges in the fracture increases, and plastic shear fragments appear at formation of facet ridges.

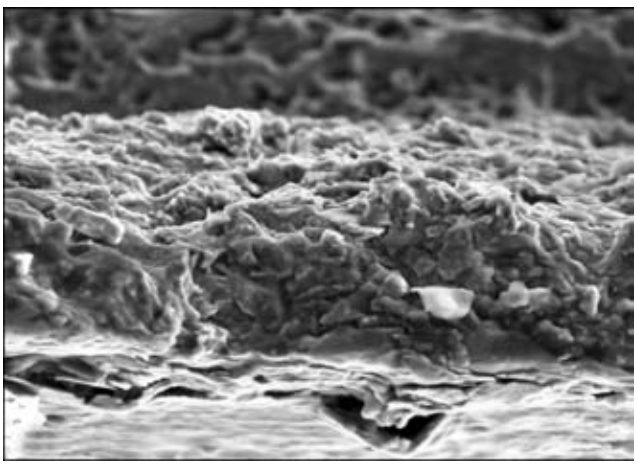

Figure 4. Fragment of the surface (×500) of fracture of AMg6 alloy welded joints near the surface of the zone of transition from the weld to base metal after fatigue testing at R_σ = –1

All together this enhances the diversity of relief morphology across the width and along the length of fatigue striation and facet structure bands. Physical basis of such a process is increase of the level of local plastic deformation of metal as a result of structural change, for instance, cleavage crack crossing the grain body or fracture (delamination) of blocks of one crystallographic order [1–3].

The relief of final fracture zone in such a sample contains a large number of pits of a parabolic shape formed as a result of the processes of tear and shear (see Figure 3). Here increase of the level of local plastic deformation in the microvolume changes the pit shape and direction of orientation, and increases the number of microcracks compared to the general pattern of final fracture zone relief. The site of initiation of primary microcracks are matrix boundaries with insoluble intermetallic inclusions or phase precipitates that points to a lowering of decohesion forces between them under the conditions of welding heating as a result of segregation of alloying elements and impurities. Research results are in good agreement with the data of [1–5]. It is noted in them that the high loading frequency as cyclic testing with the coefficient of asymmetry R_σ = 0.4 causes a fast change of the stressed state in the metal and leads both to formation of a striated relief on the fractures, and to cleavage fracture through the structural components and interphases, thus promoting appearance of secondary fatigue cracks.

High-frequency peening of the surface in the narrow zone of weld fusion with the base metal of AMg6 alloy ensures formation of a smooth geometry of weld

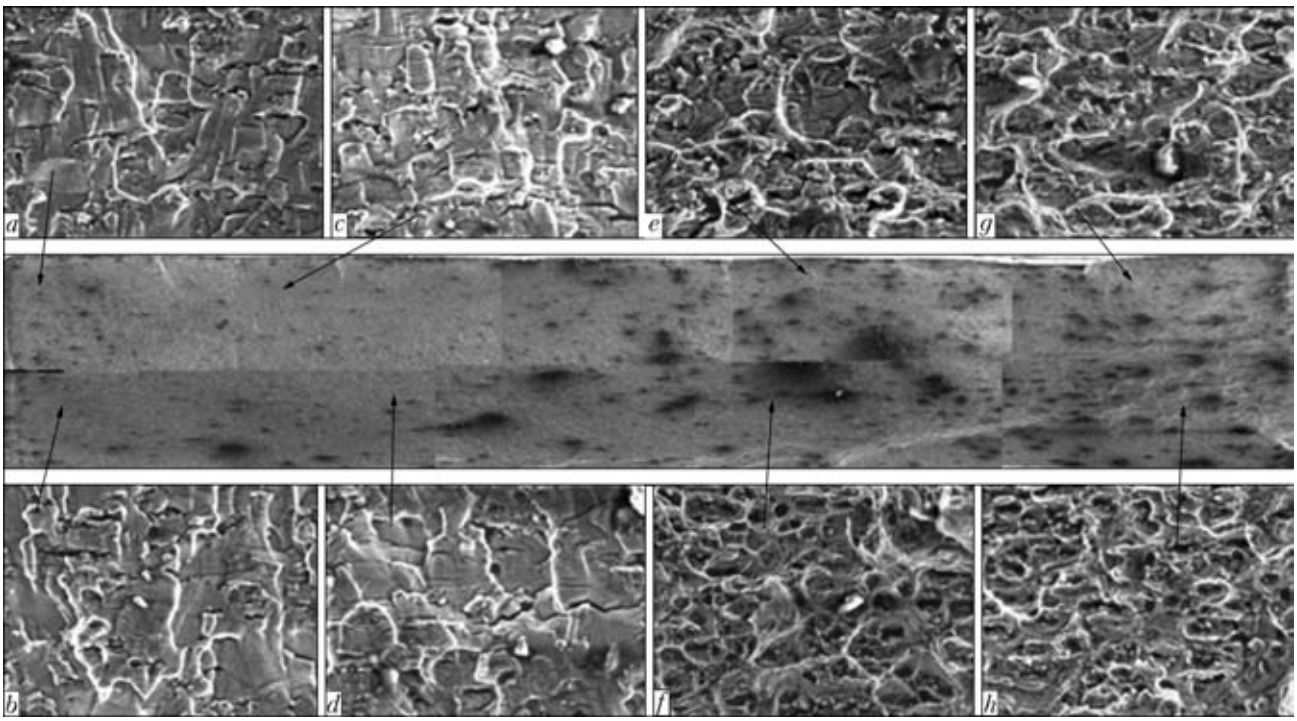

Figure 5. Fracture panorama (×13) and fractographs of its individual fragments (×500) in MIG-welded joints of AMg6 alloy treated by peening and tested at cyclic loading with coefficient of asymmetry $R_\sigma = -1$ (for *a–h* see the text)

to base metal transition and lowering of average values of the stress concentration factor. Positive effect of peening is manifested also in formation of a favourable structure, ensuring an increase of microplastic deformation resistance of the surface layer and formation of high residual compressive stresses [12]. As shown by fractographic investigations of the fracture surface of welded joint samples after cyclic testing in the low-cycle region with the coefficient of asymmetry $R_\sigma = 0.4$, effect of metal strengthening from performance of peening is small (Figure 4). Number of cycles to fracture is equal to 17000. Quasi-cleavage regions containing individual microcracks against the background of fine and small pits are located in the subsurface layer of the fusion zone on the fracture along the grain boundaries. In addition, development of an

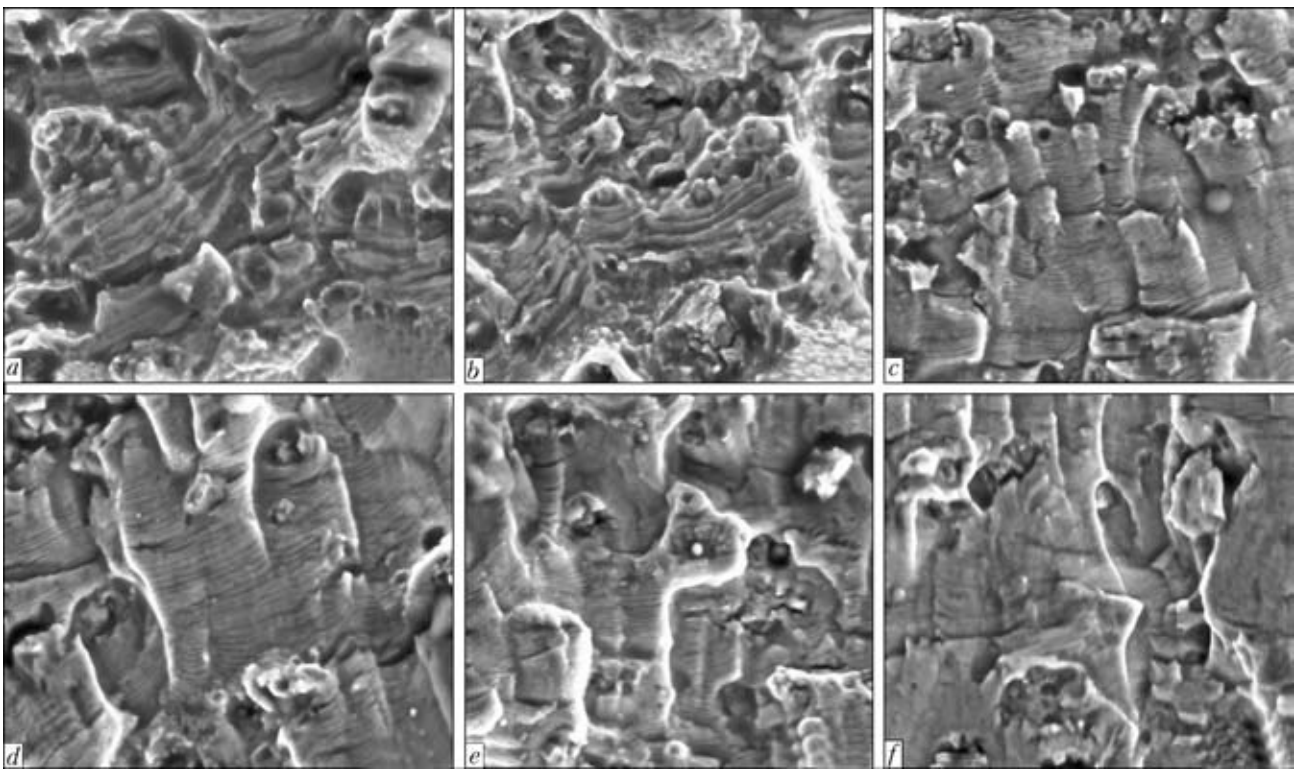

Figure 6. Examples of sections (×1000) of an abrupt transition from the tough mode of striation formation to their brittle delaminations (for *a–f* see the text)

abrupt transition from tough striation to brittle delamination is possible in the subsurface layers (Figure 5). At ×1000 magnification of the relief details one can see that the line which separates the striation from the other structural components, is a crack (Figure 6, *c*–*e*). It forms as a result of simultaneous delamination of metal along several crystallographic planes that may be due to lowering of their strength under the impact of deformation inducing compressive stresses. It should be noted that delamination is not a site of fatigue crack initiation. Therefore, the layer strengthened by peening, is involved into the process of fatigue fracture, and its site is shifted under the deformed layer. Crack propagation proceeds in the fracture section, characterized by a lower fracture resistance.

CONCLUSIONS

1. An intercrystalline mechanism of fatigue crack propagation at cyclic testing with loading cycle asymmetry $R_\sigma = 0$ of MIG-welded joints of AMg6 alloy was established. Presence of three relief zones on fracture surface is indicative of the fact that welded joint fracture on the microlevel is of a mixed and multi-site nature. Localization of plastic deformation in the welded joint and, consequently, crack initiation occur as a result of a change of the dimensions, shape and pattern of phase precipitation location, as well as coagulation of intermetallic phase inclusions occurring at welding heating, thus lowering the total resistance of the metal to fatigue crack propagation.

2. Change of the coefficient of asymmetry at cyclic testing from $R_\sigma = 0$ to more complex conditions ($R_\sigma = -1$) leads to intensification of plastic deformation localization, shortening of fatigue striation step and increase of the number of secondary microcracks, which initiate at fatigue striation and propagate normal to fracture surface in-depth of the metal. At the stage of crack propagation, fatigue striation is characterized by periodicity of the step with a small change of orientation at transition from crystallite to crystallite.

3. High-frequency peening in a narrow zone of the surface of transition of AMg6 alloy weld to base metal using steel strikers ensures formation of a smoother geometry of the zone of weld transition to base metal and lowering of average values of the of stress concentration factor. The strengthened layer relief shows quasi-cleavage regions, which contain individual microcracks along grain boundaries against the background of fine and small pits. In the subsurface layers of the fusion zone a large number of flat sections and microcracks can form, as well as an abrupt transition from tough striation to brittle delamination. The fatigue crack propagates under the peened metal layer.

1. Vladimirov, V.I. (1984) *Physical nature of metal fracture*. Moscow: Metallurgiya.
2. Botvina, L.R. (1989) *Kinetics of fracture of structural materials*. Moscow: Nauka.
3. Ivanova, V.S., Botvina, L.R., Kudryashov, V.G. (1971) *Strength and plasticity. Fracture under short-term loads. Ductile and brittle fracture*: Results of science and technology. Series Metals Science and Heat Treatment. Moscow: VINITI.
4. Kotsanda, S. (1976) *Fatigue fracture of metals*. Moscow: Metallurgiya.
5. Yakovleva, T.Yu. (2003) *Local plastic deformation and fatigue of metals*. Kiev: Naukova Dumka.
6. Herzberg, R.W. (1989) *Deformation and fracture mechanics of structural materials*. Moscow: Metallurgiya.
7. Lobanov, L.M., Kirian, V.I., Knysh, V.V. (2006) Increase in life of welded metal structures by high-frequency peening. *Fiziko-Khimich. Mekhanika Materialiv*, **1**, 56–61.
8. Gordeeva, T.A., Zhegina, I.P. (1978) *Analysis of fractures in evaluation of reliability of materials*. Moscow: Mashinostroenie.
9. Ivanova, V.S., Kudryashov, V.G., Kopeliovich, B.A. et al. (1974) Fractography and fracture toughness of aluminium and titanium alloys. *Tekhnologiya Lyog. Splavov*, **3**, 65–70.
10. (1982) *Fractography and atlas of fractographs*: Refer. Book. Moscow: Metallurgiya.
11. (1987) *Fractography as a means of diagnostics of fractured parts*. Ed. by M.A. Balter. Moscow: Mashinostroenie.
12. (1992) *Improvement of welded metal structures*. Ed. by M.M. Zherbin. Kiev: Naukova Dumka.

PECULIARITIES OF INTERGRANULAR MASS TRANSFER OF GALLIUM IN ALUMINIUM ALLOY DURING SOLID PHASE ACTIVATION OF SURFACES BEING JOINED

Yu.A. KHOKHLOVA, V.E. FEDORCHUK and **M.A. KHOKHLOV**
E.O. Paton Electric Welding Institute, NASU, Kiev, Ukraine

Peculiarities of formation of a dissimilar aluminium-steel diffusion joint in solid-state activation of the surfaces, being joined, by gallium are considered. The effect of products of gallium-aluminium interaction on a local change in mechanical properties within the zone of a permanent joint is shown.

Keywords: *diffusion welding, aluminium, aluminium alloys, reactive diffusion joint, intergranular diffusion, gallium, low-temperature activation of diffusion, indention, Berkovich indenter*

Sometimes, when producing the permanent steel-aluminium units of radio engineering purpose, it is required to reduce the temperature of technological processes down to 140 °C. One of the variants for joining steel with aluminium in a solid phase is brazing with application of pressure [1]. To prevent the formation of brittle intermetallic compounds at the interface of materials being joined the appropriate intermediate inserts of the third metal are used which are a certain diffusion barrier between materials being welded [2]. The activation of adhesive processes of the surfaces being joined is performed by deposition of layer of molten gallium with a tight pressing and consequent heating of the whole unit. Such technology of joining should provide formation of a strong joint without melting of parts and chemical refining of the surfaces being joined from oxide film.

High physical-chemical activity of gallium turns this technological task into a sufficiently complicated process which depends on the number of both positive and negative factors. Gallium is good to wet most metals, therefore they are easily subjected to «adhesion». The temperature interval of liquid state of gallium varies between 30–2204 °C [3]. Metallic «adhesives», based on gallium, impart thermal and electric conductivity, and also high rigidity to the weld. As a result of joining parts into assemblies without fusion of base metal the level of its buckling and oxidation sharply decreases. The strength at equal separation of joints produced using gallium «adhesives» is 26–30 MPa at the temperature of 20 °C. With increase of temperature the diffusion of gallium is sharply increased, and with its decrease the «adhesive» is solidified and facilitates joining of parts during seizure, even if they are not wet by the adhesive [4].

In the equilibrium diagram (Figure 1) [5] it is seen that gallium and aluminium form simple eutectic system in the point where gallium content is equal to 99.2 wt.% at the temperature of 29.7741 °C. The solubility of gallium in solid aluminium at eutectic temperature is approximately 15–20 %, the solubility of aluminium in gallium is negligible [6]. The exclusive feature of gallium is capability of its melts to overcooling: when reducing its temperature by 10–30° below the point of melting it remains in liquid state. The reason of such abnormality consists in peculiarities of molecules constitution and bonds between them under different aggregate conditions.

The joining of materials using molten gallium is a three-stage process: formation of a physical contact (wetting of surfaces being joined with molten gallium); activation of contact surfaces (removal of oxide film); volumetric development of interaction between materials (pressing of their surfaces and start of diffusion).

The mechanism of diffusion of gallium in aluminium is mainly connected with relation of atomic radii of a diffusant and components of solvent: approximation of size of atom of gallium to the size of atom of aluminium promotes the diffusion of gallium in vacancies of aluminium [7]. The rate of migration of atoms of gallium along the boundaries of grains of aluminium at the temperature of 27 °C is almost the same as the diffusion of gallium in liquid aluminium ($D = 1 \cdot 10^{-5}$ cm^2/s). The energy of interface is low and it is about 0.06–0.30 N/m. Therefore, in the

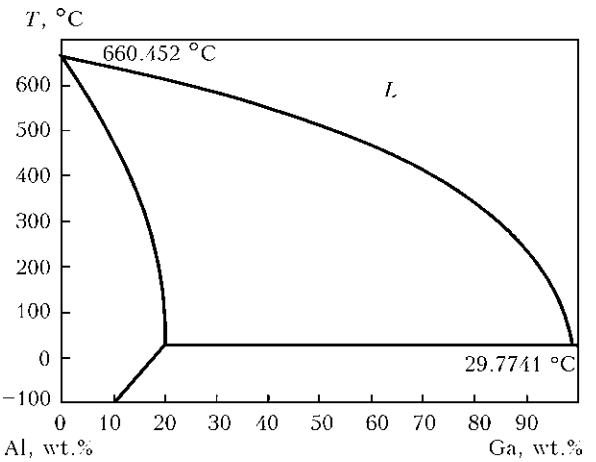

Figure 1. Aluminium–gallium equilibrium diagram

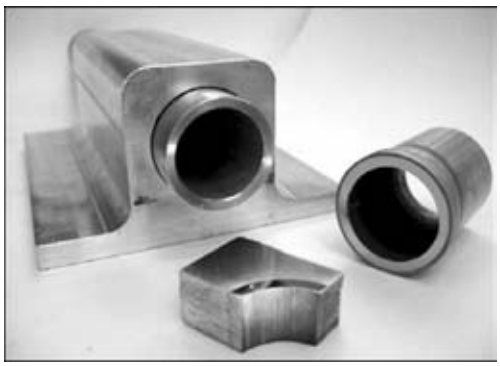

Figure 2. Appearance of the diffusion-welded parts

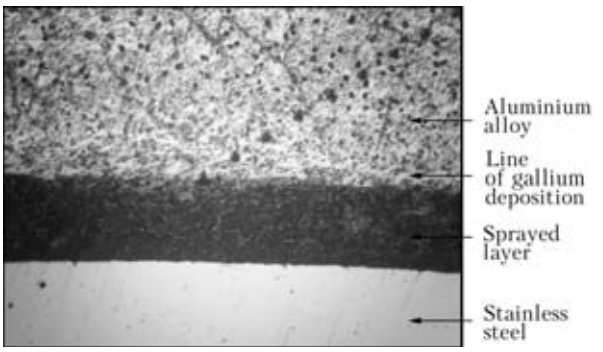

Figure 3. Microstructure (×300) of the zone of joining with dents of Berkovich indenter

presence of diffusant in liquid state at high temperature the conditions are created for grain-boundary phase transition of wetting.

At the initial stage, when the level of diffusion is negligible, the formation of homogeneous solid solution takes place due to diffusion along the grain boundaries. Then, the intermetallic compound is formed having somewhat decreased mechanical properties [8]. The tendency towards considerable decrease in strength is caused by the presence of Rehbinder effect [9, 10].

The unit of a product (Figure 2) represents by a design the joining of stainless steel 10Kh18N9T pipes of 30 mm diameter with a flange of aluminium alloy 6063 of Al–Mg–Si alloying system. To provide dissimilar joining of aluminium-steel on the outer surface of a pipe by a gas-dynamic method the layer of commercial aluminium AD1 (99.3 wt.% Al) of 300 μm thickness was deposited. The activation of adhesion processes of the surfaces being joined was performed by deposition of layer of molten gallium of 10–20 μm thickness with a tight pressing and further heating of the whole unit up to 140 °C during 2 h.

The investigation of depth of intergranular mass transfer of gallium in the process of its diffusion to aluminium was carried out each 1 h and after 60 days. The specimens were stored at the temperature of 30 °C.

Fractographic investigations of microstructure, determination of quantitative element composition and mapping of distribution of elements were performed using methods of scanning electron microscopy (SEM) and X-ray diffraction microanalysis on the basis of an analytic complex consisting of scanning electron microscope JSM-35CF (JEOL, Japan) and X-ray spectrometer with dispersion in energy of X-ray quanta of the model INCA Energy-350 (Oxford Instruments, Great Britain).

For micromechanical tests the nanoindenter «Micron-gamma» was applied designed for determination of mechanical properties using methods of continuous indentions of three-facet diamond Berkovich indenter, scanning by indenter, as well as metallographic and topographic methods [11].

The investigation of structure of specimens showed that as a result of diffusion in the sprayed layer and on the side of aluminium alloy the vast regions with changed (coarsed) structure were formed (Figure 3). The diffusion of gallium into the steel was negligible. The map of distribution of elements (Figure 4) evidences the mass transfer of gallium towards the side of aluminium alloy for the depth of up to 3 mm. The diffusion of gallium to aluminium alloy passes along the intergranular network with formation of distinctly marked boundary chains. During heating the liquid gallium wetted completely the grain boundaries, along which it was segregated, that gave it possibility to move quickly along the intergranular space to vast distances into the volume of material. The qualitative characteristic of degree of proceeding of grain boundary diffusion at each definite boundary is the width of near-boundary bands, where content of gallium reaches 85 wt.% (Figure 5, *a*). Gallium formed «islands» in the most thermodynamically beneficial places, such as clusters of eutectic mass of helium of high concentration (up to 97 wt.%) in corners of grains (spectrum 2, 4, Figure 5, *b*).

In Figure 6 the distinctions in dents of the indenter at constant minimal loading in indenting of aluminium alloy at the initial stage of diffusion are shown. It

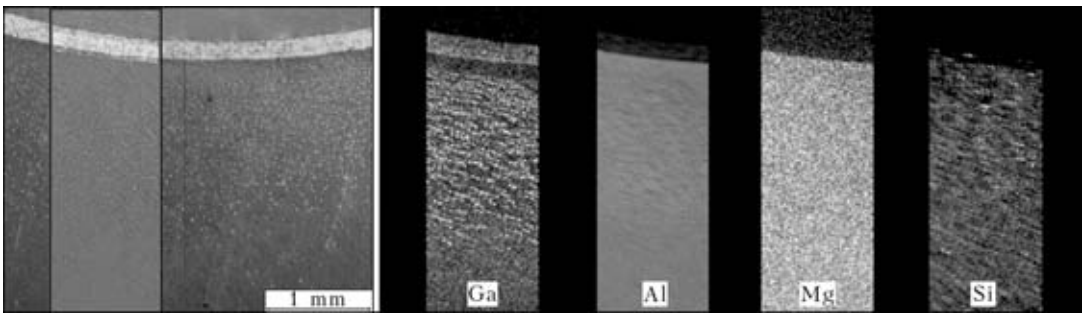

Figure 4. Map of distribution of elements in diffusion joining obtained by SEM

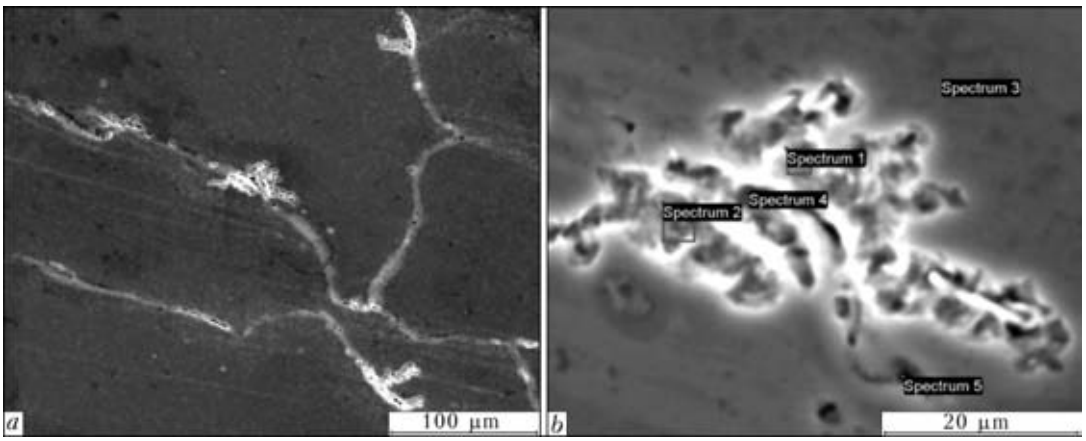

Figure 5. Pattern of intergranular clusters of eutectic mass of gallium in the aluminium alloy obtained by SEM (*a*, *b* see in the text)

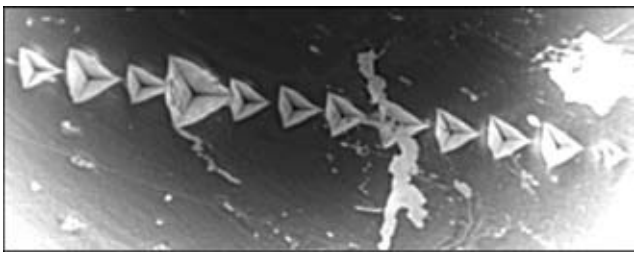

Figure 6. Dents (×600) of Berkovich indenter in the structure zones of aluminium alloy

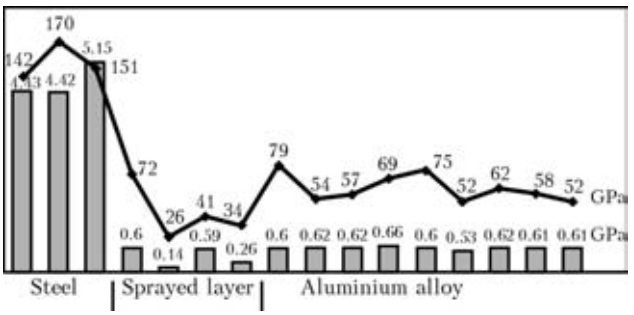

Figure 7. Diagrams of distribution of microhardness according to Meyer (*columns*) and elasticity modulus of Young (*curve*)

was produced at ultra-low (0.010–0.001 N) loading of indenter due to softening of material and impossibility of indenting at standard loading for aluminium (0.2 N) [12]. The large dents with separation of material are characteristic of intergranular boundary region filled with eutectic mass of gallium.

The jumpy change of microhardness and modulus of elasticity (Figure 7) characterizes the presence of meta-stable phases of gallium with magnesium and zinc [13–17]. The comparison of basic mechanical properties of materials being joined before the effect of gallium and properties of materials in the joint after diffusion shows the presence of general softening at the level of 10 %. At repeated heating of specimens the change in mechanical properties was not observed that proves the formation of solid solution Al_5Ga_2.

It follows from the above-described that the physical-chemical processes of interaction between the base metal (aluminium), components of aluminium alloy (magnesium and zinc) and gallium occur in the zone of formation of permanent joint. Gallium as activator of the surfaces being joined provided the removal of oxide layer at the surface (deoxidation). Its diffusion passed not only intergranually with an intensive growth of sizes of grains, but also volumetrically with a shifting of old boundaries of grains of aluminium and formation of new ones.

The distinctive feature of mass transfer of gallium in the aluminium is the formation of multistage transformation in a meta-stable phase with gallium. It resulted in formation of solid solution Al_5Ga_2 in the gap and adjacent volume of parts being joined.

1. Gab, I.I. (2008) Solid-phase brazing with pressure application. In: *Inorganic materials science*: Encyclopedia. Vol. 1, Book 2. Ed. by G.G. Gnesin, V.V. Skorokhod. Kiev: Naukova Dumka.
2. Ryabov, V.R., Ishchenko, A.Ya., Muravejnik, A.N. (1996) Current methods of welding of steel-aluminium pipes. *Avtomatich. Svarka*, **2**, 32–42.
3. *http://*en.wikipedia.org/wiki/Ga
4. Tikhomirova, O.I., Pikunov, M.V. (1969) Influence of shape and size of second component particles on properties of gallium solders. *Poroshk. Metallurgiya*, 84(**12**), 51–56.
5. *http://*www.crct.polymtl.ca/FACT/phase_diagram.php?file=Al-Ga. jpg&dir=SGTE
6. Mondolfo, L.F. (1979) *Structure and properties of aluminium alloys*. Moscow: Metallurgiya.
7. Kholyavko, V.V. (2006) *Formation of phase composition, structure and properties of quasi-crystalline alloys of Al–Cu–Fe system in reaction diffusion of gallium*: Syn. of Thesis for Cand. of Techn. Sci. Degree. Kiev.
8. Livanov, V.A. (1982) Action of gallium on aluminium and its alloys. *Tekhnologiya Lyog. Splavov*, **5**, 30–32.
9. *http://*ru.wikipedia.org/wiki/Effect_Rebindera
10. Likhtman, V.I., Shchukin, E.D., Rebinder, P.A. (1962) Physico-chemical mechanics of metals. In: *Adsorption phenomena in processes of deformation and fracture of metals*. Moscow: AN SSSR.
11. Ishchenko, A.Ya., Khokhlova, Yu.A. (2009) Evaluation of mechanical properties of microstructural constituents of welded joints. *The Paton Welding J.*, **1**, 34–37.
12. Khokhlova, Yu.A., Khokhlov, M.A. (2009) Nanoscale effect in diffusion joints with gallium. In: *Abstr. of Int. Conf. on Problems of Welding, Related Processes and Technologies* (Nikolaev, 14–17 Oct. 2009). Nikolaev: NUK, 111.
13. Larikov, L.N., Franchuk, V.I., Maksimenko, E.A. (1991) Substructural strengthening in aluminium and its alloys interacting with gallium. *Metallofizika*, 13(**10**), 3–10.
14. Larikov, L.N., Maksimenko, E.A., Franchuk, V.I. (1990) Structural changes in aluminium and its alloys during embrittlement by liquid gallium. *Ibid.*, 12(**1**), 115.
15. Franchuk, V.I., Larikov, L.N. (1992) Change of orientation of crystallites in near-surface layers of polycrystalline aluminium in diffusion interaction with gallium. *Izvestiya RAN. Metally*, **6**, 105–110.
16. Larikov, L.N., Prokopenko, G.I., Franchuk, V.I. et al. (1990) Study of embrittlement of aluminium and AMg6 alloy in interaction with liquid gallium by acoustic emission method. *Fiziko-Khimich. Mekhanika Materialov*, **3**, 5–9.
17. Larikov, L.N., Franchuk, V.I., Tikhonovich, V.V. et al. (1991) Diffusion-induced migration of grain boundaries in Al–Ga system. *Metallofizika*, 13(**8**), 56–62.

CONDITIONS FOR FORMATION OF DEFECT-FREE WELDS IN NARROW-GAP MAGNETICALLY CONTROLLED ARC WELDING OF LOW TITANIUM ALLOYS

V.Yu. BELOUS
E.O. Paton Electric Welding Institute, NASU, Kiev, Ukraine

Conditions providing defect-free welds on low titanium alloys by using narrow-gap magnetically controlled arc TIG welding were experimentally studied. The mechanisms causing deflection of the welding arc at different parameters of the welding process were established.

Keywords: *titanium alloys, TIG welding, tungsten electrode, magnetic control of the arc, deflection of the arc, weld metal*

Narrow-gap welding (NGW) by the TIG method is an efficient and cost-effective process for joining more than 16 mm thick titanium. It has certain technological advantages over the V- or U-groove welding processes, such as reduction of the weld and HAZ width, and decrease in amount of the deposited metal, which is especially important for welding titanium. In addition, NGW has labour engineering advantages as well, i.e. reduction of labour consumption in edge preparation and substantial increase in labour productivity [1]. As the major part of the heat energy of the free-burning arc is consumed for repeated penetration of the previous-pass weld metal, to successfully implement the process it is necessary to provide reliable melting of the side walls of the groove. This requires redistribution of the heat input into the welded joint, which can be achieved by mechanically moving the tungsten electrode and welding arc [2], or affecting the arc by an external controlling magnetic field [3].

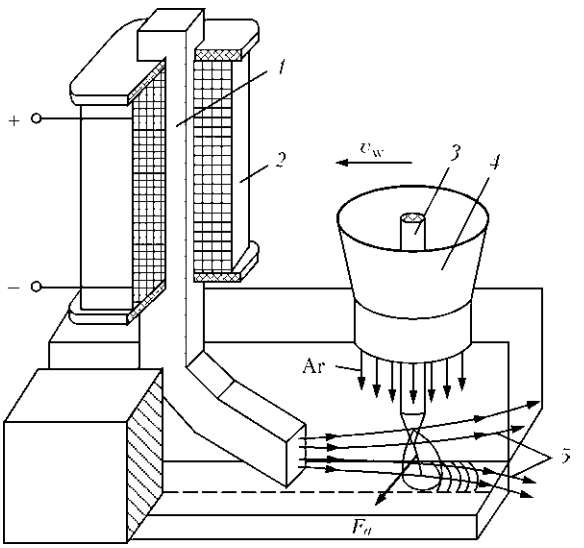

Figure 1. Flow diagram of NGW with controlling magnetic field: *1* — electromagnet core; *2* — electromagnet coil; *3* — tungsten electrode; *4* — protective nozzle; *5* — force lines of controlling magnetic field

Flow diagram of NGW of titanium by using the controlling magnetic field is shown in Figure 1. Welding was performed at a direct current of straight polarity with the tungsten electrode lowered into the groove, the protective nozzle being located over the weld edges. The magnetic field within the arc zone is formed by an electromagnet with a core. In welding it acts as a magnetic conductor, and is placed in the narrow groove. The electric current flowing through the electromagnet coil induces the magnetic field within the arc zone, the force lines of the field being oriented mostly along the welding direction (see Figure 1). This magnetic field is transverse with respect to the arc. Interaction of the magnetic field and arc current results in formation of Lorentz force F_a, which deflects the arc in a direction of action of this force. Alternate deflection of the welding arc to the side walls of the groove is caused by changes of polarity of the current flowing through the electromagnet coil.

Experimental investigation of the character of formation of the weld in NGW made it possible to establish the effect of such parameters of the controlling magnetic field as frequency of reversing and value of magnetic induction on the weld shape [4]. However, the quality of the welded joint produced by narrow-gap magnetically controlled arc TIG welding depends not only on the parameters of the controlling magnetic field, but also on welding current I_w, welding speed v_w, arc voltage U_a, and shape of the tungsten electrode tip. Therefore, to ensure conditions required for quality formation of the welded joint it is necessary to experimentally study the mechanisms causing deflection of the welding arc at changes of the welding conditions and magnetic field parameters.

The purpose of this study was to investigate conditions required for formation of defect-free welds on titanium at different welding and magnetic field parameters, as well as at different shapes of the tungsten electrode tip.

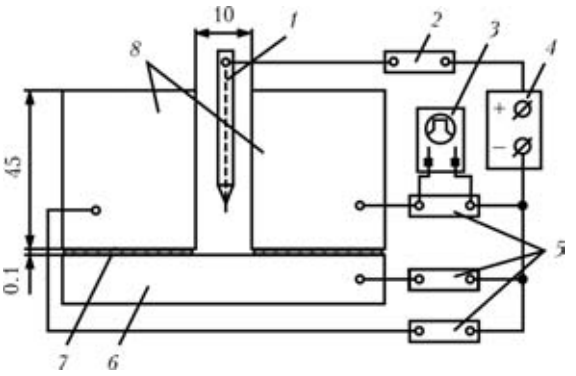

Figure 2. Scheme of the unit to measure the current flowing through the side walls of the groove in NGW with the controlling magnetic field: *1* — tungsten electrode; *2* — shunt to measure the welding current; *3* — oscillograph; *4* — power supply; *5* — shunts to measure the welding current flowing through the side and bottom walls; *6* — bottom wall of the groove; *8* — side walls

The method of measuring the electric current flowing through the side walls of the groove by the divided anode procedure was used to evaluate the character of the effect of welding conditions on deflection of the welding arc, and select the optimal welding parameters [5]. The scheme of the unit utilised to measure the current flowing through the side walls of the groove in NGW with the controlling magnetic field is shown in Figure 2. The degree of deflection of the welding arc was estimated from the value of the current flowing through the side wall of the groove by using parameter X:

$$X = \frac{I_s}{I_w},$$

where I_s is the current flowing through the side wall of the groove.

Tungsten electrodes used in the study had a cone-shaped tip, or a flat tip 2.5 mm wide. In welding they were located with their wide side across the weld axis.

Examinations of macrostructure of the welds made by NGW were performed to establish the required deflection of the welding arc. These examinations revealed a high probability of lacks of penetration at points of intersection of a vertical wall of the groove with a surface of the previous-pass weld (Figure 3). Lacks of penetration may form on one side (Figure 4, *a*) or on both sides of the groove (Figure 4, *b*), and may be either continuous or intermittent.

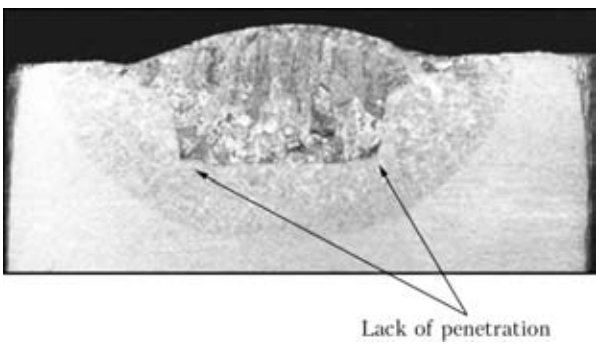

Figure 3. Macrosection of the deposited metal with lack of penetration at the groove corners (material — titanium alloy PT3V, filler wire VT1-00)

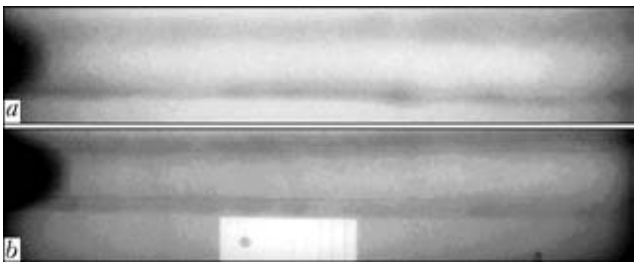

Figure 4. X-ray picture of welds with lacks of penetration at the groove corners (*a*, *b* see in the text)

Analysis of temperature conditions of the welding process showed that the difficulty of achieving the guaranteed penetration at the point of intersection of the groove wall with the surface of the previous-pass weld was caused by an intensive heat removal from the given region of the base metal during the welding process. It was determined that to achieve the guaranteed melting of the side wall of the groove at a point of its intersection with the surface of the previous-pass weld it is necessary to deflect the welding arc to such an angle, where the conditional centre of the anode spot, O, will coincide with the point of intersection of the side and bottom walls of the groove (Figure 5). In NGW, in a case where S_b is equal to S_s, the values of the current flowing through the side and bottom walls of the groove are equal, i.e. the

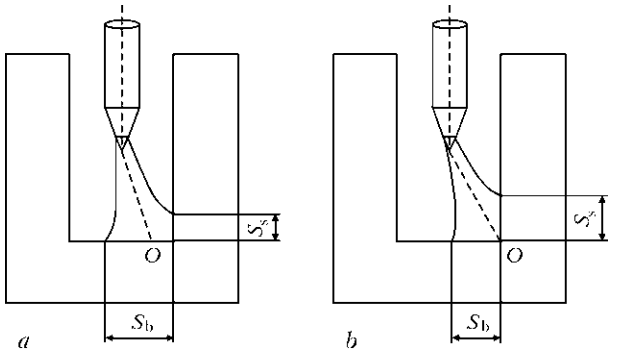

Figure 5. Schematic of location of the anode spot at insufficient (*a*) and optimal (*b*) deflection of the arc in the groove: S_b, S_s — distances from the centre to edge of the anode spot at the bottom and side walls, respectively

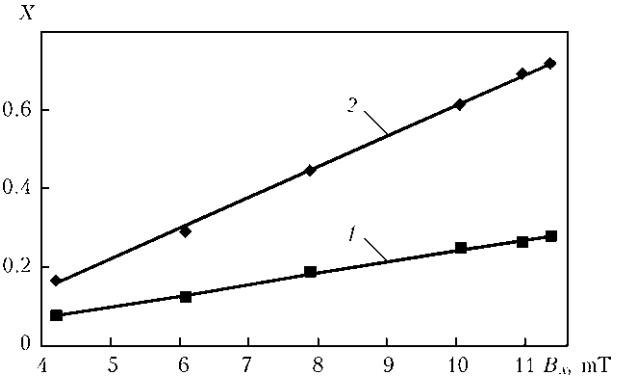

Figure 6. Dependence of the fraction of the current in a side wall of the groove on magnetic induction B_x when using tungsten electrodes with cone-shaped (*1*) and flat (*2*) tips (I_w = 400 A)

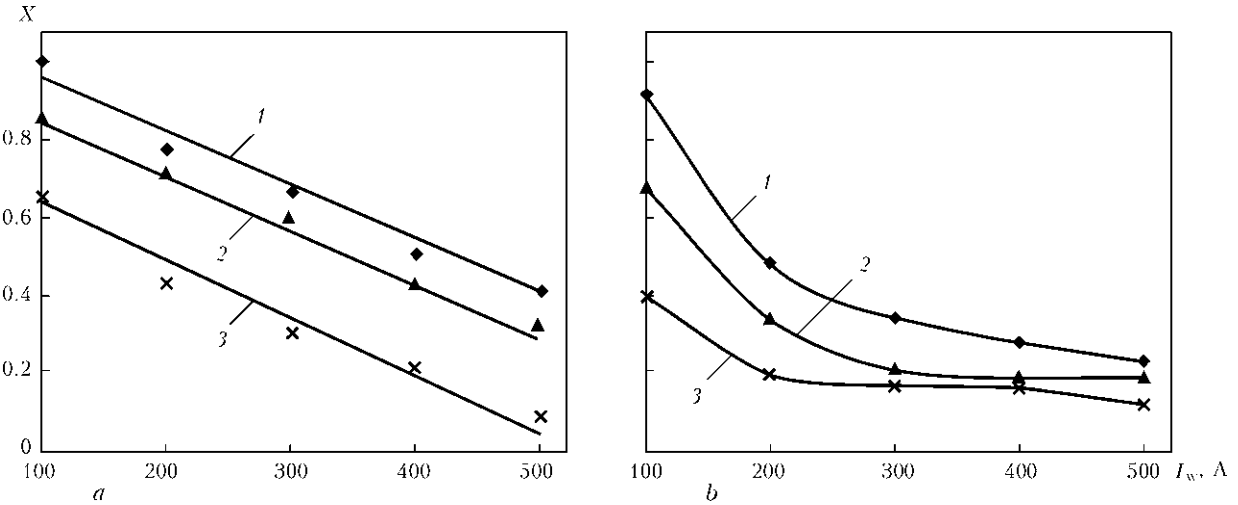

Figure 7. Dependence of the fraction of the current flowing through the side wall on the welding current when using electrodes with flat (*a*) and cone-shaped (*b*) tips: *1* — B_x = 11.4; *2* — 10.1; *3* — 6.1 mT

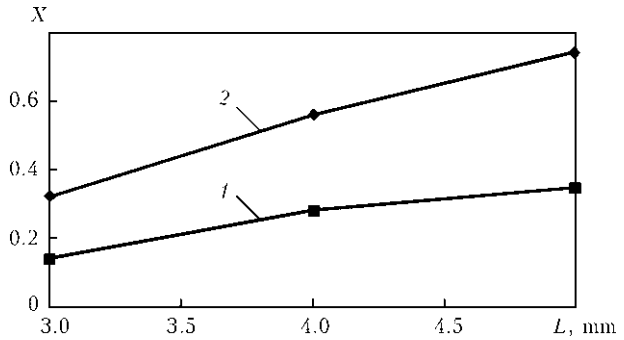

Figure 8. Dependence of the fraction of the current in a side wall of the groove on arc gap length L when using electrodes with cone-shaped (*1*) and flat (*2*) tips at B_x = 11.5 mT and I_w = 400 A

fraction of the current flowing though the side walls is 50 % of the total welding current.

As established by measurements of the current flowing through the side walls of the groove, its values are directly proportional to the values of a transverse component of magnetic induction in welding direction, B_x (Figure 6).

When using the electrode with a cone-shaped tip, the fraction of the current in the side walls is no more than 30 % of the welding current, which, based on the experimental data, is insufficient to melt the vertical walls of the groove and provide the quality formation of the weld.

To prevent lacks of penetration, the X ratio should be not less than 0.5, this corresponding to a location of the centre of the anode spot at a corner of the groove. This condition is met when using the electrodes with a flat tip. Other conditions being equal, the fracture of the current in the side walls decreases, i.e. displacement of the anode spot decreases, with increase in the welding current (Figure 7).

Increase in length of the arc gap leads to growth of the value of the current flowing through the side walls, i.e. deflection of the welding arc increases (Figure 8).

Therefore, as shown by the investigations conducted, it is necessary to form the magnetic field within the arc zone with an induction of not less than 8 mT at a welding current of 400 A and arc gap length of 4 mm to provide defect-free welds in NGW of low titanium alloys by using the controlling magnetic field. The results of examinations of macrostructure of the welds made on low titanium alloys at the above welding parameters proved the absence of lacks of penetration and lacks of fusion in the weld metal.

CONCLUSIONS

1. The mechanisms causing deflections of the welding arc in narrow-gap magnetically controlled arc TIG welding at changes of the welding and magnetic field parameters were experimentally studied. Conditions that provide the defect-free welds were optimised.

2. It was determined that narrow-gap magnetically controlled arc TIG welding requires the use of tungsten electrodes with a flat tip 2.5 mm wide.

3. It was established that deflection of the welding arc from the central plane of the groove is directly proportional to the value of a transverse component of induction of the magnetic field, B_x, and length of the arc gap, and is inversely proportional to the value of the welding current.

1. Malin, V. (1987) *Monograph on narrow-gap welding technology*: Welding research council bulletin. New York.
2. Hori, K., Haneda, M. (1999) Narrow-gap arc welding. *J. JWS*, **3**, 41–62.
3. Paton, B.E., Zamkov, V.N., Prilutsky, V.P. (1996) Narrow-groove welding proves its worth on thick titanium. *Welding J.*, **4**, 37–41.
4. Belous, V.Yu., Akhonin, S.V. (2007) Influence of controlling magnetic field parameters on weld formation in narrow-gap argon-arc welding of titanium alloys. *The Paton Welding J.*, **4**, 2–5.
5. Topolyansky, P.A., Khristofis, B.O., Ermakov, S.A. et al. (2004) Relation between effective power integral value of axisymmetric heat source on segment and function of radial density distribution of heat flow. In: *Proc. of 6th Int. Pract. Conf.-Exhibition on Technology of Repair, Restoration and Strengthening of Parts of Machines, Mechanisms, Equipment, Tools and Technological Fixture* (St.-Petersburg, 13–16 April, 2004). St.-Petersburg: SPbGPU, 3–9.

MONITORING OF CORROSION OF PIPELINES OF COOLING SYSTEM OF AUTOMOBILE GAS-FILLING COMPRESSOR STATIONS

S.A. OSADCHUK, O.V. KOTLYAR, L.I. NYRKOVA and **S.G. POLYAKOV**
E.O. Paton Electric Welding Institute, NASU, Kiev, Ukraine

Analysis of peculiarities of corrosion processes was made in carbon steel and its welded joints in cooling liquids of TOSOL type used in cooling systems of automobile gas-filling compressor stations (AGFCS). A method of monitoring the instant rate of corrosion in metal of pipes and welded joints in the cooling system at AGFCS, based on the method of polarization resistance, is offered. Sensors have been developed for estimation of corrosion rate in carbon steel and its welded joints in cooling liquid.

Keywords: *carbon steels, welded joints, automobile gas-filling compressor stations, cooling liquids, corrosion rate, method of mass measurement, method of polarization resistance, corrosion monitoring*

The present work is aimed at the investigation of a feasibility of continuous monitoring of kinetic change in corrosion rate of carbon steel and its welded joints in the cooling liquids (CL), being studied, using a method of polarization resistance.

As the practice shows, the CL becomes corrosion-active after one or two years of service due to oxidation of ethylene glycol, impurity wastes and contamination of CL itself with iron oxides. In this connection, the CL in cooling system of automobile gas-filling compressor stations (AGFCS) needs the periodic replacement or correction. Using sensors it is possible to define the time moment, when CL becomes corrosion-active with respect to pipe metal and its welded joints. Welded joints in cooling systems of AGFCS are subjected to the largest corrosion wear. Therefore, the analysis of specifics of corrosion processes was made on welded joints of carbon steel in CL of TOSOL type used in cooling systems of AGFCS. The effect of CL composition on kinetics of corrosion of carbon steel at room temperature was studied. The investigation of electrochemical characteristics of CL samples was carried out under laboratory conditions at room temperature. The methods of mass measurement, polarization resistance, polarization curves were used in the work.

It was established as a result of carried out investigations that the instant rate of corrosion of metal of pipes and their welded joints in the cooling system of AGFCS can be monitored during long time using the method of polarization resistance. The developed method allows determining the instant rate of corrosion of metal of pipes and their welded joints in the cooling system at AGFCS.

At present, the physical-chemical and protective properties of CL, used at AGFCS, are subjected to monitoring for compliance with requirements of GOST 28084–89 [1] by the following characteristics: appearance, density, temperature of crystallization beginning, hydrogen factor pH, alkalinity, corrosion effect on metals, including steel. Evaluation of corrosion effect on metals, envisaged by GOST 28084–89, is performed using the method of mass measurement, which is labor-consuming and long-time as the tests are performed during 336 h (14 days). Besides, the rates of corrosion, determined by the method of mass measurement, represent the integral characteristic averaged with time.

The following CL were selected for investigation: TOSOL (solution of ethylene glycol $HOCH_2CH_2OH$ with impurities in water), ethylene glycol ($HOCH_2CH_2OH$, molar mass of 62.07), propylene glycol ($CH_3CHOHCH_2OH$, molar mass of 76.09), and also standard media (3 % solution of NaCl and distilled water H_2O).

Physical-chemical and corrosion properties of CL were evaluated for compliance with requirements of

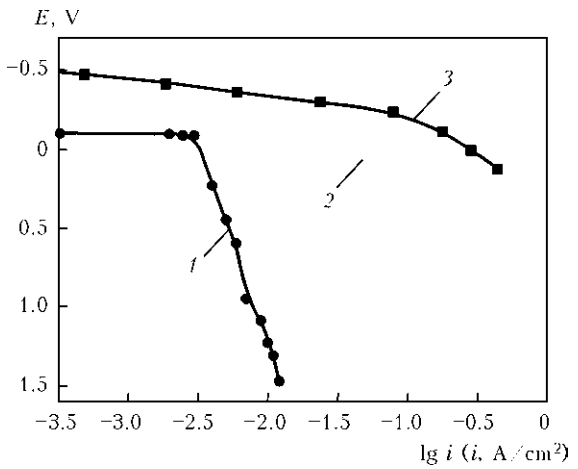

Figure 1. Anode polarization curves of carbon steel in different media: *1* — ethylene glycol in the 1:1 dilution with water; *2* — propylene glycol in the 1:1 dilution with water; *3* — 3 % solution of NaCl

Physical-chemical and protective properties of CL

Characteristic (parameter, property)	Standard acc. to GOST 28084–89		Test media				
				Ethylene glycol		Propylene glycol	
	CL-K	CL-40	TOSOL	Concentrated	In dilution with water (1:1)	Concentrated	In dilution with water (1:1)
Appearance	Transparent homogeneous liquid without mechanical inpurities						
Density, g/cm^3	1.100–1.150	1.065–1.085	1.056	1.114	1.075	1.036	1.036
Temperature of crystallization beginning, °C, not higher than	–35 in 1:1 dilution	–40	–40	–13	–38	–60	–36
Hydrogen factor (pH)	7.5–11.0	7.5–11.0	8.7	5.1	5.1	7.2	7.2
Alkalinity, cm^3, not less than	10	10	9.196	0.05	–	0.05	–
Corrosion effect on steel, g/(m^2·year), not more than	0.0041	0.0041	0.0008	0.00128	0.0056	0.00163	0.0048
Electric conductivity, S/m	–	–	0.2272	$8.364 \cdot 10^{-5}$	0.0845	$3.182 \cdot 10^{-5}$	0.073

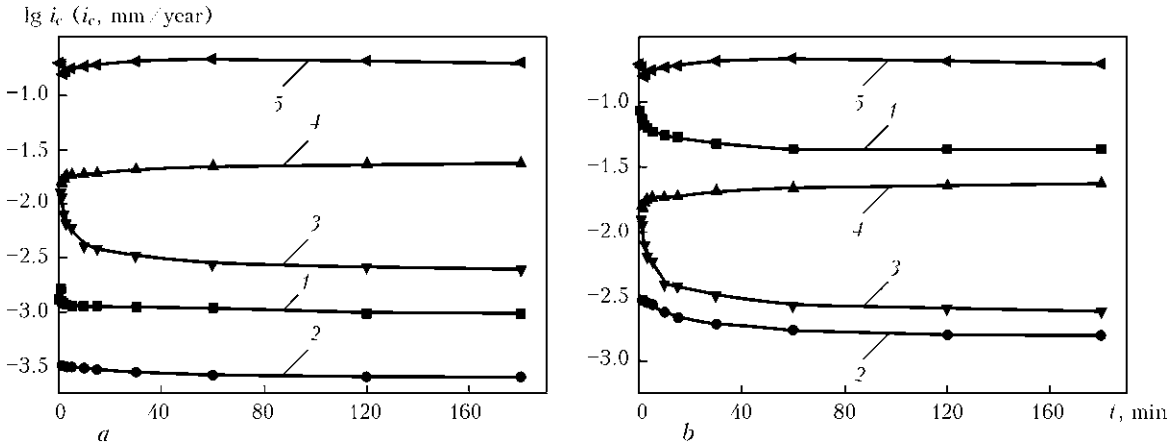

Figure 2. Kinetics of corrosion of carbon steel in concentrated (*a*) and diluted CL (*b*): *1* — ethylene glycol (1:1); *2* — propylene glycol (1:1); *3* — TOSOL; *4* — H_2O; *5* — 3 % solution of NaCl

GOST 28084–89. Results of tests of physical-chemical and protective properties of investigated CL and standard media are given in the Table.

Measurement of rates of carbon steel corrosion by the method of polarization resistance was made using the system of corrosion monitoring SKMT (TU V 33.2-01181535-014:2005) in CL, standard solution of 3 % sodium chloride and distilled water at room temperature. The rate of corrosion was calculated by formula

$$i_c = \frac{2B}{S}\frac{\Delta I}{\Delta E},$$

where B is the constant of medium, mm/(year·Ohm·cm^2); ΔI is the current, measured by the system of corrosion monitoring of SKMT type, A; S is the specimen surface area, cm^2; ΔE is the potential shifting per 10 mV.

From the data of work [2] the electrochemical processes in CL are proceeding under the conditions of passivation or diffusion control. The constant B was specified for CL and water neutral media.

CL of TOSOL type contains ethylene glycol, water and impurities, delaying the process of corrosion. To define the particular stage of monitoring the process of corrosion of steel in CL, the anode polarization curves were taken both in CL and in 3 % solution of NaCl (Figure 1). It follows after their analysis that potential of corrosion of carbon steel in CL is shifted to the region of more positive values as compared with

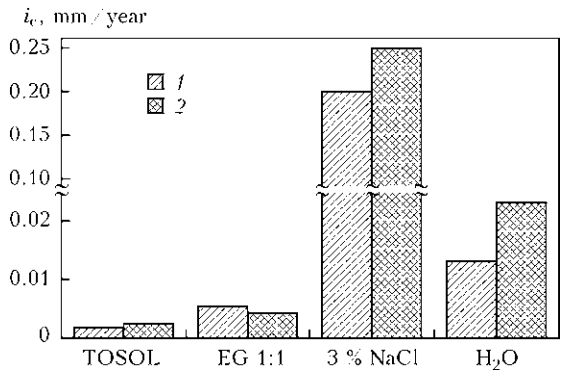

Figure 3. Diagrams of rates of corrosion of carbon steel in different media obtained by the method of mass measurement (*1*) and polarization resistance (*2*)

that in 3 % solution of NaCl. The path of curves proves the passivation of steel surface in CL as a result of delaying of anode processes, i.e. increase of slopes of anode polarization curves in propylene glycol and ethylene glycol as compared with 3 % solution of NaCl indicates the difficulty of anode reaction proceeding on the metal surface.

Kinetics of corrosion of carbon steel in concentrated and diluted CL, studied using the method of polarization resistance, is presented in Figure 2. It occurred that among the concentrated CL the TOSOL is the most aggressive for the carbon steel, and the propylene glycol is aggressive to the lowest degree. Ethylene glycol occupies the intermediate position. Results of measurement of corrosion rate in diluted CL have a good correlation with polarization curves given in Figure 1.

Ratio of rates of corrosion of carbon steels, obtained by the method of polarization resistance and method of mass measurement in different media, are given in Figure 3. It was established that the rates of corrosion, determined by the method of polarization in different media, coincide.

Thus, the application of method of polarization resistance for continuous monitoring the kinetics of changing the rate of corrosion of carbon steels and their welded joints is completely admissible.

1. *GOST 28084–89*: Cooling low-freezing liquids. General specifications. Introd. 01.07.90.
2. Chviruk, V.P., Polyakov, S.G., Gerasimenko, Yu.S. (2007) *Electrochemical monitoring of technogeneous media*. Kyiv: Akademperiodika.

DEVELOPMENT OF A PROCEDURE FOR SELECTION OF PARAMETERS OF STRIP ELECTRODE SURFACING WITH MECHANICAL FORCED TRANSFER OF LIQUID METAL

B.I. NOSOVSKY and **E.V. LAVROVA**
Priasovsky State Technical University, Mariupol, Ukraine

A procedure and equipment for investigation of the process of strip electrode melting by an arc and scheme of selection of surfacing parameter with forced transfer of electrode metal have been developed.

Keywords: *surfacing, power source, mechanical forced transfer, strip electrode, deposited layer, quality*

Surfacing with a strip electrode which distributes heat energy wider in comparison with wire one is used for obtaining a necessary chemical composition in the first deposited layer. As a result, depth of penetration and dilution of deposited metal with base metal are reduced. However, a capability of the arc to destroy interferences such as spatters and oxides on its way decreases with reduction of the penetration depth due to which local lacks of fusion are formed [1].

A character of electrode melting can be various. The electrode can be melted by a drop sequentially layer by layer (Figure 1, *a*) or chaotically (Figure 1, *b*). In this case, transfer of heat energy takes place non-uniformly that provides an increase of the possibility of lacks of fusion formation. Quality of a welded joint can be influenced by the character of movement of arc and liquid metal drop. Forced transfer of electrode metal can stabilize the process of electrode melting.

Different methods of forced transfer of electrode metal were studied. Studies [2–5] determined that the forced transfer of electrode metal in wire electrode welding reduces electrode metal loss for spattering, improves conditions of arc process excitation and stabilizes current and voltage.

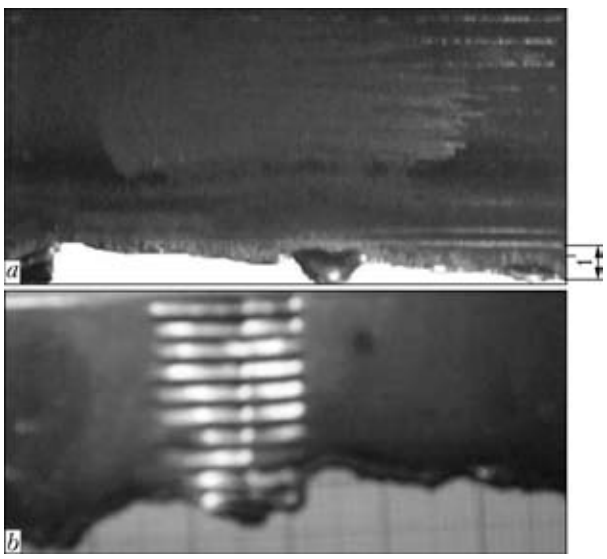

Figure 1. Appearance of the strip electrode tip melted by a drop in turn layer by layer (*a*) and chaotically (*b*)

However, existing methods of forced transfer relate only to wire electrode welding (surfacing). Data on influence of forced transfer on quality of a bead deposited by submerged arc method using strip electrode are absent. Therefore, development of a mechanism for transformation of transverse oscillations of a tip of strip electrode to longitudinal ones and investigation of influence of the oscillation parameters on the process of electrode meting and quality of deposited metal are seemed to be reasonable.

The aim of the present study is development of a procedure and equipment for determining the character of arc movement along the tip of strip electrode in submerged arc surfacing using strip electrode with mechanical forced transfer of liquid metal.

A device for mechanical forced transfer of electrode metal in submerged arc surfacing using strip electrode (Figure 2) was designed. A mechanism of transformation is situated close to the arc during automatic surfacing that reduces weight of the strip electrode performing reciprocating motions. This allows making the mechanism of transformation of transverse oscillations to longitudinal more simple. A principle of operation of presented mechanism lies in the following: shaft *7* is run by a drive; transverse movements of a strip electrode being transformed into longitudinal oscillations of its end take place due to reciprocating movement of the middle part of shaft-eccentric *9* and plates set with a gap along which the strip electrode is moved.

Proposed mechanism can be used for strips of solid section, the flux-cored electrodes cannot sustain multiple bends and vibrations since this result in uncontrolled charge spillage.

It is necessary to know the character of arc movement along the electrode tip for determining the level of influence of forced transfer on heat distribution across the width of the strip electrode.

The following methods for investigation of character of arc movement along the tip of strip electrode

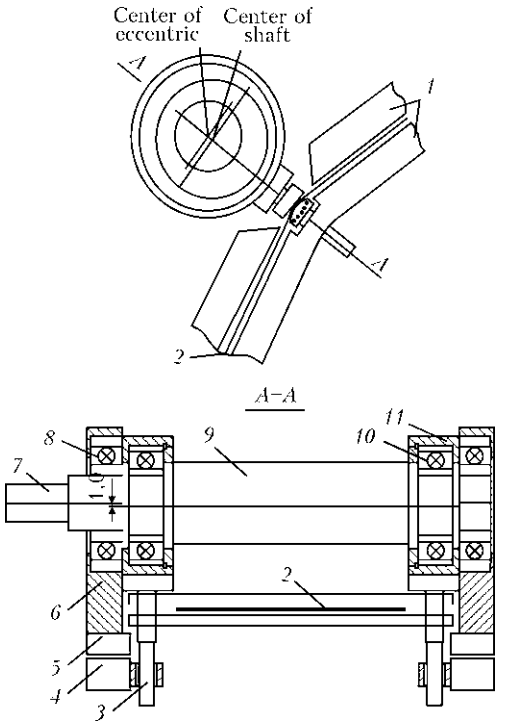

Figure 2. Scheme of transformation of transverse to longitudinal oscillations of the strip electrode tip: *1* — bent base; *2* — strip electrode; *3* — guide bolt; *4*, *5* — plate bodies; *6*, *11* — bearing bodies; *7* — shaft; *8* — shaft bearing; *9* — middle part of shaft-eccentric; *10* — eccentric bearing

are known: high-speed filming and measurement of distribution of current lines across the width of the strip electrode [1]. The letter is the most available. An attachment was developed using which a place of arcing on the tip of strip electrode (contacts) was simulated.

It is well-known [1] that arc place can be determined using the contacts situated across the width of the strip electrode. The sensors (Figure 3) were developed for control of voltage drop due current with oscillations of the tip of strip electrode and without them. A device was designed in which nine pairs of contacts (see Figure 3) are situated across the width of the strip electrode.

Strip electrodes 0.3 and 0.5 mm thick from 08A and 10Kh18N10T surfacing strips were used for practicing the procedure of performance of experimental investigations.

Arc position was simulated using the contact pressed to the tip of strip electrode. Possibility of

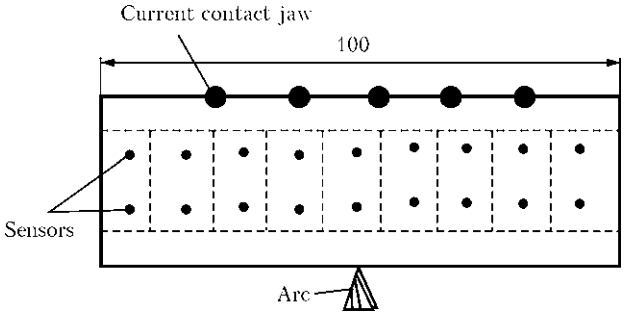

Figure 3. Scheme of position of sliding contacts (sensors) at extension of the strip electrode

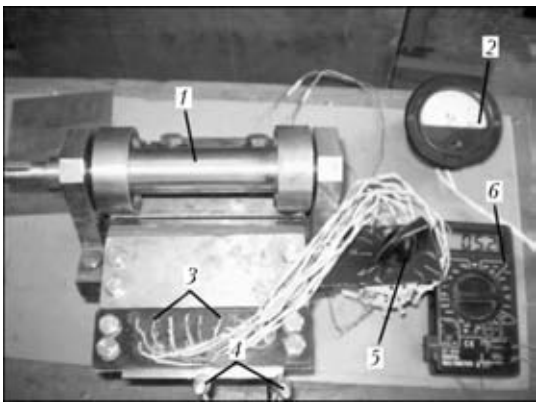

Figure 4. Appearance of device for transformation of transverse oscillations to longitudinal ones, and position of sensors of current distribution across the width of strip electrode: *1* — eccentric mechanism; *2* — ammeter; *3* — sensor of current reading; *4* — arc simulating contacts; *5* — switcher; *6* — millivoltmeter

switching-on of five sliding current contact jaws (one or combination of several) is provided for in design.

Movement of arc along the tip of strip electrode was simulated by changing contact position.

Figure 4 shows an appearance of the device for transformation of transverse oscillation to longitudinal and position of sensors for current distribution across the width of the strip electrode.

Power source with smooth regulation of voltage was used. It is three-phase autotransformer, reducing isolating transformer, to output of which a three-phase bridge rectifier is connected providing minimum pulsing of rectified voltage. Current was measured using ammeter *2* with shunt, switcher *5* switched sensors *3* by pair. Voltage drop on each sensor was measured with the help of millivoltmeter *6*.

Place for grounding must be selected for secure operation of analog-to-digital converter (ADC). For that, the current contact jaws or medium contact of low series of the sensors were grounded. Measurement results are given in Figure 5. Influence on voltage drop is insignificant in grounding of medium contact of low series of the sensors. Therefore, in future the measurements were carried out with grounded low contact of the medium sensor.

Arc (contact) position and place of current contact jaw were changed for practicing measurement proce-

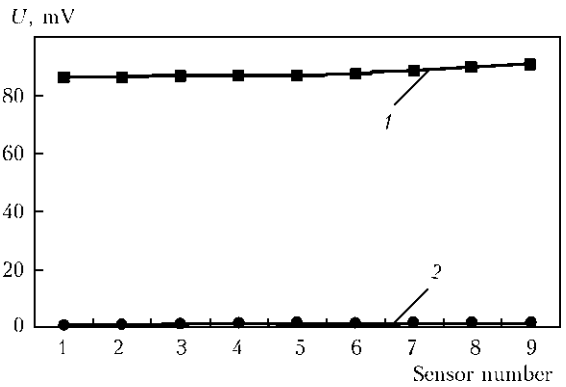

Figure 5. Dependence of voltage drop on a place of grounding: *1* — current contact jaw; *2* — middle contact of low series of the sensors

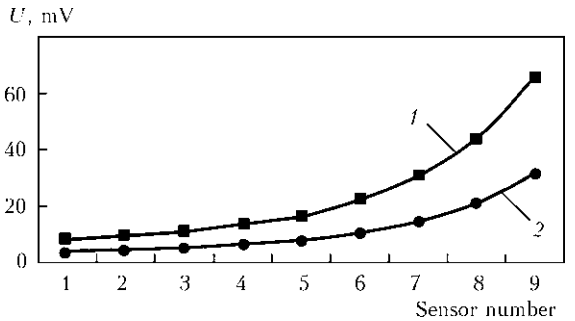

Figure 6. Dependence of voltage drop across the width of strip electrode 0.2 mm thick from 10Kh18N10T steel for different current values: *1* — 40; *2* — 20 A

dure. Measurement results are shown in Figures 6–10. As can be seen from Figure 6, the maximum of voltage drop distribution across the width of the strip electrode is situated over the contact simulating arc position at switching-on of all current contact jaws and arc position on the right end of the electrode.

Results of measurement for 0.5 mm thick strip are shown in Figure 7. Useful signal is significantly higher applying 10Kh18N10T steel in comparison with Sv-08A surfacing material. It can be seen from Figure 8 that the position as well as number of connected current contact jaws make no significant influence on character of current distribution. Experiment results, shown in Figure 9, indicate that the arc movement along the tip of strip electrode corresponds with the movement of current maximum. It is observed that the character of curves is similar using strip electrode from 10Kh18N10T and 08A, but voltage drop is significantly lower applying 08A since specific resistance of 10Kh18N10T steel is higher than that of 08A steel.

Changing of voltage drop at two contacts connected in the center and on the right end of the electrode was investigated for determining influence of shunt current or two simultaneously existing arcs. As can be seen from Figure 10, curve has two maximums at two existing arcs (contacts). A value of useful signal is higher using 10Kh18N10T material than using 08A steel.

ADC (E14-140) having 16 differential inputs or 32 inputs with common grounding is used for measurement of the parameters (Figure 11). There are 9

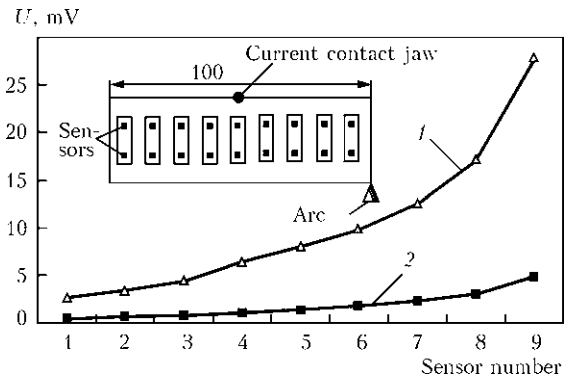

Figure 7. Dependence of voltage drop for 40 A current across the width of strip electrode 0.5 mm thick for various materials: *1* — 10Kh18N10T; *2* — 08A steel

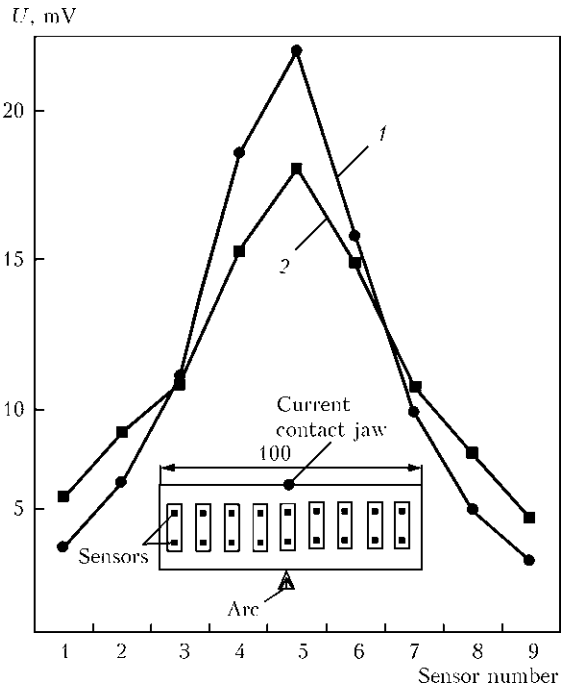

Figure 8. Dependence of voltage drop for 40 A current across the width of strip electrode 0.5 mm thick from 10Kh18N10T steel for different positions of current contact jaw: *1* — central current contact jaw is switched on; *2* — all five current contact jaw are switched on

differential sensors (Figure 11), therefore, a scheme of connection of differential inputs was used.

Shunt for 1000 A, 75 mV can be used for recording the value of arc current besides sensors of distribution of voltage drop across the width of the strip electrode. A voltage divider, parameters of which are taken in

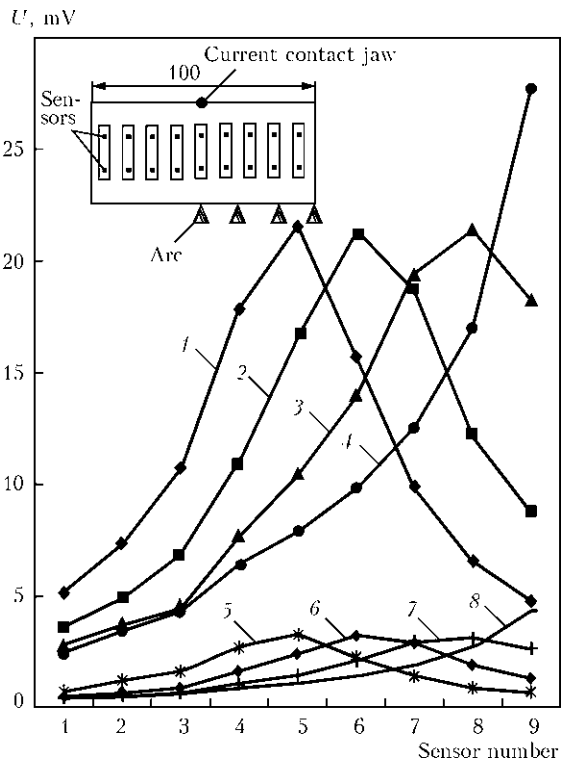

Figure 9. Distribution of voltage drop for 40 A current across the width of strip electrode 0.5 mm thick for different positions of current contact jaw: *1–4* — 10Kh18N10T; *5–8* — Sv-08A steel

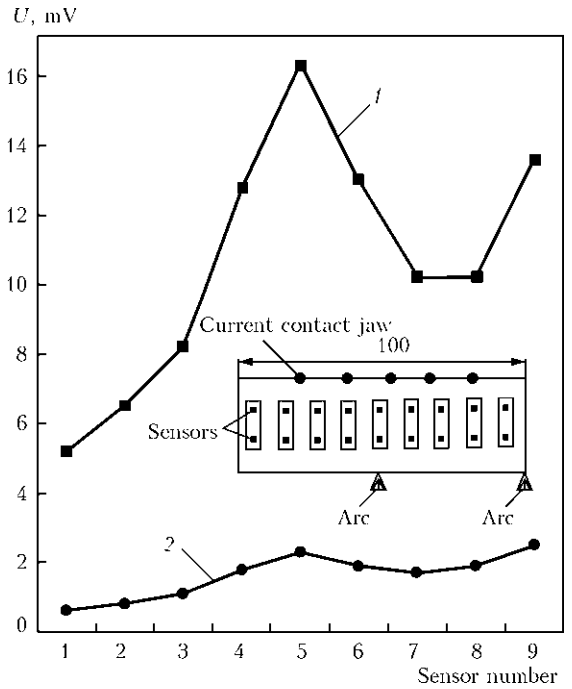

Figure 10. Distribution of voltage drop across the width of strip electrode for two arcs: *1* — 10Kh18N10T; *2* — 08A steel

account, is used for voltage measurement. Voltage drop at the electrode extension and shunt are close and arc voltage is significantly higher that is considered during programming of the device on PC.

CONCLUSIONS

1. The procedure was developed for measurement of distribution of current lines across the width of the strip electrode. It allows determining character of arc movement along the tip of strip electrode in submerged-arc strip-electrode surfacing with mechanical forced transfer of liquid metal.

2. Voltage drop distribution across the width of the strip electrode is shown.

3. Influence of the material and current on the value of useful signal was determined. It should be

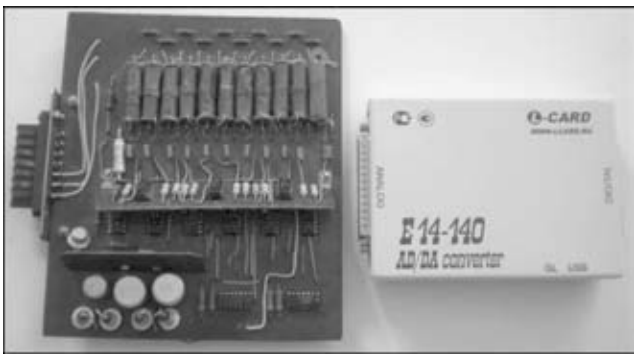

Figure 11. Device for data reading

taken into account during processing of measurement results.

4. It is determined that grounding of current contact jaw and movable contacts has significant influence on the value of useful signal. The middle contact in lower series of the sensors should be grounded for increase of measurement sensitivity and accuracy.

5. Distribution of voltage drop has two maximums at existence of two simultaneous arcs.

6. It is proved that the position of maximum of voltage drop matches with arc position at the tip of strip electrode. Consequently, the arc movement along the tip of strip electrode can be recorded using developed devices and ADC.

1. Gulakov, S.V., Matvienko, V.N., Nosovsky, B.I. (2006) *Submerged-arc surfacing with strip electrode*. Mariupol: PGTU.
2. Lebedev, V.A. (2003) Special features of designing mechanisms of pulsed feed of electrode wire in welding equipment. *The Paton Welding J.*, **3**, 39–43.
3. Lebedev, V.A. (2010) Tendencies in development of mechanized welding with controlled transfer of electrode metal (Review). *Ibid.*, **10**, 37–44.
4. Voropaj, N.N., Benidze, Z.D. (1989) Specifics of CO_2 welding process with pulsed feed of electrode wire. *Avtomatich. Svarka*, **2**, 23.
5. Nosovsky, M.B. *Metal arc welding*. Pat. 24440 Ukraine. Int. Cl. 7 B 23 K 9/12, C2.

CONTROL OF ARC IGNITION DURING EXCITATION OF ELECTROSLAG PROCESS

Yu.N. LANKIN, A.A. MOSKALENKO, V.G. TYUKALOV and **V.F. SEMIKIN**
E.O. Paton Electric Welding Institute, NASU, Kiev, Ukraine

Control of the electric arc ignition process for inducing the slag pool for ESW is described. Algorithm of contact ignition of the arc from the first touch of a workpiece by wire electrode is given. The sharpened electrode tip and feeding of voltage from the power source to the fixed-electrode short-circuited to the workpiece are decisive conditions for reliable ignition of the arc. To transfer to the steady-state process, the electrode feed should be switched on with a lag after the arc ignition. Experimental data on the arc ignition are given.

Keywords: *electroslag welding, ignition of welding arc, induction of slag pool, ignition control*

A slag pool of molten flux is necessary for beginning of the electroslag process. It can be obtained (induced) by several methods. The slag is preliminary melted in auxiliary crucible and then poured in a gap between the edges being welded [1] or a solid state conducting flux is used [2] during electroslag welding (ESW) with large section electrodes. The slag pool in most cases is induced with the help of arc in wire electrode welding. Arc ignition can be contact-free using high-voltage high-frequency generators [3, 4], but mostly it is performed with the help of contact methods. A layer of metal powder or chips of 10–12 mm thickness and then a flux layer 3–5 mm thick [5] are put into a welding zone for making arc ignition easier. A method based on break of live contact between the electrode and workpiece being welded [6, 7] became the most widespread for shielded-gas consumable electrode arc welding or submerged arc welding.

A range of papers, for example [8–11], is devoted to the theoretical issues of contact ignition of the arc. Based on them, the process of contact ignition of the arc can be shown in the following way. Short-circuit welding current (SC) starts flowing through the electrode during contact of the electrode tip with metal being welded. Heat of the electrode making it heated is released as a result of current flowing. The largest amount of heat is released in the high-resistance zones: in electrode–workpiece and electrode–current-conducting tip contacts.

If the contact resistances are relatively low than the electrode is heated up to the melting temperature closer to the middle of its extension due to intensive heat removing in the contact zones. After that the diameter of formed liquid bridge begins to reduce under the effect of surface tension forces and electromagnetic forces induced by flowing current. The bridge metal overheats up to evaporation and explodes. Significant part of the electrode, collapsed due to intensive heating, is removed out of the welding zone by explosion. The arc is not ignited due to large gap formed between the electrode. As a result of electrode feed the SC of arc gap is occured again but already with new temperature distribution along the electrode length. Initial temperature of the electrode tip will be every time higher due to heating at previous touch during repeated and following touches of the electrode to workpiece being welded. Electrode melting and bridge explosion will take place close to the electrode–workpiece contact after several SC. The electric arc is ignited [8] since formed ionized gap is sufficiently small. The SC for such a process of arc ignition is characterized by significant duration (Figure 1). Electrode wire of 3 mm diameter (feed rate of 42 m/h) and AN-8 flux were used in experiments.

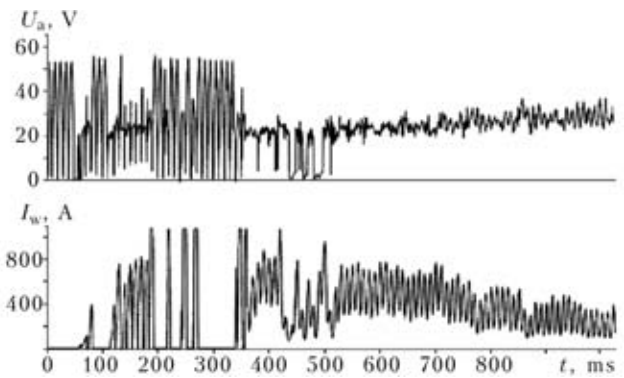

Figure 1. Process of arc ignition at relatively high electrode–workpiece contact resistance

A zone of electrode with workpiece contact appears to be the most heated at large electrode–workpiece contact resistance. Electrode melting and explosion of the liquid bridge take place exactly in this zone. The arc is ignited in a gap (electrode–workpiece) filled with ionized gas formed after the bridge explosion, i.e. the process of arc ignition occurs after the first touch of the workpiece by electrode.

Thus, a decisive condition of reliable ignition of the electrode from the first touch is increased resistance of the electric circuit in electrode tip–welded workpiece area and minimum resistance of the electrode–current-conducting tip contact.

A cross-section area of current conductor in the contact area is reduced in that or another way in order to increase the contact resistance of electrode–workpiece. Mentioned above metal chips or powder, electrode-welded metal plate of smaller cross-section than in electrode [7], vibrations of the electrode tip in the direction normal to its axis [12, 13] or sharpened electrode tip can be used for that. The latter can be obtained through reducing a size of drop remaining on the electrode tip using special algorithms for finishing of process of welding or snapping off the electrode tip with cutters better at acute angle to the axis. This method is the most simple and effective as experience shows.

The results of computer modeling of heating for sharpened and obtuse electrode tip at SC are given in study [11]. Heating conditions for these two cases have significant differences. Temperature maximum for the sharpened electrode is situated in the area very close to the tip. At the same time, the rest of the electrode is at room temperature. The area heated up to melting temperature in flat end electrode takes more extended area and situated at significant distance from the electrode tip.

If possible a form of the electrode should remain constant during the whole heating period for using advantages of the sharpened electrode to maximum. For that, initial rate of electrode feed up to arc ignition is set lower working one [6]. Otherwise, the area of electrode to workpiece contact is increased due to electrode feed at heating of sharpened electrode tip during SC up to ductility temperature and heat emission in this area is reduced. The best result is achieved at complete stopping of electrode feed for the period of arc ignition as this was done in work [14]. Process of submerged arc ignition at zero rate of electrode feed is given in Figure 2. A feed drive after touch of the welded workpiece by sharpened tip of the electrode is stopped, flux is put and welding power source is switched on. As can be seen from Figure 2, the process

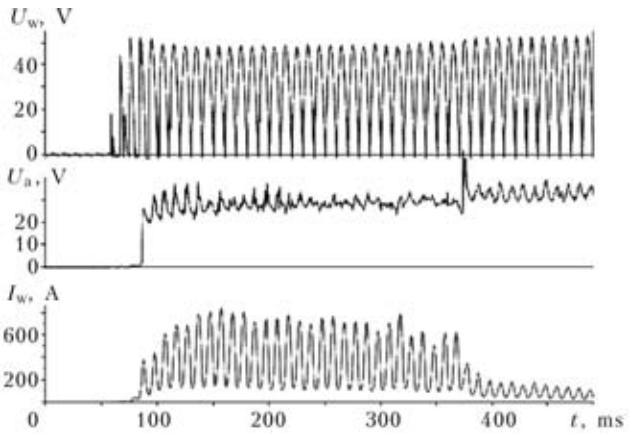

Figure 2. Electric arc ignition at zero rate of feed of sharpened tip electrode: U_w — voltage of welding source

of arc ignition is very flexible — SC current lower than 300 A, and duration is less than three half-circuits of supply-line voltage. Electrode melting by electric arc and discharge of formed drop result in increase of the arc gap up to threshold value of arcing at given voltage of power source and resultant arc extinction. The arc extinction takes place at 5 mm arc length for process parameters given in Figure 2. Duration of this process makes 350–600 ms. Therefore, electrode feed can be switched on after 150–250 ms for setting stable arc process. Further, the arcing stability depends only on parameters of power source, electrode feed rate and shielding medium, etc.

A sensor for the short-circuiting of electrode to workpiece and controller of driving of electrode feed motor and switching of welding power source were developed for automation of the algorithm of arc ignition mentioned above. The SC sensor is a low-voltage self-regulating voltage source with high internal resistance connected to the electrode in parallel to the welding power source.

A system of arc ignition is operated in the following way. START instruction switches on probing voltage of the SC sensor and electrode feed motor at low speed. Electrode voltage (Figure 3, *a*) sharply decreases at

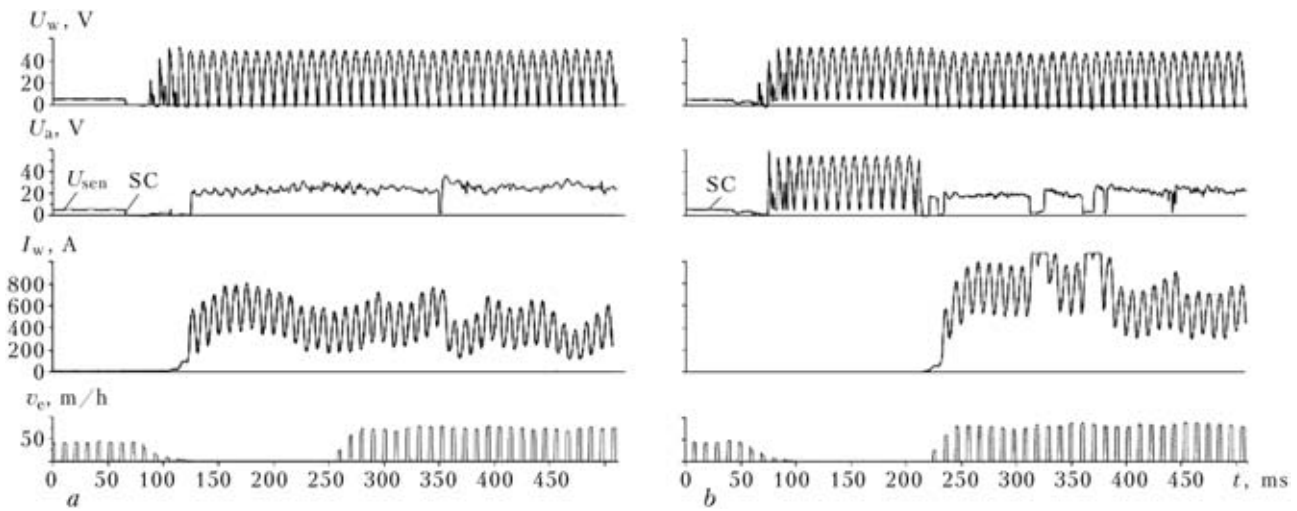

Figure 3. Automatic control of ignition of submerged arc using the electrode to workpiece touch sensor: *a* — ideal process of ignition; *b* — lag of arc ignition due to the flux film between the electrode tip and surface of workpiece being welded

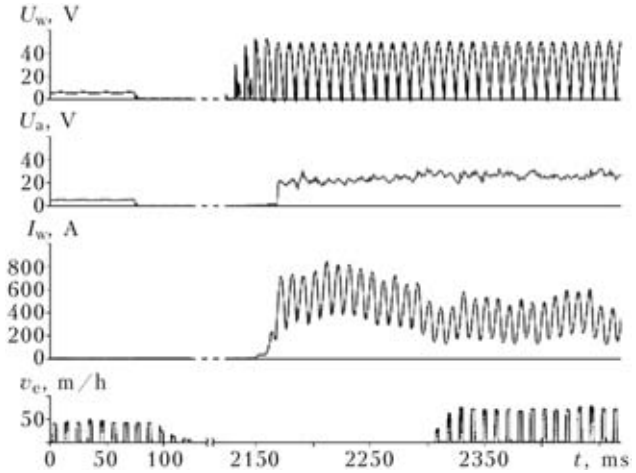

Figure 4. Automatic control of arc ignition at the flux filling after stop of electrode feed by touch sensor command

electrode SC to the workpiece. This signal stops the motor, welding power source is switched on and after around 200 ms of time lag the electrode feed motor is switched on again but already at working speed.

Unfortunately, the arc ignition occurs not as smooth as shown in Figure 3, *a* with flux preliminary filled in the welding zone. Sometimes, ultra thin flux film is formed between the electrode tip and surface of workpiece being welded. It makes worse a signal of the SC sensor and conditions of arc ignition (Figure 3, *b*) due to own low conductance. In this case the sensor acted accurately but arc was ignited not at once after welding source switching on but at significant lag. In principle, a situation is possible when the sensor can fail and motor does not stop or arc not ignite because of too low SC current (mainly it concerns only to ESW of vertical welds) due to high resistance of the flux film. Possibility of such a situation is significantly reduced in the process of relative movement of welding head and workpiece being welded during submerged arc welding.

Unreliable starting SC is eliminated when the flux filling is carried out after the SC sensor triggering (Figure 4). A difference from the processes, given in Figure 3, lies in significant increase of operation reliability of the SC sensor since its data are not influenced by the flux film on the surface of workpiece being welded. The peculiarity of the process is that the arc ignition current appears to be lower than the welding one. This is result of sharpened electrode tip. Besides, some current increase relative to its steady-state value is observed just after arc ignition. It seems that the relatively low resistance of still cold electrode extension and reduced arc voltage drop due to its small length provoked this.

Thus, ignition of the arc from the first touch of the workpiece by wire electrode for inducting the slag pool for ESW takes place in fulfillment of the following conditions:

- sharpened electrode tip;
- reliable contact of the electrode with current-conducting nozzle;
- stop of electrode feed after its short-circuited to the workpiece being welded;
- flux filling after electrode short-circuited to the workpiece;
- switching of power source only after this;
- electrode feed is switched on with 100–200 ms lag after power source switching to transfer to the steady-state process.

The SC sensor and controller of driving of the electrode feed motor and welding power source were developed for automation of performance of given algorithm.

1. Paton, B.E., Medovar, B.I., Safonnikov, A.N. et al. (1972) New method of electroslag welding. *Svarochn. Proizvodstvo*, **7**, 16–17.
2. (1980) *Electroslag welding and cladding*. Ed. by B.E. Paton. Moscow: Mashinostroenie.
3. Kavcic, A. (1987) Vzig obloka pri varjenju pod praskom. *Varilna Tehn.*, **3,** 61–62.
4. Striz, D., Kucek, L. (1989) Zapal'ovanie obluka pri zvarani pod tavivom. *Zvaranie*, **3**, 92–93.
5. Sushchuk-Slyusarenko, I.I., Lychko, I.I. (1974) *Electroslag welding technique*. Kiev: Naukova Dumka.
6. Lenivkin, V.A., Klenov, G.G., Sagirov, Kh.N. et al. (1986) Arc ignition in arc metal electrode (Review). *Avtomatich. Svarka*, **2**, 30–34.
7. Morozkin, I.S. (2003) *Arc ignition control in mechanized processes of welding*. Rostov-na-Donu: Rostov GUPS.
8. Lenivkin, V.A., Sagirov, Kh.N., Doktorsky, R.Ya. (1982) Establishment (excitation) of the arc metal welding. *Svarochn. Proizvodstvo*, **8**, 9–11.
9. Ersoy, U., Hu, S.J., Kannatey, E. (2008) Observation of arc instability and spatter generation in GMAW. *Welding J.*, **2**, 51–56.
10. Zhu, P., Rados, M., Simpson, S.W. (1977) Theoretical prediction of the start-up phase in GMA welding. *Ibid.*, **7**, 269–274.
11. Farson, D., Courardy, C., Talkington, J. et al. (1998) Arc initiation in gas metal arc welding. *Ibid.*, **8**, 315–321.
12. Paton, B.E., Chvertko, A.I., Ivanov, G.P. et al. *Device for automatic arc ignition in electric arc metal welding*. USSR author's cert. 408729. Int. Cl. B 23 K 9/6. Appl. 11.10.71. Publ. 1973.
13. Chvertko, A.I., Ivanov, G.P., Porkhun, B.V. (1973) New method of arc ignition in submerged-arc welding. *Avtomatich. Svarka*, **4**, 44–45.
14. Dilthey, U., Eichhorn, F., Groten, G. et al. (1990) Low-spatter ignition of the mig-welding arc. *IIW Doc. XII-1181–90*.

EVALUATION OF STABILITY OF THE FLASHING PROCESS IN FLASH BUTT WELDING

I.O. SKACHKOV and **E.P. CHVERTKO**
NTUU «Kiev Polytechnic Institute», Kiev, Ukraine

Procedure was developed for monitoring the process of continuous flash butt welding. The feasibility of using neural networks for evaluation of stability of the welding process was established.

Keywords: *flash butt welding, continuous flashing, process stability, defects in joints, deviation of process parameters, monitoring of quality, neuron networks*

Non-destructive testing of welded joints in flash butt welding does not always allow a reliable detection of defects. Given that properties of the welded joints directly depend on the welding process parameters, stability of the latter is often determined by the presence of their deviation from the specified values.

Normally, the satisfactory quality of the welded joints in continuous flash butt welding is achieved by providing the optimal temperature distributions in the near-contact zone over the entire cross section area prior to upsetting, as well as the upsetting value and speed. As in a number of cases the above characteristics are very difficult or impossible to measure directly, the measurements are carried out on other parameters that affect heating of workpieces, such as welding voltage, speed of feeding of workpieces, etc. Consistent values of the above indicators provide the optimal heating of workpieces and, as a result, quality of the joints. In this case, the maximum permissible deviation of open-circuit voltage from the specified value is 10 %, that of the speed of feeding of workpieces is 20 %, and deviations of the values of workpiece extension should not exceed 5 % [1]. This approach allows fixing the deviations of each of the above parameters separately, but it gives no idea of their total effect on the process stability.

The information required for evaluation of the quality of a welded joint can be obtained from the results of analysis of basic physical parameters of the welding process, the electric parameters in particular [1–3]. In continuous flash butt welding the process of formation of liquid bridges, their heating, destruction and formation of the new ones can be described by the probability methods. The course of this process is determined by instantaneous values of the welding parameters (both electric and mechanical), as well as by different kinds of random disturbances, including the technological ones, related to preparation of workpieces for welding and their arrangement in clamps of the welding machine. Effect of the disturbances on the course of the process is most often characterised by deviation of the basic process parameters from the specified values, i.e. the change of voltage during the flashing process is of a probability character, while the secondary voltage itself is one of the welding process parameters that is most sensitive to disturbances.

As preconditions that determine deterioration of quality indicators of the joints may form at all stages of the welding process, one of the variants of evaluation of the quality can be analysis of voltage oscillograms and their division into groups corresponding to deviations of the basic parameters. Therefore, the task of monitoring of the quality is reduced to the task of classification.

A procedure was developed for monitoring of the continuous flash butt welding process to reveal deviations of welding voltage in real time. Experiments on continuous flash butt welding of 14 mm diameter reinforcing rods of class A400S were conducted by using machine MSO-606 with a positive electromechanical flashing drive without feedbacks. Voltage in the secondary circuit of the machine was registered by using analogue-digital converter E-140 (L-Card, Russia).

The optimal conditions, as well as three cases of deviation of the process parameters deteriorating quality characteristics of the joints, which most often occur during welding, such as decrease in workpiece feed speed v, decrease in machine open-circuit voltage $U_{o.-c}$, and change in workpiece extension l, were evaluated.

Deviations of the process parameters were caused by inducing disturbances that exceeded those permitted by the quality assurance conditions. The joints produced as a result of the experiments differed in the heating zone and presence of defects, such as discontinuities (Figure 1). It can be seen from oscillograms of the welding voltage obtained under different welding conditions (Figure 2) that the sufficiently informative signal reflecting the course of the explosive-spark process is a frequency component, which was separated by means of a digital filter.

After primary processing of the data, the arrays were divided into blocks equal to ten periods of the industrial mains voltage, based on the permissible du-

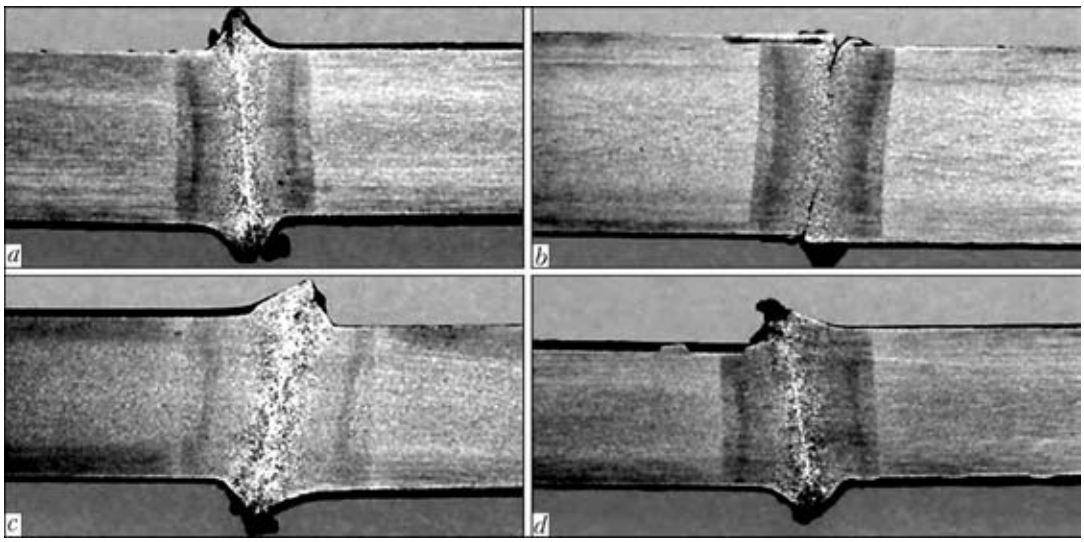

Figure 1. Macrosections of the joints produced under different welding conditions: here and below in Figures 2 and 3: *a* — optimal conditions; *b* and *c* — decreased speed and voltage, respectively; *d* — increased extension

ration of deviations during the flashing process [1]. Mathematical expectation of a random quantity module reflecting the intensity of flashing at a given stage of oscillogram was determined for each block. This resulted in the data arrays reflecting the intensity of flashing (Figure 3).

The data arrays were different even for the joints welded under conditions with the identical parameters, although the limits of variations in values of the parameters can be determined for each group of the joints. This brings about a problem of automatic classification of the arrays.

This problem can be successfully solved by using neuron networks for data classification and clustering. The Probability Neural Network (PNN), which belongs to the radial-base networks, and Learning Vector Quantization (LVQ), i.e. the network for discretisation of learning vectors, were used for classification.

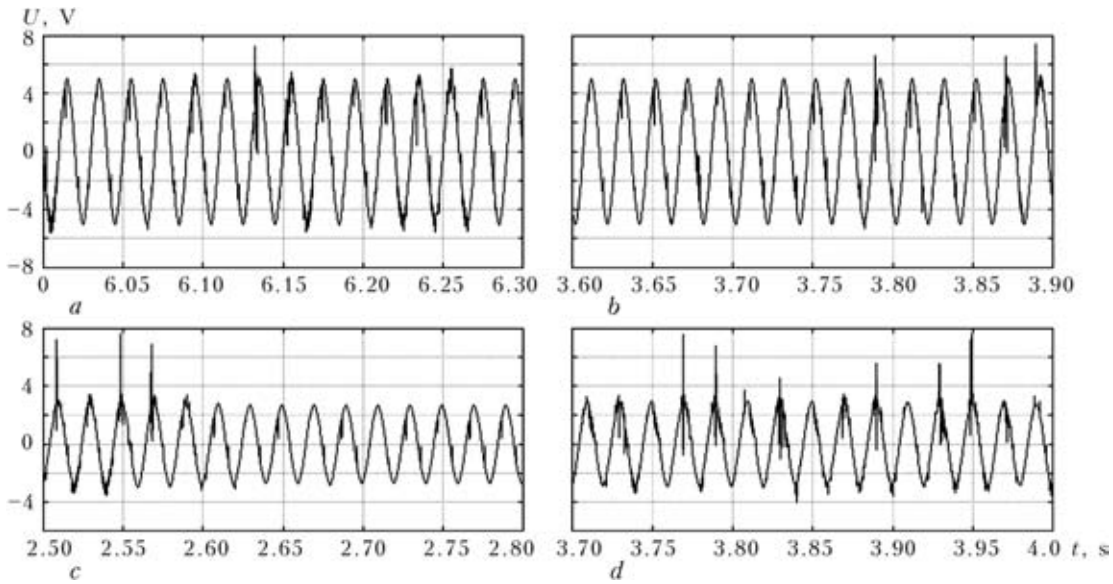

Figure 2. Typical voltage oscillograms at different welding parameters

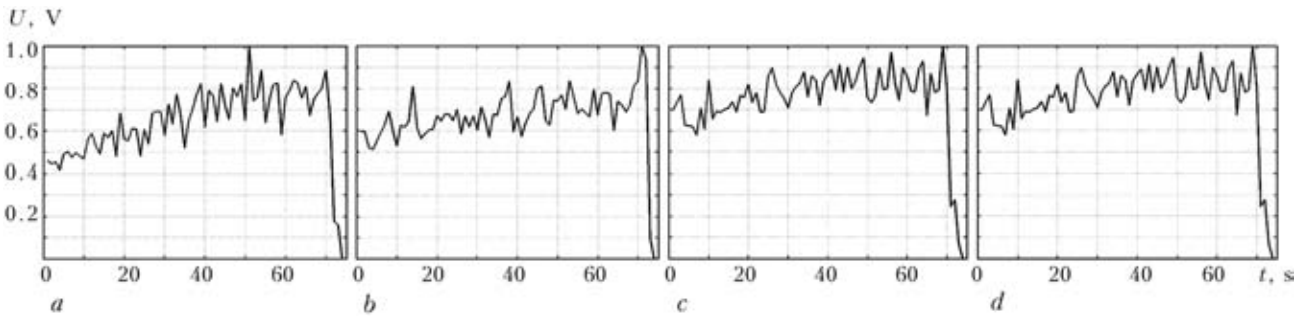

Figure 3. Typical data arrays (*a*–*d*) reflecting the intensity of flashing for groups of joints

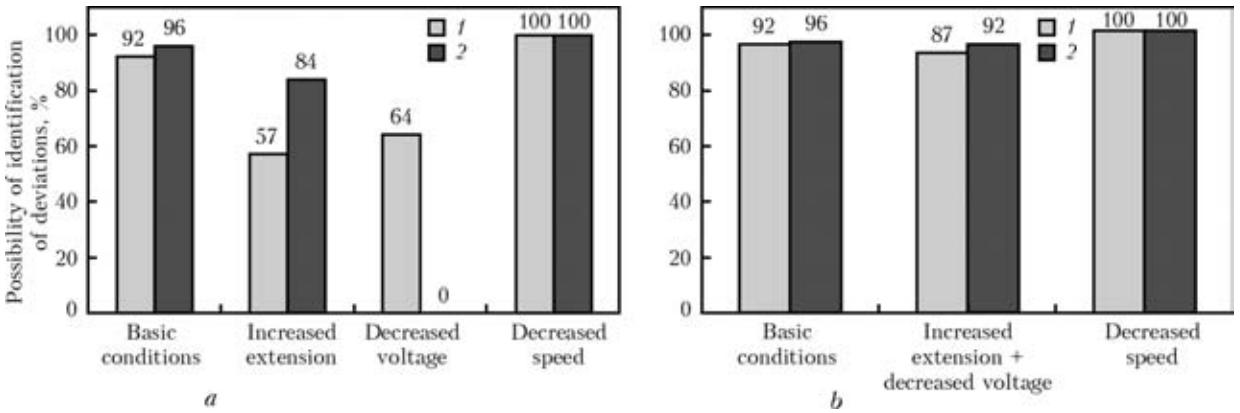

Figure 4. Results of operation of PNN (*1*) and LVQ (*2*) networks: primary (*a*) and after repeated learning (*b*)

Both networks are classed with the self-organising ones [4]. Classification was based on a criterion of the presence of deviation of one of the process parameters (v, $U_{o.-c}$, l). Therefore, the data were divided into four classes.

The data obtained during the experiments were used for network learning. One learning sequence was applied for both types of the networks. It included 15 data arrays for each group of the parameters. PNN had 4 neurons, and LVQ had 4 neurons in the second layer. Performance of the networks was tested on ranges of the values which were not used in their learning.

A relative error in identification of the data arrays for the joints welded under the optimal conditions was not in excess of 8 % (Figure 4, *a*). The data arrays belonging to a group of parameters with the decreased speed were determined unmistakably. In identification of the data arrays referring to parameters with the decreased voltage and increased extension, the error was more than 16 %. This is related to the fact that both deviations lead to formation of similar changes in the course of the process (e.g. see Figure 3).

Repeated learning of the network was carried out. For it the two groups of the joints were joined together. A new PNN network had 3 neurons, and LVQ had 3 neurons in the second layer. The network learning parameters remained unchanged. The error in revealing disturbances in this case was not in excess of 8 % for LVQ, and 13 % for PNN (Figure 4, *b*).

The results obtained proved the feasibility of using the artificial neuron networks for evaluation of stability of the process in continuous flash butt welding.

CONCLUSIONS

1. Analysis of a high-frequency component of voltage of the welding machine allows efficient realisation of 100 % monitoring of the flash butt welding process.

2. It is reasonable to use the classification and clustering neuron networks for automatic monitoring based on analysis of the intensity of flashing.

1. Kuchuk-Yatsenko, S.I. (1992) *Resistance flash-butt welding*. Kiev: Naukova Dumka.
2. Adolfsson, S., Bahrami, A., Bolmsjo, G. et al. (1999) Online quality monitoring in short-circuit metal arc welding. *Welding Res.*, **2**, 59–72.
3. Shannon, G. Gaining control of resistance welding. *http://*www.thefabricator.com/ArcWelding/Arc\ Welding_Article.cfm?ID=1689. August 8, 2007.
4. Medvedev, V.S., Potyomkin, V.G. (2002) *Neural networks: Matlab 6*. Moscow: Dialog-MIFI.

SELECTION OF THE GROOVE SHAPE FOR REPAIR OF THROUGH CRACKS BY MULTILAYER ELECTROSLAG WELDING

S.M. KOZULIN
E.O. Paton Electric Welding Institute, NASU, Kiev, Ukraine

The article gives results of calculation of the groove shape and penetration depth for repair of through cracks in thick parts by multilayer electroslag welding.

Keywords: *multilayer electroslag welding, carbon steels, band of cement kiln, through crack, repair, groove shape, gap width, penetration depth, consumable nozzle, pitch of holes*

Application of electroslag welding (ESW) to repair cracks in large-sized thick-walled expensive machine and mechanism parts makes it possible to substantially reduce the terms of their repair operations, extend their service life and save money and materials [1, 2]. The method of multilayer electroslag welding (MESW) is used to repair failed parts directly in site of their operation, particularly under erection conditions. This method allows using simple mobile small-size equipment and low-capacity power supplies [3].

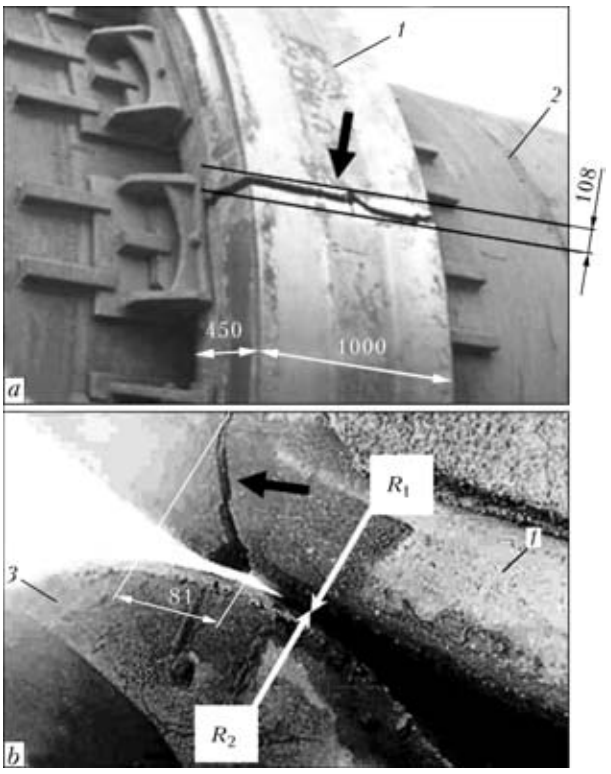

Figure 1. Through cracks in bands of rotary cement kilns 5 m in diameter: *a* — deviation of crack from the cross section plane of the band; *b* — deviation from the radial plane; *1* — band; *2* — kiln casing; *3* — bearing roller; R_1 = 3050 mm — radius of roll surface of band; R_2 = 450 mm — radius of bearing roller

A crack is grooved for welding with small regions (pits) by drilling 65–75 mm diameter holes at a pitch of 80–90 mm [4]. However, to repair through cracks having considerable branches, the shape of the groove and pitch of the deposited layers should be determined depending on the configuration and size of defects [5, 6]. For example, in repair of through cracks in bands of rotary kilns the deviations of a crack from the cross section plane may amount to 60–110 mm, and those from the radial plane — 40–100 mm (Figure 1), sizes of the failed sections being (355–500)×(900–1350) mm. High-quality grooving of such defects by drilling through holes [5] is hardly feasible, as it does not allow an entire defective region of metal to be removed. Therefore, the defective region with a crack is removed by machining or gas-oxygen cutting by making two through parallel cuts in a workpiece. The distance between the cut planes is selected such that it covers the whole crack region. Then steel plates are placed at a certain distance into the resulting gap, thus forming holes of a rectangular shape [6].

The optimal shape of the groove in MESW should provide a stable process, maximal productivity of repair, required depth and width of penetration of the base metal in the filled-in hole, guaranteed fusion of layers of the multilayer weld, and achievement of the maximal effect of auto-heat treatment with a heat released in deposition of the next layer.

Geometric parameters of the groove were calculated on the basis of the data obtained experimentally. ESW of 300–620 mm thick samples of steel 35L and 34L-ESh was performed by using units A-645, A-1304 and AShP 113M, as well as AC power supply TShS-3000-3. The use was made of 3 mm diameter electrode wires of the Sv-08GA and SV-10G2 grades and flux AN-8M. The holes made by installing the rolled metal plates were filled in sequentially by using the twin-electrode consumable nozzle at specific heat input q_w = = 70–175 kJ/cm^2. Transverse macrosections were made from the templates cut out from the welded samples in the planes normal to the multilayer weld.

The experience of repair operations shows that most often the width of the groove for filling-in of through cracks is 60–120 mm. The much larger width

of the groove (welding gap) than in traditional ESW is attributable to the necessity to fully remove the workpiece metal located in the crack branching zone.

Width S_p of the filled-in hole (pit) formed by installing the shaping spacer plates (partitions) was determined as a function of two variables from the following relationship:

$$S_p = \frac{F_d}{B},$$

where F_d is the surface area of the deposited metal, and B is the width of the welding gap.

As shown by the data given in studies [3, 4, 7–10], as well as by additional experiments on filling-in of rectangular holes by the ESW method using the consumable nozzle, the satisfactory fusion of the base metal and metal of the shaping spacer plates can be achieved in the case of the groove with a cross section area of 2500 to 4500 mm^2. Figure 2 shows the diagram of optimal ratios of gap width B to pit width S_p for MESW with the twin-electrode consumable nozzle.

Examination of transverse macrosections of specimens with the holes filled in by MESW with the twin-electrode consumable nozzle indicated that at a ratio of groove width B to filled-in hole width S_p equal to 1.1–2.4 the penetration shape in a cross section is close to ellipse. Based on this observation, a scheme (Figure 3) was worked out to calculate the expected penetration shape in MESW. It can be seen from this scheme that to provide the good fusion of filler metal to edges of the base metal it is necessary to optimise the following parameters: local width of penetration of the base metal edges in the filled-in hole, S_b; distance between the axes of the filled-in holes (pitch), t; and width of a region of repeated penetration of the base metal edges in place of installing of the shaping spacer plate after deposition of the neighbouring layer, l.

Parameter S_b characterises part of thickness of the joint welded per pass by the MESW method.

The classic ellipse equation [11] was used to calculate the above parameters. This equation allows determining coordinates of points M (x, y) and N (x, $-y$) of the chord parallel to one of the ellipse diameters (see Figure 3). Hence:

$$y = \sqrt{\left(1 - \frac{x^2}{a^2}\right) b^2}, \qquad (1)$$

where a and b are the ellipse semi-axes.

Expression (1) was used to determine the minimal required width of penetration of the base metal edges in the filled-in hole, S_b, for the preset depth of penetration of the base metal, h (see Figure 3).

By expressing the unknown value through $S_b = 2y$, and parameters x, a and b — through values indicated in Figure 3, and by making cancellations, we obtain that

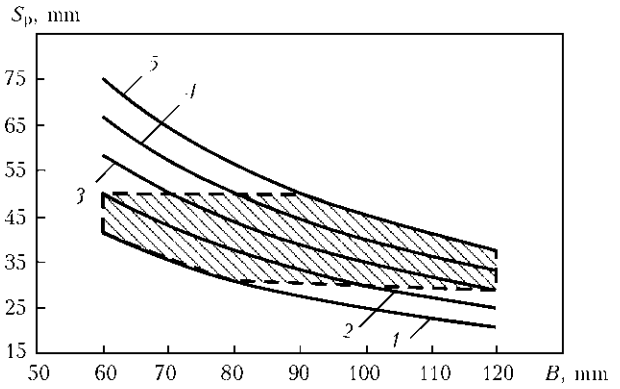

Figure 2. Range of optimal ratios of gap width B to pit width S_p for MESW with twin-electrode consumable nozzle: *1* — F_d = 2500; *2* — 3000; *3* — 3500; *4* — 4000; *5* — 4500 mm^2

$$S_b = 2\sqrt{\left[1 - \frac{B^2}{B^2 + 4h(B + h)}\right]\left(\frac{S_p}{2} + h_{pl}\right)^2}, \qquad (2)$$

where h_{pl} is the depth of penetration of the shaping spacer plate.

To reduce variables in formula (2), the diagram of the ratio of the base metal to shaping spacer plate metal penetration depth was plotted on the basis of experimental data (Figure 4). The approximated line of this diagram can be expressed in terms of a linear function [12]

$$y = mx + c, \qquad (3)$$

where m is the angular coefficient equal to tg α, and c = 13 mm

Substantiation of the m and c values taken from Figure 4 to equation (3) and replacement of the penetration variables yield the expression that characterises relationship of the base metal and shaping spacer plate metal penetration depths:

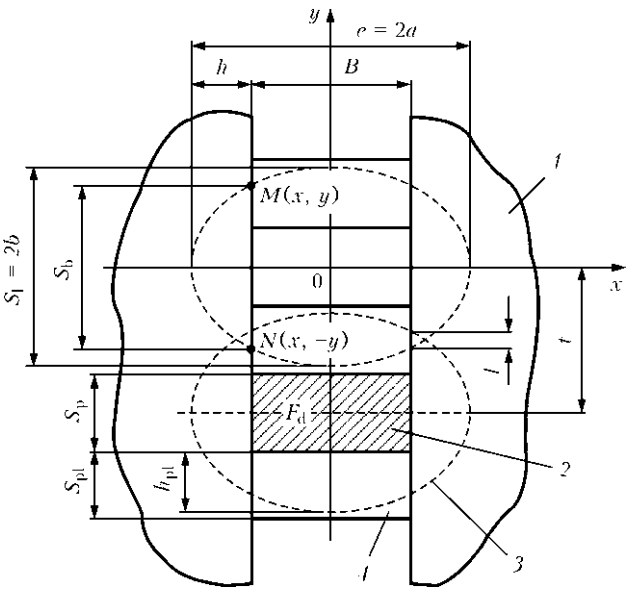

Figure 3. Scheme for calculation of groove and penetration shape in MESW: *1* — body of workpiece subject to repair; *2* — filled-in hole; *3* — penetration shape; *4* — bridge; e — width of a layer of multilayer weld; S_{pl} — thickness of shaping spacer plate; S_l — thickness of a layer of multilayer weld (see the text for the rest of the designations)

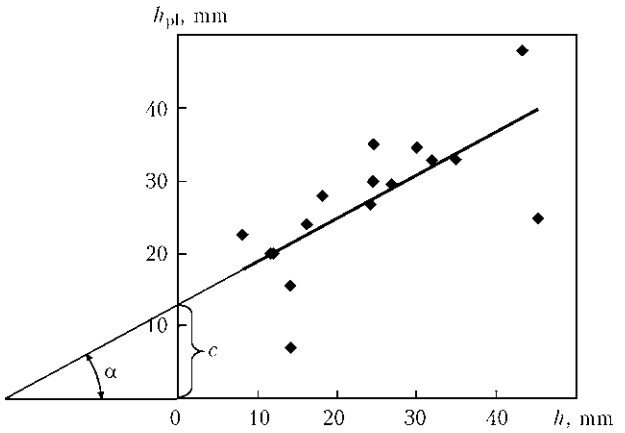

Figure 4. Ratio of base metal h to shaping spacer plate metal h_{pl} penetration depth in MESW with consumable nozzle

$$h_{pl} = 0.577h + 13. \quad (4)$$

By substantiating expression (4) to (2), we obtain the minimal required width of penetration of the base metal edges in the filled-in hole.

Pitch t of the filled-in holes (see Figure 3) should provide the guaranteed fusion of layers of the multilayer weld (Figure 5). For this, theoretically the width of the region of repeated penetration of the base metal edges, l (see Figure 3) should have a positive value (above zero). For practical calculations, allowing for permissible variations of the process parameters that occur during welding, this value should be not less than 5–8 mm.

The required value of pitch t was determined from the scheme of the groove with the expected penetration shape (Figure 6), wherefrom it follows that the unknown value can be expressed through the assumed width of penetration of the base metal edges, S_b:

$$t = S_p + S_{pl} = S_b.$$

The $t < S_b$ inequality should be met for the guaranteed fusion of layers of the multilayer weld.

To allow for the above required value of l, the t value can be expressed as follows:

$$t = kS_b, \quad (5)$$

where $k = 0.85–0.95$.

Substantiation of expression (2) to (5) yields

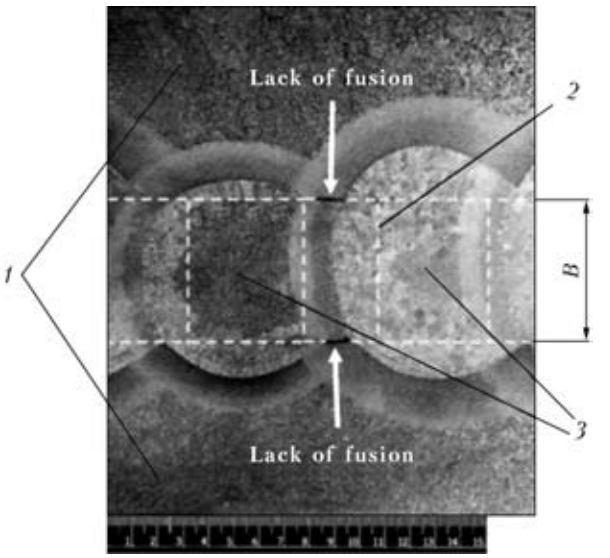

Figure 5. Transverse macrosection of a fragment of multilayer weld with defects: *1* — specimen pieces welded; *2* — shaping spacer plate; *3* — weld layers

$$t = 2k\sqrt{\left[1 - \frac{B^2}{B^2 + 4h(B+h)}\right]\left(\frac{S_p}{2} + 0.577h + 13\right)^2}. \quad (6)$$

This expression allows determining the required pitch of the filled-in holes to select the groove size and shape for MESW.

The calculated values were experimentally checked by making instrumental measurements of the above parameters in the scanned photos of transverse macrosections (Figure 7). The measurements were made by using software KOMPAS-3D V8.

Results of the calculations and measurements of geometric parameters of the penetration zone are summarised in the Table.

Comparative evaluation of the calculated and actual parameters of the shape and depth of penetration of the weld edges showed the following:

• the calculated shapes of penetration satisfactorily coincide with the actual shapes of penetration of the base metal and shaping spacer plates. Deviation of the actual fusion line from the calculated one is observed only in the closing (at the joint end) layers of the multilayer electroslag weld, this being caused by the end effect [13];

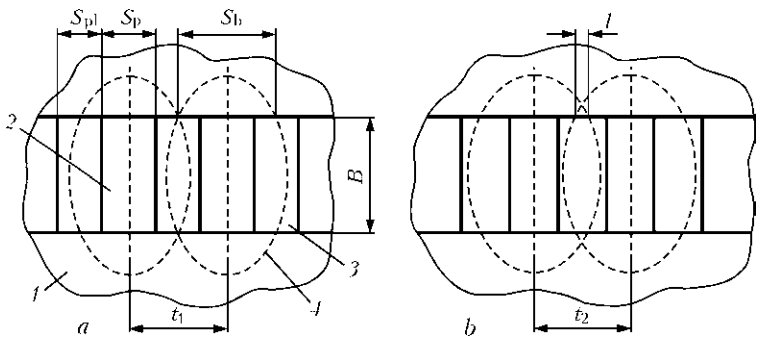

Figure 6. Scheme of groove and expected penetration shape in MESW with consumable nozzle: *a* — $l = 0$; *b* — $l > 0$; *1* — body of workpiece subject to repair; *2* — filled-in hole; *3* — shaping spacer plate; *4* — isotherm of melting; t_1 and t_2 — distances between axes of filled-in holes (pitch)

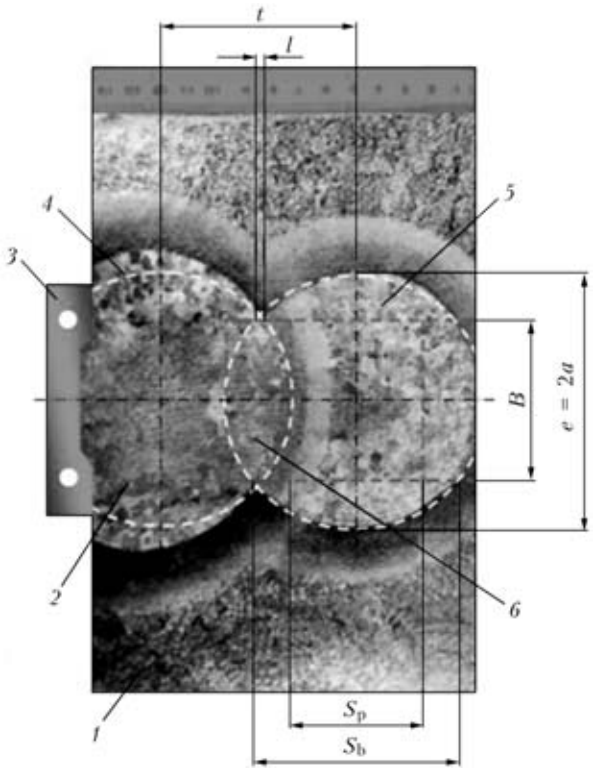

Figure 7. Transverse macrosection of a fragment of multilayer electroslag weld: *1* — workpieces welded; *2* — shape of groove for MESW; *3* — water-cooled shaping device; *4* — calculated shape of fusion line (zone); *5* — weld layer; *6* — shaping spacer plate

Calculated and experimental values of groove shape and penetration depth in MESW with consumable nozzle

B, mm	S_p, mm	h, mm	Number of weld layer	Calculated values, mm				
				$2a$	$2b$	S_b	t	l
60	50	15	3	90	93.40	69.9	66.40	3.50
			4					
70	45	30	5	130	105.62	89.0	75.65	13.35
			3					

Cont.

Actual values, mm					
h	e ($2a$)	S_l ($2b$)	S_b	t	l
15.0–17.5 / 16.25	90	98	76.0–77.0 / 76.5	74	3.4–4.2 / 3.8
24	108	–	–		
28–32 / 30	127	112	91.0	73	14.0–15.5 / 14.75
28.5–37.5 / 33	140	109	91.0–98.0 / 94.5		

• the actual values of parameters of the penetration zone differ from the calculated ones by not more than 10 %, which is acceptable for engineering calculations. The actual value of penetration depth h, local width of penetration of the base metal edge, S_b, and width of the region of repeated penetration of the base metal edge, l, are a bit higher than the calculated values of these parameters, which provides the guaranteed fusion of layers of the multilayer weld for the selected groove shape.

Therefore, the procedure proposed allows calculation of the groove shapes at which the guaranteed fusion of layers of the multilayer electroslag welds is ensured.

1. (1980) *Electroslag welding and cladding*. Ed. by B.E. Paton. Moscow: Mashinostroenie.
2. Sushchuk-Slyusarenko, I.I., Lychko, I.I., Kozulin, M.G. et al. (1989) *Repair electroslag welding and cladding*. Kiev: Naukova Dumka.
3. Sushchuk-Slyusarenko, I.I. (1977) *Electroslag welding and cladding*: Results of science and technique. Series Welding. Vol. 9. Moscow: VINITI.
4. Sushchuk-Slyusarenko, I.I., Vergela, A.G., Shevchenko, N.T. (1969) Electroslag welding-up of cracks. *Avtomatich. Svarka*, **4**, 72–73.
5. Kozulin, S.M., Lychko, I.I., Kozulin, M.G. (2007) Methods of reconditioning rotary kilns (Review). *The Paton Welding J.*, **10**, 33–39.
6. Kozulin, S.M., Lychko, I.I., Kozulin, M.G. (2010) Increase of resistance of welds to formation of crystalline cracks in repair of bands of kiln furnaces using electroslag welding. *Ibid.*, **1**, 32–34.
7. Irausch, R., Huttenes, K., Becken, O. (1969) Instandsetzung eines gebrochenen Hammerbaeren mit Hilfe des Kanalschweissverfahrens. *Reinstahl-Technik*, **3**, 124–133.
8. Sushchuk-Slyusarenko, I.I., Koval, I.M., Cherkashina, L.S. et al. (1974) *Electroslag welding of cruciform joints*: Inform. Letter 68/905. Kiev: PWI.
9. Sushchuk-Slyusarenko, I.I., Lychko, I.I. (1974) *Technique of electroslag welding*. Kiev: Naukova Dumka.
10. Filchenkov, D.I., Moshnikov, S.V., Kozulin, M.G. (1977) Repair of casting defects by electroslag welding. *Svarochn. Proizvodstvo*, **11**, 48–49.
11. Bronshtejn, I.N., Semendyaev, K.A. (1980) *Reference book on mathematics*. Ed. by G. Groshe and V. Tsigler. Moscow: Fizmatlit.
12. Vygodsky, M.Ya. (1957) *Reference book on elementary mathematics*. Moscow: Gostekhteorizdat.
13. Rykalin, N.N. (1951) *Calculations of heat processes in welding*. Moscow: Mashgiz.

IMPROVEMENT OF THE QUALITY OF WELDED ASSEMBLY FOR BRANCHPIPE CUTTING INTO THE WALL OF OIL STORAGE TANK

A.Yu. BARVINKO and **Yu.P. BARVINKO**
E.O. Paton Electric Welding Institute, NASU, Kiev, Ukraine

Performance of the assembly for cutting branchpipes for process pipelines and hatches in lower rings of the wall of high-capacity oil storage tanks is considered. It is shown that one-sided grooving of holes for the branchpipes followed by circumferential welding on the inside of tank wall, specified by industry standards, cannot guarantee the required complete penetration. It is suggested that the two-sided non-symmetrical edge preparation should be made, providing substantial improvement of welding conditions and quality of the circumferential welds.

Keywords: *arc welding, oil storage tanks, wall, branchpipe cutting-in assembly, one-sided welding, complete penetration*

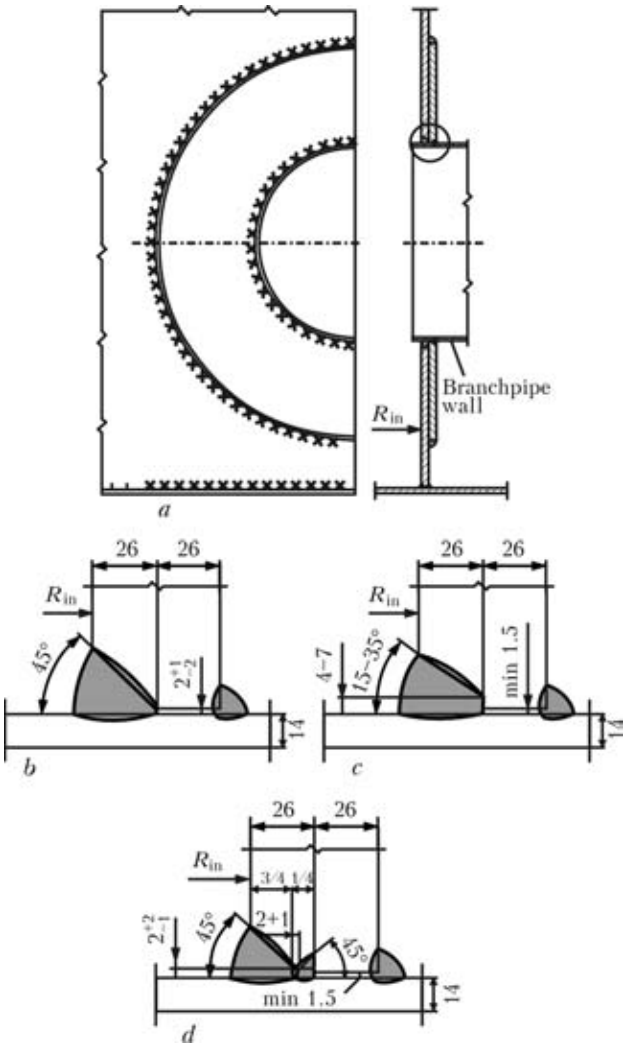

Figure 1. Design solutions of the assembly (*a*, *encircled*) of the joint of the wall of 50,000 m^3 tank RVS PK with the shell in keeping with PB 03-605–03 norms (*b*), standard API 650 (*c*) and PWI solution (*d*): R_{in} — wall inner radius

In keeping with technological requirements, cutting-in of various branchpipes for process piping and hatches is performed in the lower ring of the wall of vertical cylindrical tanks for oil storage. Cutting-in sites are located in the wall region, which is subjected to the impact of circumferential and bending stresses of edge effect caused by rigid connection of the wall to the bottom. In order to ensure the required serviceability of branchpipe cutting-in locations, the current technological norms envisage reinforcement by special coverplates, while complete penetration of the wall to branchpipe joint (Figure 1, *a*) should be in ensured [1, item 3.10.1.6] and [2, item 3.7.2.1].

Holes under the branchpipes are cut out manually by oxygen cutting in site. Gap between the wall and branchpipe, in keeping with the technological norms [1], should be equal to 0–3 mm. At tank wall thickness of 20 mm and more and one-sided welding of position butt joint with the above gap, it is difficult to cut-out and soundly grind the root of such a weld with the abrasive wheel, because of branchpipe wall and groove curvature. Depth of cutting out the weld root from the reverse side reaches 4–6 mm (Figure 1, *b*). In the absence of an efficient method of control and methods to repair the available defects, the quality of weld formation depends on welder qualification.

Experience of operation of tanks with the design of branchpipe cutting-in assemblies, recommended in [1], is indicative of the fact that cutting-in locations are zones of increased stress concentration, and they can be the sites of crack initiation and propagation. Figure 2 shows cracks propagation in the circumferential weld, made on the fastening of reinforcing coverplate to 16 mm wall of the oval hatch on an oil tank RVS PK of 20,000 m^3 capacity from 09G2S-12 steel. Crack initiation and propagation are largely promoted by the presence of a coverplate on the vertical axis of in-site butt weld. Figure 3 shows another case of failure of a circumferential weld, made at welding-in of Dn 300 branchpipe into 26 mm wall of RVS PK tank of 50,000 m^3 capacity from S390 type steel. A

Figure 2. Crack propagation in the circumferential weld made on reinforcing coverplate of the oval hatch in the oil tank of 20,000 m^3 capacity from 09G2S-12 steel with 16 mm wall thickness

water leak through the control hole in the coverplate developed at hydraulic testing. After complete draining of the water, dye penetrant flaw detection in the circumferential weld inside the tank was performed, revealing the presence of through-thickness circumferential and transverse cracks predominantly in the weld lower part (see Figure 3). Alongside the deficiencies of the welding technology, there also exist a number of other negative factors that lead to crack initiation and propagation. These are the difficulties of achieving complete penetration of the wall across its thickness, particularly in the weld root.

To improve the conditions of producing the weld of required quality in keeping with the current norms [2], a somewhat different groove geometry in the wall hole is recommended (see Figure 1, *c*), when the gap between the tank walls and branchpipe should be increased to 4–7 mm. In order to reduce the volume of deposited metal, groove angle is selected equal to 15–35°. However, welding brachpipes into the wall of RVS PK tank of 50,000 m^3 capacity showed that increasing the gap at reduction of groove angle does not solve the problem of sound penetration of circumferential weld root. At the gap of 5–7 mm the volume of deposited metal in the weld root increases significantly, and the end face of weld root has 3–8 mm recession on the outside, that does not allow performing its sound grinding and subsequent back-up welding. On the other hand, in all the illustrations to the norms [1, 2] there are no direct recommendations on the need for grinding and back-up welding of weld root with subsequent cutting off of reinforcement flush with the wall to ensure a tight fit of the reinforcing coverplate.

Analysis of engineering solutions, proposed in the current norms, for ensuring complete penetration of the wall of RVS PK tank of 50,000 m^3 capacity at its joining to the wall of welded-in branchpipes, showed that at more than 20 mm thickness of the lower ring standard solutions do not guarantee producing a circumferential weld of the required quality. It is proposed to move over to a two-sided welding of the circumferential weld with two-sided edge preparation of the hole in the wall. In the solution presented in Figure 1, *d*, preservation of groove angle of $\alpha = 45°$ provides the conditions sufficient for sound welding of the weld root and filling the weld groove, while wall grooving from the outside gives good access for root cleaning and performing its sound back-up welding. Root weld reinforcement can be removed with an abrasive wheel or by making a chamfer on the coverplate.

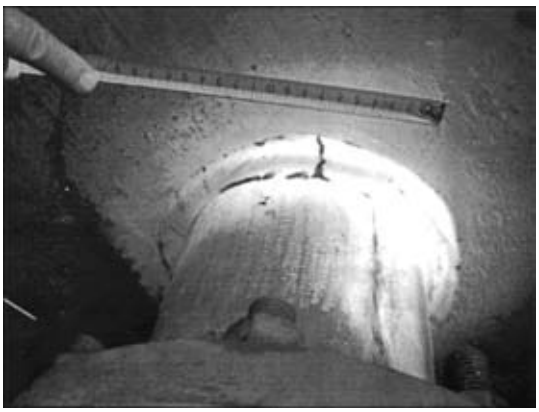

Figure 3. Cracks in the circumferential weld at welding-in of Dn 300 branchpipe in the first ring of the wall of 50,000 m^3 oil tank RVS PK from S390 steel with 26 mm wall thickness

Technology of welding branchpipes into the lower rings of tank walls also has certain peculiarities. The main of them consists in that the circumferential weld is made under the conditions of a rigid contour, when there is no compliance of welded elements and the transverse shrinkage deformations of the weld should be compensated by ductile properties of the metal of the wall and the weld proper. In order to compensate the above deformations, the current norms make special additional requirements to the tank wall metal: required ratio of yield point to tensile strength is equal to $\sigma_y/\sigma_t \le 0.75$ [2], value of reduction in area is $\psi_z \ge$ $\ge 25\,\%$ [3], and the circumferential weld proper should be subjected to heat treatment (tempering). When the tank is made of high-strength steels (S390 type, etc.) it is recommended to apply preheating and post-weld local heating of its wall sections, adjacent to the circumferential weld, that improves the conditions for realization of high ductile properties of the base metal and weld metal. Used welding consumable should provide a sufficient ductility of the weld metal and, particularly, the root passes.

1. *PB 03-605–03*: Rules of construction of vertical cylindrical steel tanks for storage of oil and oil products. Moscow.
2. *API 650*: Welded steel tanks for storage of oil products. American National Standards Institute FNSI/STD 650. Introd. May 1993.
3. *GOST 28870–90*: Steel. Methods of tensile tests of plate iron in thickness direction. Introd. 01.01.92.

SHIELDING MATERIALS AND PERSONAL GEAR FOR WELDER PROTECTION FROM MAGNETIC FIELDS

O.G. LEVCHENKO, V.K. LEVCHUK and **O.N. TIMOSHENKO**
E.O. Paton Electric Welding institute, NASU, Kiev, Ukraine

Issues related to development of personal protective gear for welder protection from magnetic fields in resistance welding are considered. Investigation results on protective properties of shielding materials made from magnetically soft strips of amorphous cobalt-base alloy (Co–Fe–Cr–Si–B) are presented. An apron has been developed to protect welders from electromagnetic radiation.

Keywords: *resistance welding, electromagnetic radiation, magnetic field intensity, protection methods, protective magnetic materials, permalloys and amorphous metal alloys, shielding apron*

Variable electromagnetic fields (EMF) of a broad frequency range and electromagnetic radiation of radiofrequency ranges are the main factors of hazardous impact on the body of electric welding operators. Application of special protective clothing could complement the known traditional methods of protection by time and space [1], as their realization is not always possible or rational in view of the scope and nature of operations performed by personnel.

The main component of electromagnetic background is low-frequency EMF, which is generated by power lines, household appliances and electrical equipment of industrial enterprises. It is known that electrical component of low-frequency field is readily shielded using metal sleeves and cases of distribution boards. However, shielding EMF magnetic component (that fully applies also to welding processes) is a complicated engineering task, if we are talking about elastic magnetic shields for personal protection gear (PPG) of the workers.

Table 1. Required effectiveness of protection from MF in resistance welding

Resistance welding process	Required effectiveness of protection at exposure for 8 h, times*
Spot:	
manual (tongs)	6–7**
mechanized stationary	3–4**
mechanized capacitor	2
Seam	2–3**
Projection	2–3**
Butt	2–3**

*Effectiveness of protective devices E_{sh} means a ratio of MF maximum amplitude intensity H_m in the work place to its TLV H_{th} ($E_{sh} = H_m/H_{th}$).
**Tentative value in welding with one pulse of full-wave current of up to 1 s duration.

Problems of shielding high-frequency magnetic fields (MF) in welding were studied at PWI [2], and methods to design electromagnetic shields have been developed [3–5]. However, parameters of intermittent-pulsed MF generated in welding, with allowance for their spectral composition, are so complicated that selection of effective shields for them can only be performed experimentally.

Experimental studies of magnetic radiation conducted by the authors [6, 7] at different electric welding processes showed that the highest MF level is characteristic of resistance welding, where the service personnel particularly needs PPG based on elastic magnetic shields. Tentative data obtained by us on the need for efficient protection of the welder in the working zone against MF using shielding at different resistance welding processes are shown in Table 1.

As is seen from the Table, maximum shielding effectiveness should lower MF intensity 7 times for an eight hour working day (MF frequency is equal to 0–1000 Hz). This is highly problematic for the known modern metallic shield materials, which should be solid and have sufficient elasticity. However, taking in account the fact that the net welding time during the working day is usually limited to 5 h, shielding efficiency can be reduced by approximately 1.3 times. Using the additional traditional methods of protection by time and distance, shielding effectiveness (to increase PPG elasticity at reduction of shielding layer thickness) can be reduced further by 2–3 times. Such a comprehensive approach to solving the problem of electromagnetic safety when using the procedure for MF level measurement developed at PWI yields positive results.

Development of PPG against low-frequency MF requires materials with high magnetic permeability ($\mu \geq 15000$) and high stability of magnetic properties. Complexity of development and manufacturing of shielding magnetic materials, which would be efficient both in the low- and in the high-frequency MF ranges, is related to the fact that their development makes it necessary to study various physical principles of op-

eration and technological aspects of their manufacture. For instance for low-frequency MF (up to 1 kHz) the protective coating should be in the form of a continuous shell, and for high-frequency fields, measured in mega- and gigahertz, it is necessary to study the regular structure of the coating with gaps, the width of which is determined by the shielded field wave length.

Shielding material selection. Protective shielding in the general case is designed for protection both from MF, and from EMF. The versatility of such a solution, however, is not only dubious, but also not rational. Shields and coatings designed for protection from EMF and radiation of certain ranges of frequency and amplitude are considered to be the most suitable, as the magnetic properties of both the metallic and amorphous materials depend not only on their chemical composition, but also on their manufacturing conditions, modes of mechanical, heat and magnetic treatment. Selection of treatment modes allows manufacturing materials with the specified properties, the most efficient for EMF of certain ranges of frequency and amplitude. At development of such materials and their application as protective shields, it is necessary to determine the dependence of the coefficients of shielding or magnetic permeability on MF (EMF) amplitude-frequency characteristics and material treatment modes, providing maximum values of the above parameters at the manufacturing stage. In the first approximation, material magnetic permeability can be an indication of shielding properties of the selected material.

The most widely accepted materials for MF shielding are electric steels with 2.8–3.8 % Si made in the form of iron strips and sheets. Their magnetic properties are much higher along the rolling direction than in the transverse direction (magnetic permeability is up to 5000). Steel of 0.35–0.50 mm thickness is used at MF of 50 Hz frequency, and thinner steel — at MF of 400 Hz and higher frequency. Coefficients of shielding of these materials are not always satisfactory and depend on the modes of their preliminary heat treatment. In addition, if during manufacturing of parts (for instance, transformers), steel is subjected to even small plastic deformation (chipping, bending), its magnetic properties markedly deteriorate.

The most suitable thin shields for protection from MF generated by welding equipment are iron-nickel alloys (permalloys) and amorphous metal alloys with a high cobalt content [8]. Permalloys made in the form of sheets (or strips) 0.0015–2.5 and 3–22 mm thick contain from 45 up to 89 wt.% Ni. Alloys of 79NM, 80NKhS, 68NMP grades, which have up to 80 wt.% Ni (high-nickel permalloys), are used as magnetic shields. Letter P in the latter alloy grade indicates the rectangular shape of hysteresis loop and strong dependence of the alloy magnetic properties on the level of external MF. Permalloys have a high (up to 50000) magnetic permeability, but are highly sensitive to mechanical impact (work hardening). For instance, magnetic properties of a shield from permalloy of 79HM grade after its deformation by 10 % decrease by almost 18 times.

During the last decade considerable success has been achieved in the field of materials science, namely in development and putting into production of new polymer, composite and metallic materials with unique physical properties. One of the promising developments in this field is creation of new magnetically soft materials — amorphous metal alloys, which are characterized by a high magnetic permeability and saturation induction, and have various applications. The required physical properties of these materials can be achieved due to their heat and magnetic-thermal treatment. Predictable variation of magnetic properties, acceptable mechanical properties, as well as a constant lowering of the cost of manufacturing and pre-treatment of amorphous alloys, make them promising in development of elastic coatings for protection of personnel and technical means from MF and electromagnetic radiation of anthropogenic origin.

The composition of amorphous metal alloys suitable for practical application includes the main metals (iron, nickel, cobalt) and amorphoidizing additives (phospohorus, boron, silicon, carbon, aluminium). The most widely accepted materials are 85KSP and 71KNSP alloys with a high cobalt content [9]. Amorphous metal alloys are made in the form of very thin (down to several tens of microns) strips that is due to the technology of high-speed quenching (so-called spinning) of the melt.

It is known that the relative magnetic permeability of amorphous alloys can vary in a broad range. For instance, relative magnetic permeability of the high-cobalt alloy (80 wt.% Co) in MF with 10 kHz frequency and amplitude intensity H_m = 800 A/m after thermomagnetic treatment in a constant MF with the intensity of 1000 A/m at the temperature of 300 °C increases from 120,000 up to 300,000.

Analysis of the influence of the level of MF intensity on shielding properties of permalloy and high-cobalt amorphous alloy in MF of industrial frequency (50 Hz), depending on shielding materials with plant heat treatment, is given in [10], from which is follows that shielding efficiency of the above alloys is much higher than that of permalloy. It is also noted that at application of the same shielding materials, their properties are significantly improved with increase of MF frequency, even in low-frequency MF, the dependence of these properties on amplitude level of the latter becoming more complicated.

Thus, one of the main problems, arising in development of systems of electromagnetic shielding, consists in that the range of MF frequency, in which modern technical devices operate, is very broad, and protective materials ensure shielding in just a limited

frequency range. As was noted earlier, such materials as permalloy, are highly sensitive to mechanical impacts. In amorphous metal alloys, as a rule, high uniaxial magnetic anisotropy is realized, however, the amorphous state is metastable. In this connection, amorphous materials are characterized by the ageing effect, particularly, at increased temperature.

Investigations conducted at TsNII CM «Prometey» (RF) showed that amorphous magnets of one grade, but from different manufacturers, differ essentially in their magnetic properties. As Ukraine has both the scientific-technical and production facilities for manufacturing amorphous magnets (G.V. Kurdyumov Institute of Metal Physics of the NAS of Ukraine and MELTA Ltd., Kiev), development of protective structures and overalls similar to foreign developments, is not always rational.

The above-said leads to the conclusion that at present there is no universal solution for ensuring electromagnetic shielding of specific objects. Taking organizational-technical decisions on electromagnetic shielding requires thorough theoretical and experimental studies of the processes of thermal and magnetothermal treatment of amorphous materials to optimize their properties for application as magnetic and electromagnetic shields. At present amorphous alloys can be regarded as the most promising materials for protection of technical and biological objects from adverse influence of MF and electromagnetic radiation. Development of elastic protective shields for electromagnetic devices and protective clothing should be oriented to local magnetically soft materials.

Development of elastic magnetic shield for welder's protective clothing. During performance of welding operations the following harmful and hazardous production factors are in place: sparks and spatter of molten metal and slag with up to 2000 °C temperature, radiant energy from the welding arc of different spectral composition and intensity, thermal radiation of up to 84 J/(cm^2·min) (20 cal/(cm^2·min)), MF of 80–10000 A/m intensity of 0–2000 Hz frequency, dust and fume levels in welder breathing zone with harmful substance concentration exceeding the TLV, meteorological factors, when working in open air, depending on the season and climatic zone.

In keeping with the labour conditions and nature of impact of these harmful and hazardous factors, all the clothing for welding fabrication workers is divided into five groups based on the common protective, service and hygienic properties. By the earlier existing classification the protective clothing for resistance welding of metal of small cross-sections (spot, seam, projection and butt welding) was classified as group 3A, and was to provide protection from MF of 80–10000 A/m intensity (amplitude value) without indication of any frequency ranges. Welder's PPG should include suit (coat and trousers), gloves and mittens, headwear and footwear [11, 12].

A protective outfit is known which consists of a cap and short skirt [12], where permalloy of 79NM-I, 80NKhS, 76NKhD grades was used in the form of thin metal threads mixed with cotton threads, which protect from external impact and act as electrical insulation. Thus, a cloth with a regular structure forming a net with 0.5 × 0.5 mm mesh was used as the shield. There is a lack of data on shielding properties of such a material designed for protection from low-frequency MF, and its effectiveness is highly doubtful.

PWI staff had the goal of developing a protective magnetic shield that could be the basis for welder's protective clothing, allowing for the modern sanitary norms of magnetic safety. Here, it was to be decided what is the meaning of «elasticity» term for protective clothing. Elasticity (from the Greek for flexible) is the ability of a structural material or product to stand considerable elastic reversible deformations without fracture at relatively small loads. The term «elasticity» exists side by side with the term «resilience». Elasticity is achieved both through selection of material (for instance, rubber), when it is due to the features of the molecular structure of the body, and due to design. In the latter case high deformations of the item develop at small material deformations. It is the issue of conditional use of «elasticity» term for composite material for the protective clothing, which essentially is a functional material and ensures MF shielding in addition to the traditional properties of protective clothing. The need to include a metal layer into the composition of protective clothing material, and possibly, also additional functional layers (electrically insulating, protective, adhesive, etc.), as a rule, lowers such a parameter as flexibility, the limit value of which is equal to 0.50–0.55 kN for textiles, designed for protective coverplates, stripes, etc. [13].

Tentative structure of a material for protective clothing should have the following component layers-parts: one or two inner layers of the magnetic shield; two external electrically-insulating layers (if required); two external layers from a material traditional for this type of protective clothing; two inner layers (or a coating) of a technological purpose (for instance, adhesive).

Known is an engineering solution for protective clothing against MF [9], in which the shield is formed by longitudinal strips of an amorphous alloy with overlaps across the width, thus providing a continuous protective shielding coating of the textile. The method of strip joining to each other and to the textile was not considered in this work, but in any case it promotes an increase of rigidity of the shield design, both in the longitudinal and in the transverse directions, as a result of rigid fastening of individual layers into a whole. In our opinion more promising is the design of an elastic magnetic shield, consisting of strips, which are connected to each other due to their so-called linen weave with zero gaps between the strips

located in one direction without a rigid connection to each other. In this case the structure is completed without using any additional materials or elements during shield assembly. It provides the maximum magnetic shielding in two directions normal to each other (in connection with the anisotropy of magnetic properties of the strip).

The required protective properties can be obtained at the expense of increase of the total number of shields in the pack or strips woven in one shield without a rigid connection to each other. In this case use of several shields from single strips is preferable, as a result of their assembly into a pack with the shifting of points and lines of intersection of strips in one shield relative to the other the total effective thickness of the latter is increased, and its continuity for magnetic lines of force is ensured at maximum possible elasticity. Contacting of shield strips and individual shields with each other occurs both due to weaving, and due to elastic properties of the material and its certain residual magnetization. With reduction of the width and thickness of the composite strips of the shield its elasticity increases, but the labour consumption in its manufacture increases at the same time, which is not of principal importance, considering the urgency of the problem.

It is anticipated that the number of woven shields in the pack will not exceed two. If the double shield does not provide a sufficient level of protective properties, increase of shielding effectiveness can be achieved through additional thermomagnetic treatment of the strips that will increase the effectiveness further approximately by 2 times. However, mechanical properties of the shield material (in particular, number of bending cycles) deteriorate as a result of such a treatment. In this connection, it is initially intended to manufacture these shields from a material with a minimum (up to 70 %) content of deficit cobalt and without additional thermomagnetic treatment.

Available numerous data on the dependence of magnetic features of magnetically soft alloys on the level of external MF and coefficients of shielding for materials with different treatment conditions often are contradictory and need more precise definition. Reliable data on the dependence of coefficients of shielding of low-frequency range (0–1000 Hz) of external continuous or pulsed MF are also absent.

Experimental study of protective properties of shields in the laboratory. The main characteristic of a protective shield is the shielding effectiveness E_{sh}, which includes the relationship of electric field intensity E, magnetic field intensity H or power flow density (PFD) in a given point in the absence of a shield and E_{sh}, H_{sh} or PFD in the same point in the presence of a shield:

$$E_{sh} = \frac{E}{E_{sh}} = \frac{H}{H_{sh}} = \frac{PFD}{PFD_{sh}}.$$

It is rational to determine protective properties of materials experimentally by measurement of MF level behind the protective shield, as described in [10]. Diagram of a laboratory facility for testing pilot samples of shields is given in Figure 1.

MF generator allows in the first approximation simulating continuous MF with the spectral composition and intensity, characteristic for the working zone in resistance welding. Relative position of the generator, MF sensor and shield-partition in the experiments (allowing for the model scale factor) can be taken to be arbitrary, therefore, measurement of the intensity of the initial MF and field behind the shield was conducted in three planes normal to each other, which was followed by calculation of the resultant MF value (geometrical mean). Note that the effectiveness of the shield-partition theoretically is lower than that of protective clothing in the form of open or closed cylinder. However, this factor is not critical, considering that model studies were preliminary and comparative, and the final test of shielding effectiveness is conducted with samples of protective clothing in the shop.

Integral effectiveness of shielding in keeping with sanitary norms [14] was experimentally determined as

$$E_{sh} = \frac{\sum\limits_{n} H_{1\,mn}^2}{\sum\limits_{n} H_{2\,mn}^2},$$

where $H_{1\,mn}$, $H_{2\,mn}$ is the amplitude dependence of initial MF and that beyond the shield, respectively.

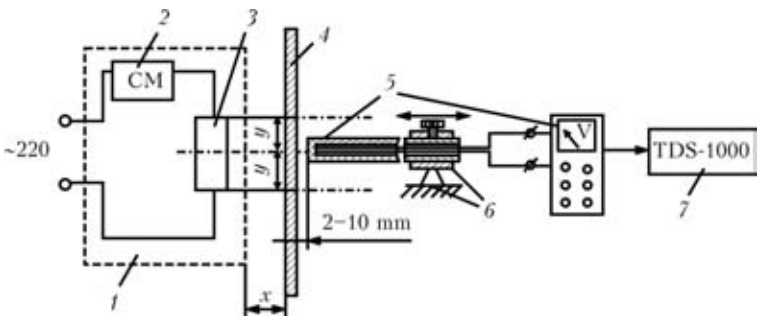

Figure 1. Schematic of a laboratory facility for testing pilot samples of protective shields: *1* — MF generator; *2* — control module (CM); *3* — solenoid; *4* — studied magnetic shield (elastic); *5* — magnetic induction Hall transducer with conversion; *6* — fastening of magnetic induction sensor; *7* — digital storage oscilloscope with the function of fast Fourier transformation (x, y have variable values)

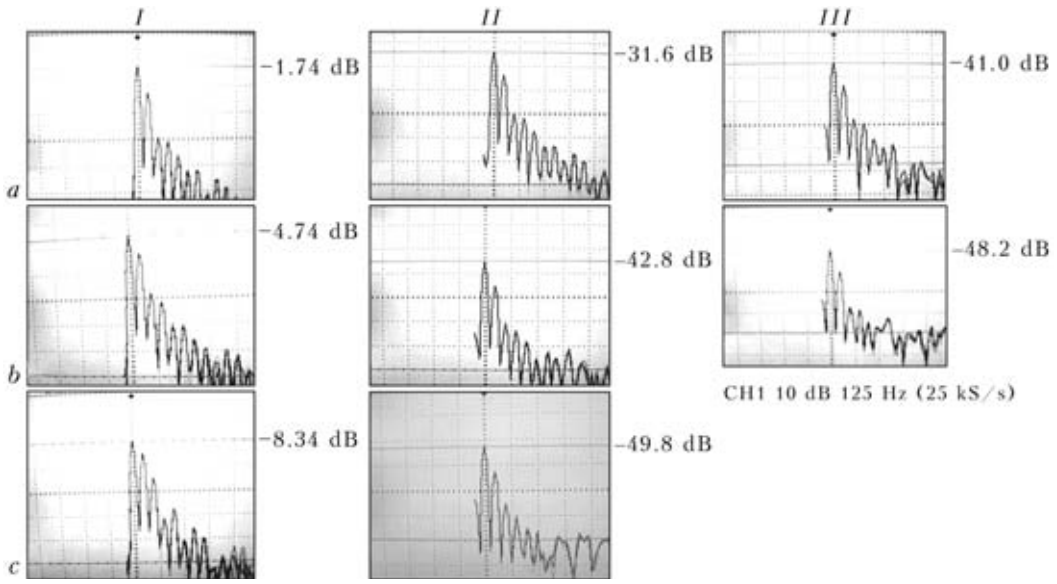

Figure 2. Nature of weakening of output MF by experimental shields: *a* — manual spot welding, H_m = 14000 A/m ((by the first 50 Hz harmonics); *b* — spot welding in stationary machines, H_m = 420 A/m; *c* — projection, seam, butt welding, H_m = 150 A/m; *I–III* — without the shield, with single and double shields, respectively

Here it was taken into account that the distance between the sensor plane and the shield equal to 2–10 mm (see Figure 1), corresponds to the actual gap between the human body and the shielding protective clothing [15].

Spectrographs (Figure 2) of MF of various intensities show the nature of differential weakening of each MF harmonics by open experimental single and double shields from strips of an amorphous metal alloy MM-5Co (Co–Fe–Br–Si) of width b = 27.5 mm and thickness δ = 0.0225 mm, assembled using linen weave. At small distances between the shield and sensor MF intensity in each of the points located along the shield strips, periodically changes slightly, reaching a minimum directly above the strips. Therefore, MF intensity was determined as the arithmetic mean of three values of intensity, measured directly under the strips of a single- (δ = 0.045 mm) and two-layer (δ = = 0.09 mm) shield, as well as in the middle between adjacent strips of different directions (δ = 0.0225 and 0.045 mm, respectively) and in the nodal points of the weave (δ = 0 and 0.045 mm, respectively).

Preliminary results of laboratory studies (Tables 1, 2) indicate that experimental shields have a certain reserve of shielding effectiveness in operation in MF, similar to fields, which form in the considered resistance welding processes, except for manual spot welding with MF intensity H_m > 1000 A/m (by the first 50 Hz harmonic). At operation of resistance welding machine with a manual tool (tongs) effectiveness of MF shielding using this shield does not provide the required protection of the welder.

Comparison of the data in Tables 1 and 2, as well as general considerations set forth in this work, allow selection of a single-layer shield with linen weave of the strips.

Thus, shielding layer in protective clothing from Ukrainian magnetically soft amorphous cobalt-based metal alloys (Co–Fe–Cr–Si–B) with sufficient mechanical functionality, can generally provide the necessary level of protection of the welder in the immediate working zone when using a product in the form of an elastic open shield in MF of medium intensity

Figure 3. Test sample of welder's protective apron without a lining (reverse side view)

Table 2. Anticipated effectiveness of experimental elastic shields with the main resistance welding processes

Resistance welding method	Effectiveness of protection by a shield with linen weave of strips, times	
	Single-layer	Double-layer
Spot:		
manual (tongs, guns)	1.2	2.0
mechanized stationary	14.4	26.0
Seam	4.4	18.4
Projection		
Butt		

($H_m \leq 500$ A/m by the first 50 Hz harmonic) in the frequency range of 500–1000 Hz.

Proceeding from the performed research, a functional sample of protective apron for the welder (Figure 3) [16] for operation in stationary machines for resistance welding with vertical location of electrodes (spot, seam, projection, capacitor, etc.) was manufactured. Testing of the shielding apron under production conditions at spot welding in MT-2202 machine demonstrated results similar to those obtained in laboratory experiments.

1. Levchenko, O.G., Levchuk, V.K. (2008) Electromagnetic safety in welding production. *Svarshchik*, **3**, 50–53.
2. Pismenny, A.S. (2008) *High-frequency welding of metallic items*. Kiev: PWI.
3. Apollonsky, S.M. (1982) *Calculation of electromagnetic shielding shells*. Leningrad: Energoizdat.
4. Apollonsky, S.M. (1988) *Reference book on calculation of electromagnetic screens*. Leningrad: Energoatomizdat.
5. Pentegov, I.V., Tarasenko, O.A. (1983) Calculation of efficiency of screening with flat screens. *Tekhn. Elektrodinamika*, **2**, 8–12.
6. Levchenko, O.G., Levchuk, V.K. (2006) Hygienic evaluation of magnetic fields in working places using arc welding of metal structures. In: *Problems of residual life and safe service of structures, constructions and machines*: Coll. of papers on results obtained in 2004–2006. Kiev: PWI.
7. Levchenko, O.G., Levchuk, V.K. (2008) Safe level of electromagnetic field intensity in resistance welding. *The Paton Welding J.*, **5**, 38–46.
8. Bogoroditsky, N.P., Pasykov, V.V., Tareev, B.M. (1985) *Electrotechnical materials*. Leningrad: Energoatomizdat.
9. Kuznetsov, P.A., Farmakovsky, B.V., Aksinazi, A.Yu. et al. *Magnetic and electromagnetic shield*. Pat. 2274914 Russia. Int. Cl. G 12 B 17/02. Publ. 20.04.2006.
10. Zaporozhets, O.I., Lukianchikov, A.V., Gliva, V.A. (2007) Evaluation of protective properties of magnetically soft materials. *Problemy Okhorony Pratsi v Ukraini*, Issue 14, 53–60.
11. *DSTU EN 470-1–2003*: Protective clothing used in welding and other high-temperature processes. Pt 1: General requirements. Valid from 01.07.2004.
12. (1988) *Means for individual protection of workers in production*: Catalogue-refer. book. Moscow: Profizdat.
13. (1975) *New textiles and materials for protective clothing*. Moscow: All-Union Institute of Light Industry Items and Clothing Standards.
14. *DSN 3.3.6.096–2002*: State sanitary standards and rules in operation with electromagnetic field sources. Kyiv: Ministry of Public Health of Ukraine.
15. (1973) *Protection against electromagnetic field action and electric current in industry*. Moscow: All-Union Central Sci.-Res. Institute of Labour Protection.
16. Lobanov, L.M., Levchenko, O.G., Levchuk, V.K. et al. *Welder's apron*. Pat. 50293 Ukraine. Int. Cl. G 12 B 17/00. Publ. 25.05.2010.

NEWS

HIGH-RELIABLE DRILL BITS

The mines of Donetsk basin have high saturation of layers with methane, which does not only complicate the service of mines and increases service costs, but also constantly creates dangers of explosions with grave consequences, including human victims. Besides, the experience of the Zasyadko mine shows that it is possible not only to decrease the probability of accidents at the mines due to explosions of methane, but also to efficiently use the latter both to satisfy the needs of mines (power saving, application for transport, etc.) as well as the needs of local inhabitants.

Drill bit and calibrator for extraction of sprayed mining methane

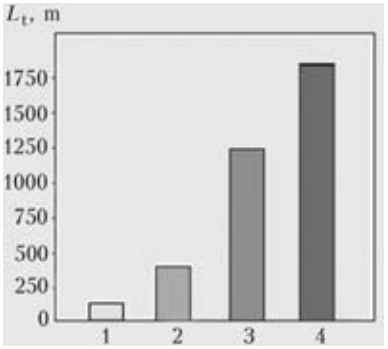

Average value of tunneling of a drill bit manufactured at the Institute of Superhard Materials (ISHM) (1); jeintly by ISHM and PWI (2); PWI (3); PWI + repair (4)

The weak point for mass application of this technology was low service life of drill bits manufactured in Ukraine, which were much inferior to foreign analogues.

At the E.O. Paton Electric Welding Institute

- high-strength cadmium-free brazing alloys and technological process of drill bits manufacture, and
- advanced design of drill bit and stabilizer were developed.

Renewed design and technology of manufacture allowed tunneling to be several times increased.

MULTIFUNCTIONAL POWER SOURCE

The E.O. Paton Electric Welding Institute (PWI) of the NAS of Ukraine has developed the new small-sized functional power source MP-50 for microplasma welding and powder surfacing. It is designed to provide technological processes of manual and mechanized microplasma welding of ferrous, non-ferrous, refractory metals, alloys of small thicknesses (from 0.3 to 1.5 mm) and can be used as a main or auxiliary plasma power source in technological installations for microplasma-powder surfacing and hybrid laser-microplasma welding.

In accordance with functional purpose the power source provides formation of microplasma arc with power and thermophysical characteristics in operation

required for preset technological processes at the following basic modes:

• mode A — welding using direct current of straight polarity with smooth adjustment of current from 5 to 50 A;

• mode B — welding using pulsed current of straight polarity with smooth adjustment of current from 5 to 50 A and discrete adjustment of duration of pulses and pauses between them in the range from 1 to 99 ms with a pitch of 1 ms;

• mode C — welding using variable-polarity current pulses with smooth adjustment of current of straight polarity from 5 to 50 A and discrete adjustment of duration of pulses and pauses between them in the range from 1 to 99 ms with a pitch of 1 ms and current of reversed polarity in the range from 1 to 99 s with a pitch of 1 ms.

The source can be used in electromechanical industry, automobile industry, manufacture of products of aerospace engineering, machine building and manufacture of industrial plants, chemical and food industry, medicine engineering.

For operation, the supply of working gases and water cooling should be connected to plasmatron (powder feeder) and outer systems.

NEW METHOD OF BRAZE WELDING

Braze welding of a single-fiber wire with multi-fiber ones. For butt joining of multi-fiber wires with one-fiber ones where melting temperature of material of multi-fiber wire is not higher than melting temperature of metal of one-fiber one (for example, for termination of wires of resistance alloys by copper multi-fiber wires), the new method of braze welding was developed at the E.O. Paton Electric Welding Institute.

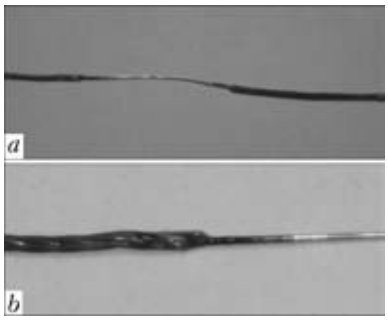

The photos of typical joints of copper wire of 7 × × 0.42 mm section with wire of 0.5 mm diameter of nichromium (*a*) and stainless steel (*b*) are presented in the Figure.

The method allows automation of joining process. The strength of joints produced with keeping of Technological Instructions corresponds to the strength of a copper wire, i.e. rupture at tension always occurs in copper wire.

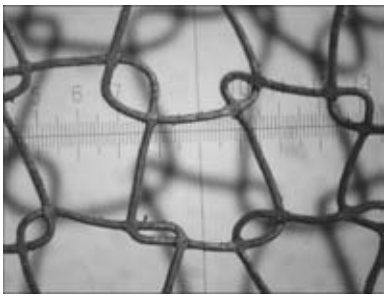

Welding of meshes of metallic grid. During manufacture of grid of a thin wire, produced of soft metal, the necessity in joining this grid in meshes to preserve sizes of a grid often appears. This task is solved by a new method of joining the grid meshes in the process of its knitting. The strength of a joint allows coiling a grid, its bending at sharp angle, manipulating at different types of service.

SUBSCRIPTION
FOR «THE PATON WELDING JOURNAL»

If You are interested in making subscription directly via Editorial Board, fill, please, the coupon and send application by fax or e-mail.

The cost of annual subscription via Editorial Board is $324.

Telephones and faxes of Editorial Board of «The Paton Welding Journal»:

Tel.: (38044) 200 82 77, 200 81 45

Fax: (38044) 200 82 77, 200 81 45.

«The Paton Welding Journal» can be also subscribed worldwide from catalogues of subscription agency EBSO.

SUBSCRIPTION COUPON

Address for journal delivery _____

Term of subscription since _____ **20** **till** **20**

Name, initials _____

Affiliation _____

Position _____

Tel., Fax, E-mail _____

ADVERTISEMENT
IN «THE PATON WELDING JOURNAL»

External cover, fully-colored:
First page of cover (190×190 mm) – $700
Second page of cover (200×290 mm) – $550
Third page of cover (200×290 mm) – $500
Fourth page of cover (200×290 mm) – $600

Internal cover, fully-colored:
First page of cover (200×290 mm) – $350
Second page of cover (200×290 mm) – $350
Third page of cover (200×290 mm) – $350
Fourth page of cover (200×290 mm) – $350

Internal insert:
Fully-colored (200×290 mm) – $300
Fully-colored (double page A3) (400×290 mm) – $500
Fully-colored (200×145 mm) – $150
Black-and-white (170×250 mm) – $80
Black-and-white (170×125 mm) – $50
Black-and-white (80×80 mm) – $15

- Article in the form of advertising is 50 % of the cost of advertising area
- When the sum of advertising contracts exceeds $1000, a flexible system of discounts is envisaged

Technical requirement for the advertising materials:
- Size of journal after cutting is 200×290 mm
- In advertising layouts, the texts, logotypes and other elements should be located 5 mm from the module edge to prevent the loss of a part of information

All files in format IBM PC:
- Corell Draw, version up to 10.0
- Adobe Photoshop, version up to 7.0
- Quark, version up to 5.0
- Representations in format TIFF, color model CMYK, resolution 300 dpi
- Files should be added with a printed copy (makeups in WORD for are not accepted)